UNIVERSITA' DEGLI STUDI DI PADOVA

Sede Amministrativa: Università degli Studi di Padova

Dipartimento di Principi e Impianti di Ingegneria Chimica "I. Sorgato"

SCUOLA DI DOTTORATO DI RICERCA IN : Ingegneria Industriale
INDIRIZZO: Ingegneria Chimica
XXI CICLO

DEVELOPMENT OF CELL CULTURE TECHNOLOGY FOR THE EXPANSION OF HOMOGENEOUS POPULATIONS OF HUMAN STEM CELLS

Direttore della Scuola : Ch.mo Prof. Paolo Bariani
Supervisore : Ch.mo Prof. Nicola Elvassore

Dottorando : Camilla Luni

To my parents

"The human understanding is of its own nature prone to suppose the existence of more order and regularity in the world than it finds."

Sir Francis Bacon

Table of contents

Chapter 3

Microliter-bioreactor array stirred by thermoconvection

Sommario

E' stato prospettato l'impiego di cellule staminali per terapie volte al mantenimento, alla rigenerazione o alla sostituzione di tessuti malfunzionanti. Tuttavia non sono ancora state risolte alcune limitazioni legate principalmente alla scarsa disponibilità di cellule staminali e ai problemi di sicurezza clinica connessi alla qualità cellulare. L'ottimizzazione del processo di espansione cellulare è un sfida ingegneristica, oltre che biologica.

Scopo di questa tesi è lo sviluppo di una tecnologia sperimentale e di un quadro razionale che consenta di comprendere e controllare l'espansione di cellule staminali *in vitro*, sia considerando le proprietà medie che la loro distribuzione nella popolazione cellulare prodotta.

E' stata realizzata un'analisi razionale dei principali fenomeni coinvolti nella coltura cellulare, ponendo in evidenza le fonti di eterogeneità sia nei sistemi di coltura convenzionali che nei bioreattori mescolati.

Da un punto di vista sperimentale, sono stati progettati e sviluppati due tipi di bioreattori fino a realizzarne dei prototipi. Il primo, un sistema di bioreattori di volume dell'ordine dei microlitri, è stato progettato basato su un meccanismo di termoconvezione; questo apparato sperimentale è particolarmente adatto per un'ottimizzazione multiparametrica delle condizioni di coltura. Il secondo, un bioreattore in sospensione multipozzetto con un volume operativo di 10 ml/pozzetto, è stato pensato e costruito per un'ottimizzazione di processo meno dettagliata o, alternativamente, per una produzione su piccola scala di cellule staminali; una versione più avanzata è stata sviluppata per effettuare colture di cellule staminali in condizioni di ipossia. Entrambi i dispositivi sono stati

vantaggiosamente utilizzati per coltivare cellule staminali ematopoietiche, ricavate da cordone ombelicale umano, che sono poi state caratterizzate secondo i metodi di analisi biologica convenzionali.

Per ottimizzare razionalmente il processo di espansione delle cellule staminali, è stato sviluppato un modello computazionale, basato su un bilancio di popolazione, che tiene conto della distribuzione di recettori e di complessi recettore-ligando nel campione cellulare. Il modello descrive ragionevolmente l'eterogeneità intrinseca, intra- e intergenerazionale, derivante dal processo di divisione cellulare.

Questi risultati possono dare un riscontro positivo in fase di progettazione degli esperimenti e di definizione delle condizioni operative a cui effettuare colture in bioreattore, al fine di minimizzare l'eterogeneità estrinseca e intrinseca della popolazione cellulare e di effettuare un ulteriore avanzamento verso un processo di espansione di cellule staminali umane clinicamente sicuro ed affidabile.

Summary

Stem cell-based therapies have been proposed as promising for the maintenance, regeneration, or replacement of malfunctioning tissues, but suffer from limitations mainly due to scarce cell availability and clinical safety concern related to cell quality. Optimization of stem cell expansion process is an engineering challenge, besides a biological issue.

Aim of the work presented is to develop the experimental technology and the rational insight to understand and control stem cell expansion *in vitro*, in terms of both average and distributed properties of the cell population produced.

A rational analysis of the main phenomena involved in a cell culture was achieved, underlining the sources of stem cell heterogeneity in both conventional culture systems and stirred bioreactors.

From an experimental point of view, two types of bioreactors were designed, developed, and prototyped. The first, a microliter bioreactor array, was designed based on thermoconvective mixing; this experimental setup is particularly convenient for multiparametric optimization of cell culture conditions. The second, a six-well suspension bioreactor with a working volume of 10 ml/well, was designed and fabricated for coarse process optimization or, alternatively, for small-scale stem cell production; an improved setup was developed to perform stem cell cultures under hypoxia conditions. Both devices were advantageously used to culture human cord blood-derived hematopoietic stem cells, which were then characterized according to the currently available biological assays.

In order to rationally optimize the stem cell expansion process, a computational model, based on a population balance approach, was developed, that takes into

account receptor and receptor-ligand complex distribution in the cell sample. The model fairly describes intrinsic intra- and inter-generational heterogeneity arising from the process of cell division.

These findings could give interesting feedback to experimental design and to define the operative conditions for bioreactor cultures, in order to minimize extrinsic and intrinsic heterogeneity, and to make a step towards a clinically safe and reliable human hematopoietic stem cell expansion process.

Foreword

The work of this PhD program was performed at "Dipartimento di Principi e Impianti di Ingegneria Chimica" of Università di Padova. Part of the computational section was carried out at University of California at Santa Barbara (UCSB), under the supervision of Prof. F. J. Doyle III.

I would like to thank here my supervisor Prof. N. Elvassore, for his constant challenging collaboration, and my co-supervisor, Prof. F. J. Doyle III, for the opportunity of profitably working at UCSB.

Due to the high interdisciplinarity of this topic, the work in this thesis has benefited from external collaborations, and I would like to thank the following research groups:

- Prof. Paolo De Coppi (Department of Paediatric Surgery, Institute of Child Health, London, UK)
- Prof. Carl Meinhart (Department of Mechanical Engineering, University of California at Santa Barbara, USA)

I am grateful to Ministero Italiano dell'Università e della Ricerca (MIUR), Università di Padova, and Città della Speranza, for the financial support to the research activity.

During the period of the PhD program, a patent application was deposited at Camera di Commercio Industria, Artigianato e Agricoltura of Padova (PD2008A000371).

During of the period of the PhD program, the following publications have been produced:

Flaibani M, Luni C, Sbalchiero E, Elvassore N. Flow cytometric cell cycle analysis of muscle precursor cells cultured within 3D scaffolds in a perfusion bioreactor. Biotechnol Progr. In press.

Luni C, Strumendo M, Boldrin L, Piccoli M, De Coppi P, Elvassore N. Modeling of human skeletal muscle stem cell ex vivo culture by a population balance equation. To be submitted.

Luni C, Feldman H, Meinhart C, Pozzobon M, De Coppi P, Elvassore N. Multiwell bioreactor for hematopoietic stem cell expansion under thermoconvective flow. In preparation.

Luni C, Albania L, Pozzobon M, Piccoli M, De Coppi P, Elvassore N. Six-well stirred bioreactor for hematopoietic stem cell expansion. To be submitted.

Luni C, Doyle III FJ, Elvassore N. Optimizing ligand administration for hematopoietic stem cell expansion in bioreactor through a population balance model approach. To be submitted.

Luni C, Cimetta E, Elvassore N. Understanding the dominant regimes to tailor the stem cell niche. In preparation.

Part of the work in this thesis was presented at international conferences, including: the American Institute of Chemical Engineering (AIChE), Biomedical Engineering Society (BMES), International Conference on Systems Biology (ICSB).

Chapter 1

Clinical use of hematopoietic stem cells

In this chapter clinical relevance, problems, limitations, and current perspectives of hematopoietic stem cell use are presented. The rational analysis of these topics in view of a process design will be analyzed in Chapter 2. At the end of this chapter, the outline of the thesis is reported.

1.1 Clinical motivation

The use of living cells as therapeutic agents for the maintenance, regeneration, or replacement of malfunctioning tissues has been proposed in last decades (Kirouac *et al*, 2008). Stem cells are the basis for cell therapy. They are functionally undifferentiated cells that retain the ability to differentiate in one or more mature cell types under appropriate conditions, and to self-renew, representing a potentially inexhaustible cell source (Alberts *et al*, 2002).

There are two main sources of stem cells. Adult stem cells are present as a small fraction in most tissues of the human body, and are mostly committed to

differentiate only in the mature cells of the tissue where they reside. Embryonic stem cells are used in the form of immortal cell lines that were derived from the inner mass of the blastocyst during embryogenesis, they are multipotent as they are able to differentiate in mature cells derived from all three germ layers (Alberts *et al*, 2002).

Cell-based therapies use either autologous or allogeneic stem cells, depending if the recipient is the same as the donor or not, respectively. While autologous cell therapy has the advantage of complete immunological compatibility, there are many situations where allogeneic cell transplantation is necessary for therapeutic efficacy (Cortesini, 2005). Therapeutic strategies that make use of stem cells have been proposed for many clinical applications for example, Parkinson's and Alzheimer's diseases, spinal cord injury, stroke, burns, heart disease, diabetes, osteoarthritis, and rheumatoid arthritis (stemcells.nih.gov).

Despite the efforts in stem cell research, cell therapy is still not widely applied clinically, because severe limitations reduce their potential benefits. There some general issues that need to be solved in most of the clinical applications, such as the need to have a sufficient number of cells that maintain the appropriate phenotype and perform the required biological functions; the choice of the stem cell source considering availability, invasiveness of cell harvesting, and histocompatibility; safety challenges as the product is the living cells themselves, and the extensive proliferative potential that makes stem cells attractive also confers the risk associated with their tumorgenicity (Polak *et al*, 2006).

1.1.1 HSCs from bone marrow: clinical relevance and limitations

A particularly promising cell-based therapy is hematopoietic stem cell (HSC) transplantation, because it has a wide range of applicability, for example in the

treatment of blood cancers, hereditary blood disorders, or, in some cases, to replace cells destroyed by chemotherapy (Weissman, 2000).

Adult hematopoiesis *in vivo* is performed by HSCs present in bone marrow, as shown in Fig. 1.

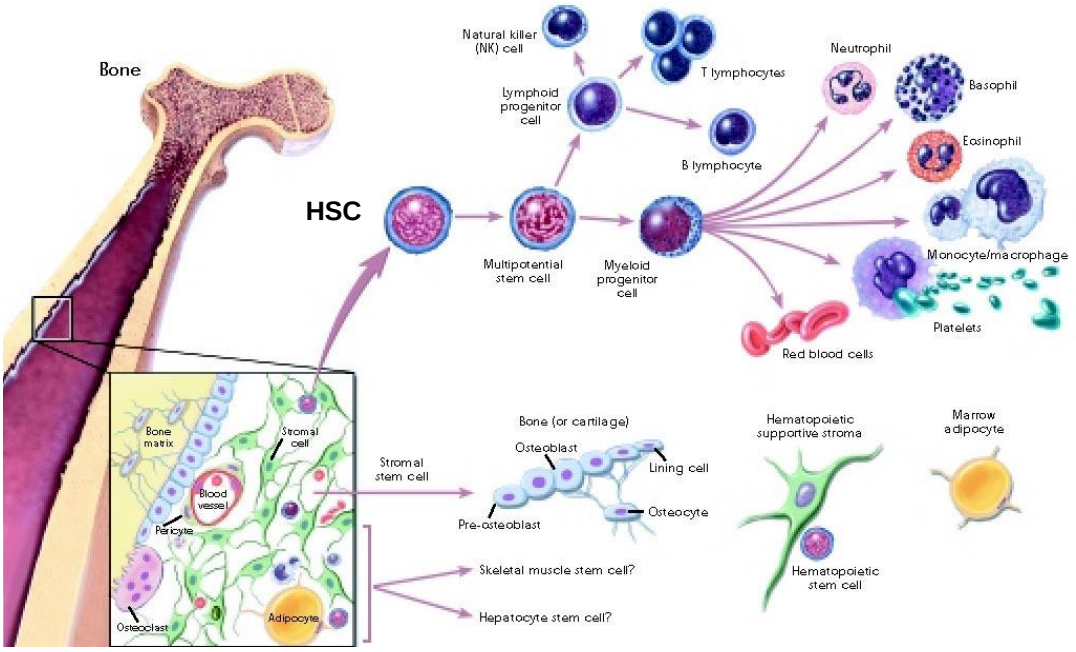

Figure 1. Location of HSCs in the bone marrow, and differentiation tree that produces the different classes of mature blood cells (stemcells.nih.gov).

According to molecular signals from the local microenvironment, HSCs proliferate and differentiate, producing the different classes of blood cells. In this process different steps are generally identified that correspond to distinct intermediate cell phenotypes, as reported in Fig. 1. Each phenotype is characterized by a specific morphology and cell surface markers. During differentiation cells progressively become committed to only one type of mature cell and loose their proliferative potential (Alberts *et al*, 2002). While progenitors seem to play a role in the immediate period after transplantation, only HSCs are able to give rise to long-term bone marrow reconstitution (Weissman, 2000).

Despite its therapeutic potential, bone marrow transplantation have several limitations. First, the large HSC dose required, which is a crucial parameter for a successful therapy, but makes bone marrow harvesting a more invasive procedure for the donor. Then donor availability, considering the importance of histocompatibility issues. Except in the case of homozygous twins, there is always a certain severity of immunological response, called graft-versus-host disease, after transplantation. The donor cells have different surface proteins, called human lymphocyte antigen (HLA), that produce an immunological response from the host. Furthermore bone marrow from the donor includes T cell lymphocytes that do not recognize host cells, giving rise to a double immunological response. Thus, a requirement for bone marrow transplantation is the HLA matching between donor and patient. Consequently patients with uncommon HLA-types can face difficulties in finding a matching donor. However the high degree of HLA polymorphism makes a random match between unrelated humans a rare event in any case, and even between siblings the probability of a HLA match is 25%. All these medical implications result in very long times before a suitable donor can be found and transplantation performed. For completeness, it is worth to highlight that, although autograft bone marrow transplantations overcome the histocompatibility issue, they are not feasible in many cases from a clinical perspective. A minor issue is the risk of donor morbidity, that requires careful control of donor cells and further delays the transplantation (Weissman, 2000).
An alternative source of HSCs is umbilical cord blood (UCB).

1.1.2 UCB as a promising source of HSCs for transplantation

The presence of HSCs in UCB was discovered in the 80s (Broxmeyer *et al*, 1989). Since then, various works have studied UCB as a possible alternative to bone

marrow in HSC transplantations. There are several advantages connected with UCB use, even if a definitive assessment of its comparable therapeutic efficacy with respect to bone marrow has not been given in clinical trials yet, because of the difficulty to compare data that inevitably present a high variability (Shoemans *et al*, 2006).

The main advantage of UCB as a HSC source is its availability. Cord blood banks select, purify, classify, and store UCBs from donors (Shoemans *et al*, 2006). The bank network is growing all over the world, making an UCB unit ready to use in a day because it is HLA-typed before storage. Bone marrow usually requires 3-4 months, as it is donor-dependent. HSCs from UCB give rise to less histocompatibility problems and require a less HLA-match, because they have more immature surface antigens and T cell lymphocytes are absent. The risk of donor morbidity is also reduced (Eapen *et al*, 2007).

The main limitation for UCB success in transplantations is the fixed HSC content of a unit of UCB, considering that the minimum number of cells required for transplantation is $2.5 \cdot 10^7$ cryopreserved nucleated cells/kg of patient. As transplantation outcome is correlated with the cell dose infused, this restricts UCB use mainly to pediatric patients (Eapen *et al*, 2007). Different strategies try to overcome this limitation, like the injection of multiple cords, that resulted in a higher engraftment but also in an increased graft-versus-host disease. Expansion *ex vivo* of HSC from a unit of UCB is a promising strategy. Up to now the increased number of cells obtained is mainly due to hematopoietic progenitors which are helpful in the immediate recovery after transplantation, but a higher number of HSCs is also required, and efficient strategies for effective stem cell expansion *in vitro* have not been developed yet (Eapen *et al*, 2007).

1.2 HSC expansion and cell quality assessment

In vivo HSC expansion is regulated by a network of chemical, mechanical, and electrical signals from the local surrounding environment, called stem cell niche. *In vitro* HSCs are conventionally cultured in single-well Petri dishes, multiwell, or flasks, where they grow settled at the bottom without surface attachment. Their proliferation rate is regulated by exogenous and endogenous growth factors that are present as soluble molecules in the culture medium. Besides proliferation, growth factors affect the phenotypic characteristics of the cell population, for example in terms of morphology, degree of differentiation, and tumorigenicity properties (Kirouac *et al*, 2008).

The optimization of protocols for HSC expansion needs to span a wide range of experimental conditions, in terms of type, timing and dose of soluble growth factors to reproduce *in vitro* stem cell niche signals (Verfaillie, 1992).

The first requirement of a cell-based therapy is its efficacy in the human patient. A robust correlation between measurable HSC properties and clinical success is not available yet. Most of the assays, developed to characterize the cells, associate cell characteristics to short-term engraftment more than to long-term bone marrow reconstitution (Purton *et al*, 2007).

Despite this limitation, the characterization of cells from a cell culture is important to understand different aspects of the expansion process, such as repeatability and heterogeneity inside the HSC population, to increase our understanding of cell behavior, and to detect the retain of multipotency after the expansion process.

The most common assays used for cell quality assessment are flow cytometry, colony-forming cell assays, *in vivo* assays in model animals, and then clinical trials. Currently, results from clinical trials are the only ultimate response of the effective expansion of HSCs, whereas it is uncertain if experiments in animals are

representative of the human response. Colony-forming cell assays are informative about the progenitor cell content of a population of interest, but do not measure the HSC fraction of a cell population, they are used to detect the retention of multipotency in the expanded cells (Purton *et al*, 2007). Flow cytometry is a powerful technique used to analyze the pattern of protein markers present on the surface of cells at different stages of differentiation, it will be described in further detail in Chapter 2.

1.3 From discovery to clinical use

The road map that brings HSCs from umbilical cord blood to the clinic is a long process (Fig. 2), that involves people with different skills, like biologists, engineers, and physicians.

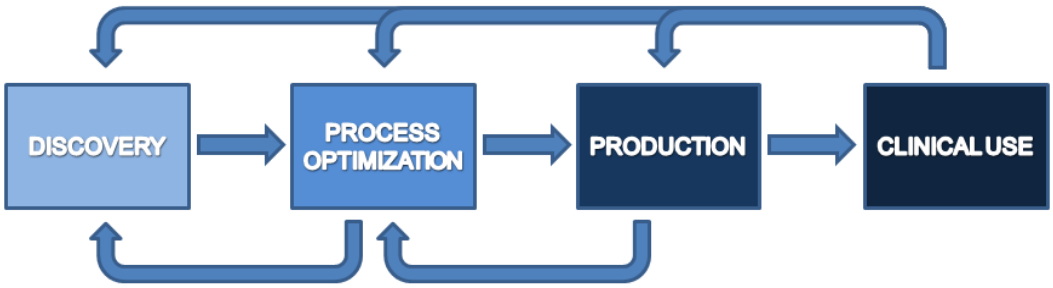

Figure 2. Schematic representation of the road map from hematopoietic stem cell discovery to their clinical use.

- Discovery is the first step, which gives the basis for a feasible clinical application. It involves the identification of HSCs, and of the basic signaling they receive from the stem cell niche, like endogenous and exogenous growth factors.
- Process optimization involves the understanding of the relative importance of the different processes in order to find the proper conditions for an

effective stem cell expansion. Wide screening of experimental conditions occurs at this stage, that includes for example the choice of materials used for cell culture and definition of local conditions for cell expansion, along with the development of reliable cell quality detection assays. The cell quality after *in vitro* culture is the main goal of this step. Process development occurs on a small scale to provide increased insight and understanding.

- Once the key design parameters for HSC expansion are known, the process needs to be implemented for a production at the clinical scale. At this stage other variables come into play, such as the development of a cost-effective process, robustness and reproducibility in the methodology of cell expansion, detection of key measurements for cell quality control and process monitoring.
- The last step is clinical use of HSCs.

This road map that brings HSCs to the clinic is not just a sequence of steps, because different development phases feed back on one another. For example, as clinical trials are today the only evidence of therapeutic efficacy, motivated by the lack of other reliable tests, they give a feedback to the whole process development pipeline.

Food and Drug Administration (FDA), the American agency responsible for protecting and promoting public health, indicated the guidelines and regulations to develop stem cell clinical applications, underlining the importance of quality control not only of the final cell product, but also of the manufacturing methods that need to be robust and repeatable (FDA, 2004). This task is further complicated

by the fact that besides average properties, also their distribution in the cell population affects the clinical success of the cell-based therapy (Bryder *et al*, 2006).
Thus, process optimization and production are not only biological problems, but also engineering challenges.

1.4 Thesis outline

The aim of this thesis is to develop the technology to expand HSC populations under definite conditions, and to define and describe the average properties of the system and eventual sources of intrinsic and extrinsic variability or heterogeneity in the cellular quality outcome.

In Chapter 2 a rational analysis of the biological and physical phenomena relevant for the development of cell culture technology is discussed. In particular, the key variables to take into account in bioreactor design are discussed, and the strategy to collect experimental data are presented.

In Chapter 3 the design and application of a microliter bioreactor array is presented, in view of a wide screening of experimental conditions for stem cell culture under stirred-suspension conditions.

In Chapter 4 a clinical-scale bioreactor prototype is described, along with the results from biological experiments, where human umbilical cord blood hematopoietic stem cells were cultured.

In Chapter 5 a theoretical analysis of the intrinsic heterogeneity in a stem cell population is presented. This study is performed by a mathematical model based on a population balance approach.

In Chapter 6 conclusions are presented, along with future perspectives.

1.5 References

Alberts B, Johnson A, Lewis J, Raff M, Roberts K, Walter P. 2002. Molecular Biology of the Cell, 4th ed. New York:Garland.

Broxmeyer HE, Douglas GW, Hangoc G, Cooper S, Bard J, English D, Arny M, Thomas L, Boyse EA. 1989. Human umbilical cord blood as a potential source of transplantable hematopoietic stem/progenitor cells. PNAS 86:3828-3832.

Bryder D, Rossi DJ, Weissman IL. 2006. Hematopoietic stem cells - The paradigmatic tissue-specific stem cell. Am J Pathol 169(2):338-346.

Cortesini R. 2005. Stem cells, tissue engineering and organogenesis in transplantation. Transplant Immunology 15:81-89.

Eapen M, Rubinstein P, Zhang M-J, Stevens C, Kurtzberg J, Scaradavou A, Loberiza FR, Champlin RE, Klein JP, Horowitz MM, Wagner JE. 2007. Outcomes of transplantation of unrelated donor umbilical cord blood and bone marrow in children with acute leukaemia: a comparison study. Lancet 369: 1947-1954.

FDA. 2004. Guidance for industry: PAT—A framework for innovative pharmaceutical development, manufacturing, and quality assurance (http://www.fda.gov/cder/guidance/6419fnl.htm).

Kirouac DC, Zandstra PW. 2008. The systematic production of cells for cell therapies. Cell Stem Cell 3:369-381.

Polak JM, Bishop AE. 2006. Stem cells and tissue engineering: Past, present, and future. Ann N Y Acad Sci 1068:352-66.

Purton LE, Scadden DT. 2007. Limiting factors in murine hematopoietic stem cell assays. Cell Stem Cell 1(3):263-70.

Schoemans H, Theunissen K, Maertens J, Boogaerts M, Verfaillie C, Wagner C. 2006. Adult umbilical cord blood transplantation: a comprehensive review. Bone Marrow Transplantation 38:83–93.

Verfaillie CM. 1992. Direct contact between human primitive hematopoietic progenitors and bone marrow stroma is not required for long-term *in vitro* hematopoiesis. Blood 79(11):2821-2826.

Weissman IL. 2000. Translating Stem and Progenitor Cell Biology to the Clinic: Barriers and Opportunities. Science 287:1442-1446.

Chapter 2

Rational design principles

In this chapter the biological processes involving stem cell behavior, connected to the topic of this work, are reviewed. The methods to experimentally detect cell quality at population level are described. The theoretical analysis of the processes generating heterogeneity is then performed, anticipating the content of next chapters.

2.1 Stem cell behavior

Stem cell behavior strongly depends on interactions with signal molecules in the extracellular environment. *In vivo* these molecules are produced by neighboring cells or by cells further away inside the organism. Cells are able to detect and respond to the presence of these molecules in the local environment by a variety of cell-surface receptor proteins. A type of receptor is specific for detecting only the complementary ligand signal molecule. When a receptor-ligand complex is formed, an intracellular signaling cascade is generated inside the cell, affecting its behavior (Alberts *et al*, 2002).

Stem cell niche is the local tissue microenvironment that maintain and regulate stem cells *in vivo* (Scadden, 2006). Besides by soluble factors, stem cell behavior is also influenced by surface contact, and mechanical and electrical stimuli. But they are out of the scope of this thesis.

Cell surface receptors are important markers that characterize a cell, because they are an index of cell ability to respond to specific external stimuli. Nonetheless a straight relationship between certain kind of receptors and cell "stemness" has not been found yet. Even if some markers are associated with primitive cell behavior, they are not fully specific for stem cells (Morrison *et al*, 2008).

HSC-environment interactions *in vitro* can be schematically described as in Fig. 1, where a main distinction is made among:

- exogenous soluble factors, that are provided by the culture medium;
- endogenous factors, that are produced by cells to influence neighbor cells;
- autologous factors that cells both release and uptake.

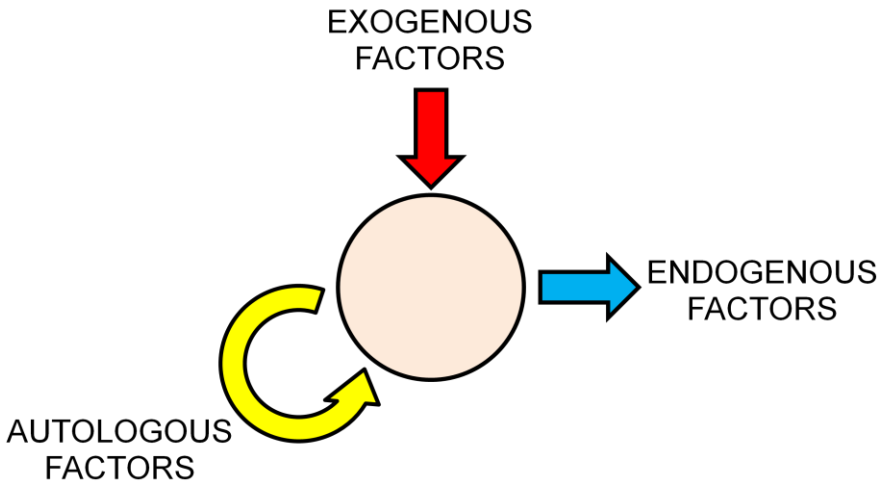

Figure 1. Schematic of the soluble factors involved in cell-environment interaction. Exogenous factors present in culture medium, endogenous factors released by the cell, and autologous factors that are both released and up taken by the cell itself.

The commitment of a stem cell to different differentiation lineages (Fig.1, Chapter 1) is dependent from these signaling molecules. Thus, they play a key role in stem cell culture strategies. Growth factors represent the operative variables that need to be controlled during *in vitro* expansion (Verfaillie *et al*, 1992).

In vivo, hematopoietic stem cells (HSCs) reside primarily in the bone marrow, that contains both hematopoietic and non-hematopoietic cells. In response to signals from the local microenvironment, cells proliferate. Proliferation occurs also *in vitro* if culture conditions are suitable.

Cell cycle is the sequence of steps that cells undergo to divide. It is mainly composed by four phases, as indicated in Fig. 2. During S-phase cells double their DNA, whereas during M-phase they effectively divide their biological material between the two daughters. G_1 and G_2 phases are gap phases of variable duration that are inserted between S- and M- phases. A further cell state exists called G_0-phase, typical of cells that perform normal cellular functions, but are in a status of proliferative quiescence. Stem cells are recognized to be in G_0 in many adult tissues *in vivo*, where they reside before external signals make them enter the cell cycle (Alberts *et al*, 2002).

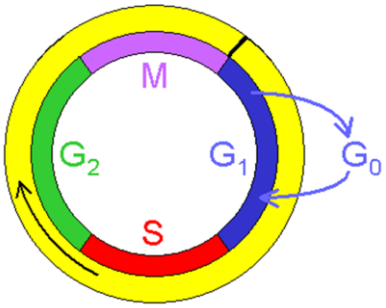

Figure 2. Schematic of the main phases of the cell cycle. G0 is a phase of proliferative quiescence, in S cells duplicate their DNA, in M biological material is split between the two daughter cells. G1 and G2 are gap phases that separate S and M.

2.2 Stem cell characterization at population level

Various experimental methods are available to assess cell quality at population level. They detect both average and distributed properties. Flow cytometry and Coulter counter are detailed below.

2.2.1 Flow cytometry

Flow cytometry is a powerful means to analyze samples of about 10^4 cells in few minutes. Cells are stained with different types of fluorescent probes that bind specifically defined cell components. Then their fluorescence is analyzed, while one cell at a time passes in front of a laser beam (Ormerod, 2000).

As reported in §2.1, cells proliferate undergoing a cell cycle. By flow cytometry it is possible to study the asynchrony of a cell population detecting the fraction of cells in each phase of the cell cycle. In Appendix A, a study is reported of a flow cytometric cell cycle analysis of muscle precursor cells cultured in a perfusion bioreactor (Flaibani *et al*, in press).

In this thesis more emphasis is given to flow cytometry as an analysis tool to detect various types of cell surface markers. Different markers can be contemporarily detected if cells are stained with fluorescent probes of different wavelengths. In Fig. 3 an example of the distribution of marker c-kit, also called CD117, is reported. As shown, it is possible to detect the distribution of fluorescence intensity, and thus marker content, in the cell population.

In Chapter 3 and 4 a detailed analysis is presented on characterization of human cord blood-derived HSCs after culture in the two different bioreactor systems developed.

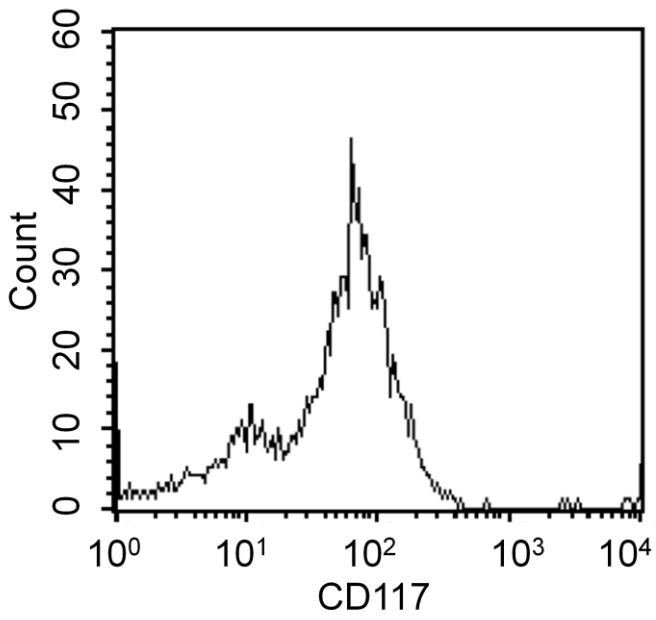

Figure 3. Example of measurement of c-kit (CD117) distribution in a population of cord blood-derived cells.

2.2.2 Cell morphology

Cell morphology can be analyzed by a Coulter counter. An instrument that detects cell number and volume distribution in the cell population. The counter measurement is based on the change in electrical conductance of a small aperture when fluid containing cells pass through.

Cell volume heterogeneity in a population of satellite cells – a type of stem cells present in adult skeletal muscle – was analyzed in a previous work that is reported in Appendix B. An example is shown in Fig. 4.

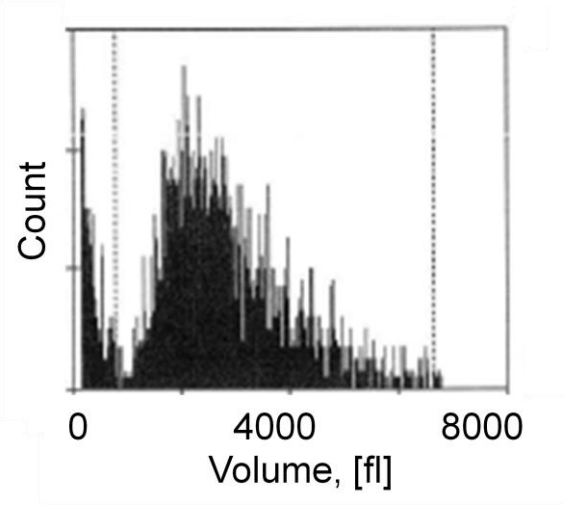

Figure 4. Example of a measurement of muscle satellite stem cell volume distribution by Coulter counter.

2.3 Stem cell culture methods

2.3.1 Static culture

Static culture systems, such as polystyrene Petri dishes, multiwells, or flasks, have been the most widely used culture devices. HSCs are conventionally cultured in these containers, and put inside a biological incubator, where two physical parameters are regulated: temperature and pH. Temperature is usually set at 37°C, whereas pH control is performed by maintaining an atmosphere at 5% CO_2 concentration, which corresponds to the physiological pH of 7.2. The main sources of variability among different culture protocols reside in medium composition, cell seeding density, and time intervals between cell dilutions, called cell passages, and medium changes. Conventional cultivation methods are in need of both optimized protocols and *ad hoc* technology (Cabrita *et al*, 2003).

2.3.2 Stirred suspension bioreactor

The road map from stem cell discovery to clinical use involves a sequence of phases (see Fig. 2, Chapter 1), bioreactors of different scales can be useful in the two steps of process optimization and production, where cost reduction and product quality control are needed (Kirouac *et al*, 2008).

A cell suspension bioreactor is a closed stirred vessel where it is possible to inline monitor and control some culture parameters, and to take samples from the vessel without disrupting culture conditions. It can be run in different configurations, such as batch, fed-batch, and in perfusion mode, with a system to prevent cell wash-out (Cabrita *et al*, 2003). The main advantage of a suspension bioreactor is related to the reduction of spatial gradients. The homogeneity in the vessel ensures more defined and repeatable culture conditions, making easier the scale-up of the process with a consequent cost reduction. Other pros are the possibility to control the process inline, and to attain higher cellular densities, because, as cells are suspended, the culture becomes three-dimensional (Blanch *et al*, 1997).

While biopharmaceutical microbiologic production processes are currently performed in stirred bioreactors, the adaptation of the setup of these systems to stem cell culture requires a more careful choice of biocompatible materials, and a minimization of the shear stress caused by the stirring (Nielsen, 1999).

Presently, research is performed in bioreactors with volume in the range of about 100-1000 ml to culture embryonic, mesenchymal, neural (for references, see King *et al*, 2007; Kirouac *et al*, 2008), and HSCs (Sardonini *et al*, 1993; Zandstra *et al*, 1994; Collins *et al*, 1998). HSCs are particularly suitable to be cultured in suspension bioreactors as they do not require surface attachment to grow.

Many protocols available have been developed for static culture conditions. Using these protocols in suspended bioreactors requires their adaptation to a completely

different system. For example, bioreactors are made of different materials, such as glass, that requires a coating to have a suitable cell-contact surface (Zandstra *et al*, 1994), but exogenous and endogenous factors have different adsorption constants on these materials respect to, for example, polystyrene. Furthermore, pH control is performed by feeding a gas mixture on medium surface, thus the efficiency of this control is dependent on medium surface-volume ratio and mixing rate, and is completely different to that under static conditions. Besides tubing used for gas inlet can also play a role.

In Fig. 5 a bioreactor with a minimum working volume of 300 ml is shown. This system was initially used in the experiments at the beginning of this PhD program, but all the limitations just described, and, in particular, the costs for handling in such a large volume very valuable materials, induced to the development of more sustainable culture systems, described in Chapter 3 and 4.

Figure 5. Large scale stirred suspension bioreactor. Provided with water jacket for temperature control, gas inlet and outlet for pH control by CO2, stirring system, pumps or on line sampling and feeding. Minimum working volume is 300 ml.

2.3.3 Analysis of characteristic times

A useful means to understand stem cell behavior is the study of the interplay between the relative rates of different biological, chemical, and physical phenomena involved. A qualitative analysis of these crucial aspects, restricted to endogenous and exogenous soluble factors, is now reported for the two culture conditions presented: culture under static conditions and in a stirred bioreactor.

2.3.3.1 Static culture characteristic times

When cells are cultured under static conditions, medium in the well is stagnant. The small convective flow due to random local temperature gradients will be neglected in this analysis. Soluble factors are present in the medium, and are up taken and released by the cells, depending if they are exogenous or endogenous (Fig. 1). The competitive processes in these culture conditions are transport by diffusion and cell uptake/release of soluble factors. Only uptake will be considered in this theoretical analysis.

The characteristic time of diffusion, τ_1, is given by:

$$\tau_1 = \frac{\lambda^2}{D} \ , \tag{2.1}$$

where λ is a the characteristic diffusion length, and D the diffusion coefficient. While for endogenous factors λ is equal to the average cell-cell distance at well bottom, δ_{cc1} (Fig. 6 A), which is cell density dependent, λ is reasonably given by medium height, *H*, for exogenous factors (Fig. 6 A).

A simple kinetics of uptake is assumed for the reaction between receptor, *R*, and ligand, *L*:

$$R + L \underset{}{\overset{k_{on}}{\rightleftarrows}} RL$$

where RL is the complex formed. The uptake characteristic time, τ_2, can be defined as:

$$\tau_2 = \frac{1}{k_{on} \cdot [L]} \ . \tag{2.2}$$

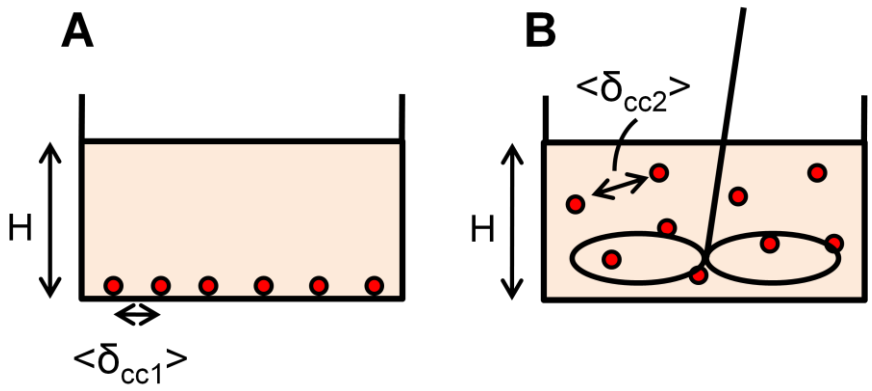

Figure 6. Schematic representation of the characteristic lengths in a static (A) and in a stirred (B) culture systems.

The concentration at cell surface is dependent on the ratio between these two characteristic times, and can have values in the range between null and bulk concentration. Thus, as cells feel only the concentration of signaling molecules at their surface, assuming they are subjected to the same conditions of the bulk volume is not always a good approximation.

It is important to notice from (2.1) that in some conditions soluble factors with the same diffusion coefficient can be either diffusion- or uptake-limited, depending if they are exogenous or endogenous. Besides, endogenous factors with different diffusion coefficients can be either diffusion- or uptake-limited, even in the same culture conditions. The same is true for exogenous factors with different diffusion coefficients. Thus, some soluble factors can be homogeneously distributed, while

others can be diffusion-limited at the same culture conditions, and these equilibria are further complicated by cell density changing with time.

2.3.3.2 Dynamic culture characteristic times

When cells are cultured in a stirred bioreactor the same considerations on the importance of characteristic times ratio hold, but the situation is further complicated by convection coming into play.

The case when medium is mixed and cells homogeneously suspended in the whole volume is now analyzed.

- Diffusion characteristic time is still given by (2.1), but the characteristic length is now the average cell-cell distance for cells distributed in the whole working volume δ_{cc2} (Fig. 6 B), both for endogenous and exogenous factors. Thus, under stirred suspension culture conditions, it is removed the difference in diffusive mass transport of endogenous and exogenous factors, as they have the same characteristic length.

- Under the assumption of a ratio between well height and diameter closed to unity, medium convection has a characteristic time, τ_3, given by (Nienow, 1997):

$$\tau_3 = \frac{3.9}{N_s} \ , \tag{2.3}$$

  where N_s is the impeller stirring rate.

- The characteristic time of cell convection, τ_4, is given by:

$$\tau_4 = \frac{\lambda}{v_{0,cell}} \tag{2.4}$$

where $v_{0,cell}$ is cell terminal falling velocity with respect to the medium, given by Stokes' law, and analyzed in Chapter 3. The characteristic length, λ, is given by the average cell-cell distance, δ_{cc2} (Fig. 6 B), and is then cell density dependent.

- Eq. (2.2) still holds for the characteristic time of uptake.

Some general considerations can be drawn. Uptake and mass transport are processes that act in series, thus the slower is the limiting one. Whereas diffusion and convection processes are parallel phenomena, and the faster is the dominant one.

An intermediate condition between static and stirred suspension culture is given by a situation when medium is mixed, but cells lie at the well bottom without being suspended. Similar considerations on characteristic times hold in this case, where different characteristic lengths should be considered.

The lack of quantitative knowledge on stem cell kinetics of uptake/release and the huge number of different molecules acting, limit the feasibility of a thorough definition of the local microenvironment surrounding the cells. However an insight of the key processes that should be considered is still important at this stage.

An overview of the characteristic times and lengths just described is reported in Fig. 7 to give a taste of the complexity of the system under study. There are three different characteristic lengths involved: cellular, niche, and culture system lengths. However characteristic times of different processes are not distinct, and can be overlapped for competitive processes, depending on culture conditions (e.g. static vs. dynamic culture, high vs. low cell density), molecule of interest (different diffusive coefficient, and uptake kinetics), and type of cells considered (different

cell dimension, and tendency to form clusters). Parameters used to generate this figure are given in figure caption and are useful to give an idea of the order of magnitude of different processes.

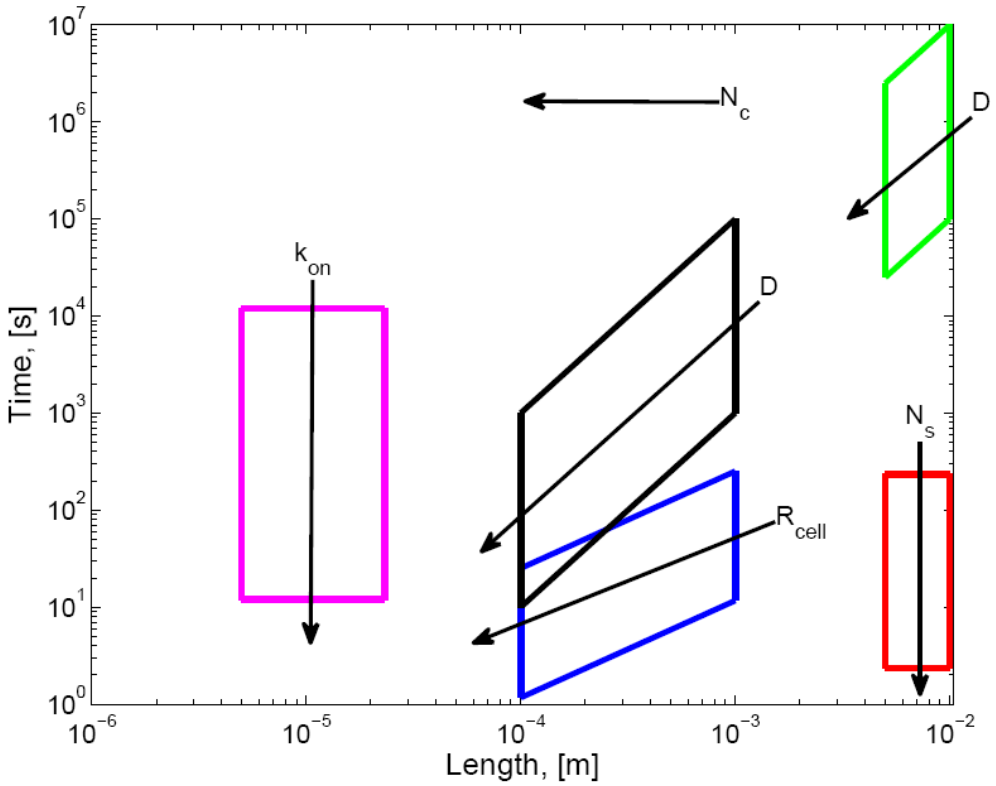

Figure 7. Range of characteristic times and lengths for different biological and physical phenomena in cell interaction with soluble factors. — Characteristic time of cell uptake of soluble factors according to (2.2) for a ligand concentration of 50 ng/ml with a molecular weight of 10 kDa. — Characteristic time of diffusion under static conditions according to (2.1). — Characteristic time of diffusion in stirred culture according to (2.1). — Characteristic time of cell relative motion with respect to the medium according to (2.4). — Characteristic time of mixing according to (2.3). The three length scales are, from left to right: cell/cluster radius ($5 \div 2.5 \cdot 10^{-5}$ um), niche length (calculated as $N_c^{-1/3}$), system length (0.5÷1 cm). k_{on} ($10^{6} \div 10^{9}$ M^{-1} min^{-1}, from Lauffenburger *et al*, 1993): kinetic constant of the receptor-ligand forward reaction, Nc ($10^{3} \div 10^{6}$ cell/ml): cell density, D ($10^{-9} \div 10^{-11}$ m^2/s, from Lauffenburger *et al*, 1993): diffusion coefficient, R_{cell} ($5 \div 2.5 \cdot 10^{-5}$ µm, the second value represents the approximate radius of a cluster formed by 100 cells): cell/cluster of cells radius, Ns (1÷100 rpm): stirring rate.

2.4 Intrinsic cell population heterogeneity

As highlighted from experimental data drawn from stem cell characterization at population level, heterogeneity is always present in a stem cell sample at different levels, such as marker expression, asynchrony, and morphology. In Section 2.3 some considerations on mass transport and uptake/release kinetics were reported to show how different cell behavior can be generated because of a different local microenvironment. Thus, cell population heterogeneity is partly generated as a consequence of spatial concentration gradients of important signaling molecules and local inhomogeneities of cell density in culture. This environmental heterogeneity, dependent on culture conditions, will be next referred to as extrinsic heterogeneity. However, another important source of heterogeneity, which is intrinsic in the cell population, is cell division. A theoretical study is reported in Chapter 5 on this topic.

2.5 Concluding remarks

In this chapter, some topics on cell population heterogeneity were discussed. First how it is experimentally detectable, then the different mechanisms that affect cell quality products not only terms of average properties, but also in terms of heterogeneity in the cell population. Because of the complexity of biological and physical phenomena that come into play, it is difficult to design a cell culture system that completely avoids heterogeneity. One of the main reason for that is that our ability to keep the system homogeneous is limited by the need to keep low the shear stress, that poses an upper bound to the feasible stirring rates. Besides, even under perfectly homogeneous external conditions, heterogeneity intrinsically arises in the population because of cell division process. On the overall, the important

conclusion from this analysis is that we cannot completely eliminate heterogeneity, but to design safe manufacturing processes we need to be aware of the sources that generate it and of the variability in the system.

2.6 References

Alberts B, Johnson A, Lewis J, Raff M, Roberts K, Walter P. 2002. Molecular Biology of the Cell, 4th ed. New York:Garland.

Blanch HW, Clark DS. 1997. Biochemical engineering. New York: Marcel Dekker Inc. 702 p.

Cabrita GJM, Ferreira BS, da Silva CL, Gonçalves R, Almeida-Porada G, Cabral JMS. 2003. Hematopoietic stem cells: from the bone to the bioreactor. Trends Biotechnol 21:233-240.

Collins PC, Nielsen LK, Patel SD, Papoutsakis ET, Miller WM. 1998. Characterization of hematopoietic cell expansion, oxygen uptake, and glycolysis in a controlled, stirred-tank bioreactor system. Biotechnol Prog 14(3): 466-472.

Flaibani M, Luni C, Sbalchiero E, Elvassore N. Flow cytometric cell cycle analysis of muscle precursor cells cultured within 3D scaffolds in a perfusion bioreactor. Biotech Prog DOI: 10.1002/btpr.40. In press.

King JA, Miller WM. 2007. Bioreactor development for stem cell expansion and controlled differentiation. Curr Opin Chem Biol 11:394-398.

Kirouac DC, Zandstra PW. 2008. The systematic production of cells for cell therapies. Cell Stem Cell 3:369-381.

Lauffenburger DA, Linderman JJ. 1993. Receptors. Model for binding, trafficking and signaling. New York:Oxford University Press.

Morrison SJ, Spradling AC. 2008. Stem cells and niches: mechanisms that promote stem cell maintenance throughout life. Cell 132:598–611.

Nielsen LK. 1999. Bioreactors for hematopoietic cell culture. Annu Rev Biomed Eng 01:129-152.

Nienow AW. 1997. On impeller circulation and mixing effectiveness in the turbulent flow regime. Chem Eng Sci 52(15):2557-2565.

Ormerod M. 2000. Flow cytometry. A practical approach. Oxford University Press.

Sardonini CA, Wu YJ. 1993. Expansion and differentiation of human hematopoietic cells from static cultures through small-scale bioreactors. Biotechnol Prog 9 (2):131-137.

Scadden DT. 2006. The stem-cell niche as an entity of action. Nature 441(29):1075-1079.

Verfaillie CM. 1992. Direct contact between human primitive hematopoietic progenitors and bone marrow stroma is not required for long-term *in vitro* hematopoiesis. Blood 79(11):2821-2826.

Zandstra PW, Eaves CJ, Piret, JM. 1994. Expansion of hematopoietic progenitor cell populations in stirred suspension bioreactors of normal human bone marrow cells. Bio/Technology 12:909-914.

Chapter 3

Microliter-bioreactor array stirred by thermoconvection

In this chapter the design and development of an array of up to 96 microliter-bioreactors to perform parallel experiments of cell culture in suspension is presented. A validation of a prototype is performed using human umbilical cord blood hematopoietic cells. The device is useful for exploring a wide range of experimental conditions at the stage of process optimization (Fig. 1, Chapter 1).

3.1 Introduction

The number of cells in a donor-derived cell sample is usually too small for therapeutic applications. If, in an efficient large-scale production, bioreactors play a fundamental role, process optimization needs a high-throughput small-scale technology, but suitable to transfer information on a larger scale. Further progress should be made in process optimization, reproducing *in vitro* stem cell niche signals, principally playing on time-dependent dosing of soluble factors (Verfaillie, 1992). The optimization of protocols for stem cell culture needs to span a wide

range of experimental conditions, in terms of type, timing and dose of growth factors. Even supported by experimental design strategies, such a wide experimental campaign has prohibitive costs in bioreactors that have volumes of hundred of milliliters.

The present work presents a system for medium stirring when cells are cultured in a 96-well plate. This number of wells can fit to the requirement of wide screening in process optimization, and this well volume is sufficient to have an enough number of cells for biological characterization of the culture outcome. Mechanical stirring at this scale would result rather complex. Thus, in the system developed in this work, mixing is provided by a mechanism of thermoconvection (Fig. 1). A micrometric heater is put in correspondence of each well bottom to generate a very localized temperature increase. As a consequence of the temperature gradient, a convective flow arises into the well, homogenizing the culture medium.

In the past Dexter *et al*. (1977) were able to maintain hematopoiesis *in vitro* for a long period of time culturing cells at 33°C, thus up to 4°C of temperature difference at the well bottom are acceptable, but even less is sufficient for mixing and keeping cells suspended. Shear stress is not a concern even at 4°C temperature difference (Hua *et al*, 1993).

As the temperature gradient at the well bottom and the temperature profile in the well are not directly measured, a mathematical model is used to correlate temperature and velocity profiles in the well to the experimental operative variables. The model is validated by experiments of micro-particle image velocimetry, before being used to define proper operative conditions for experiments of cell culture.

Parameters important for a successful stem cell culture are temperature and pH, besides biocompatibility of the materials used. It is possible to dispense with

complex control of temperature and pH, as the device is put inside the biological incubator, what makes the system proposed easily usable also by people not familiar with engineering equipment. The cell culture is in contact only with the polystyrene multiwell, which is a well-know biocompatible material (LaIuppa *et al*, 1997).

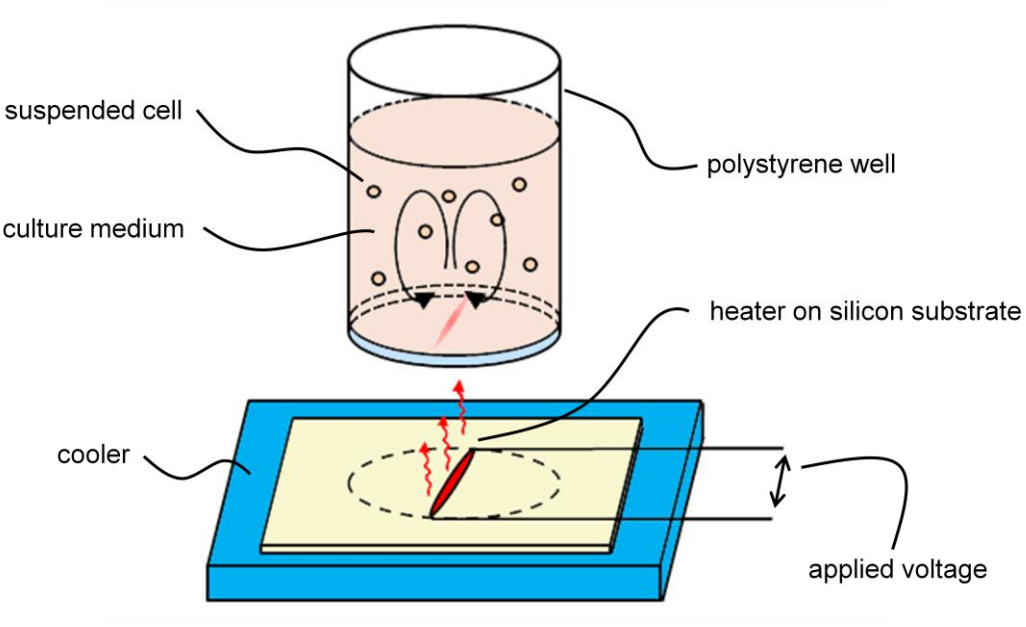

Figure 1. Schematic of one micro-liter bioreactor stirred by thermoconvection. Suspension cell culture is performed in a polystyrene well. A temperature gradient at the well bottom generates a stirring inside the well by natural convection. The gradient is produced by placing the well on a silicon substrate where a micro-fabricated heater provides a very localized heat flux. Under the silicon wafer a cooler is used to maintain the heat localization. All the system is incubated at the same temperature as the cooler.

The bioreactor array developed is tested with preliminary cultures of human cord blood-derived $CD34^+$ cells. Five different low-mixing conditions are investigated

in six repeated one-week experiments. Results of cell count, viability and CD34 expression are presented.

While the system developed is suitable for culturing HSCs, as they grow as single-cells, its application can be extended to cells that form agglomerates, as long as medium mixing is required without cell suspension.

3.2 Materials and methods

3.2.1 Bioreactor device

3.2.1.1 Complete bioreactor system

Fig. 2 illustrates the main components of the microliter-bioreactor array. Cells are cultured in a 96-well plate (CLS3614; Sigma-Aldrich, Milan, Italy) with lid (CLS3099; Sigma-Aldrich, Milan, Italy). This multiwell is made of polystyrene, and has a flat bottom of 0.127-mm thickness.

A silicon wafer, see details below, is put in contact with the bottom of the multiwell. A miniaturized electrical circuit, including an electrical resistor at the bottom of each well, is printed on its surface. Electrical wires (1 mm diameter) are attached to the electrical connections of the circuit on the wafer. For this purpose, first a conductive epoxy (Chemtronix, Georgia) is applied over night, and then, to guarantee a stronger mechanical fixing, a 2 Ton Clear Epoxy (Devcon, Danvers, MA) is applied for 2 hours. The wires are then connected to a DC power supply (6220B, Hewlett-Packard) which provides a stable voltage.

A thermoelectric cooler (CP-031; TE Technology, MI) is used to regulate the temperature below the wafer. An aluminum block (90x60x8 mm) is put between the wafer and the cooler to guarantee a better temperature homogeneity. A

temperature probe (PT100 ,10mm, class A; RS Components, Milan) monitors the temperature on the upper surface of the aluminum block. It is connected to a PID controller (998D-22CC-JARR; Watlow, MN) that regulates the temperature by turning on and off the cooler regulating its connection to a DC power supply (Digimaster, PS3003DA).

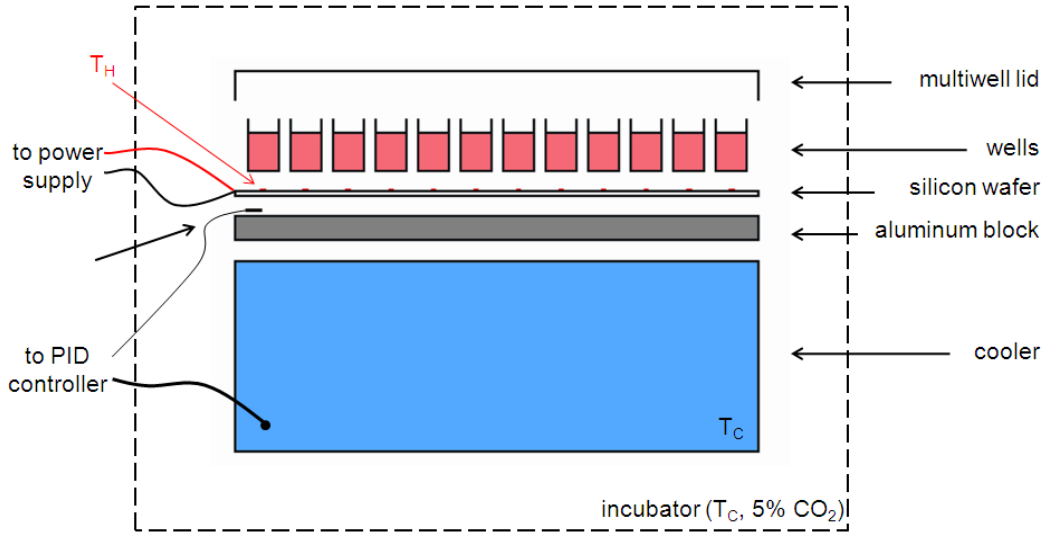

Figure 2. Schematic of the micro-liter bioreactor array. A conventional 96-well plate is placed on a silicon wafer, where a micro-fabricated electrical circuit provides a heater at the bottom of each well. A thermoelectric cooler is used to maintain localized the hot spot at the bottom of each well, regulating the temperature around the spot at T_C. An aluminum block is put between the silicon wafer and the cooler to enhance temperature homogeneity. A PT100 temperature probe is put on the aluminum block top surface, and is connected to a PID controller that regulates the activation of the cooler. All the system is placed inside an incubator whose temperature is fixed at T_C.

The 96-well plate with lid, the silicon wafer, the aluminum block, the temperature sensor, and the cooler are the only components that are put inside the biological incubator. The electrical wires provide the connections with components outside.

3.2.1.2 Miniaturized electrical circuit fabrication

A miniaturized electrical circuit is micro-fabricated (University of California at Santa Barbara Nanofabrication facility) on a silicon substrate. A 2-µm layer of insulating silicon dioxide (SiO_2) is thermally grown using an oxidation furnace.

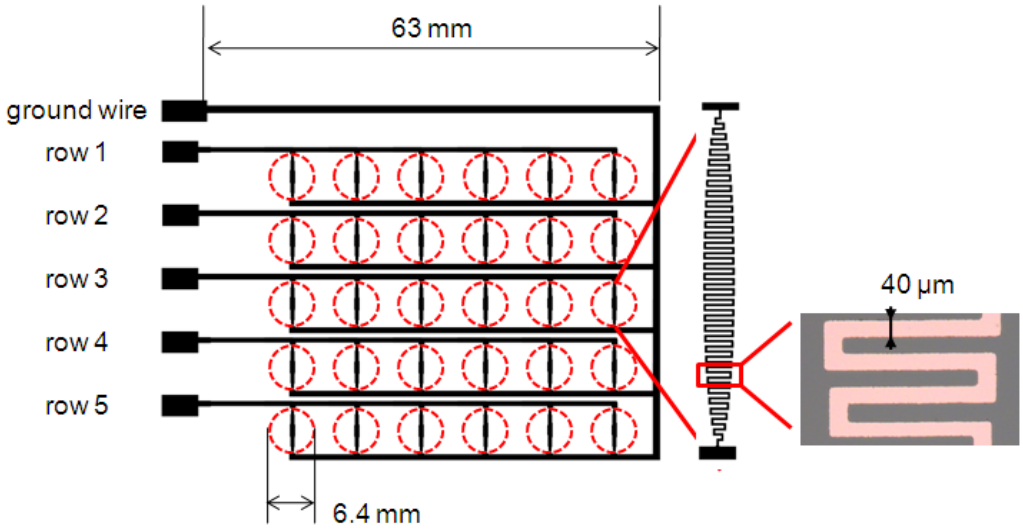

Figure 3. Top view schematic of the micro-fabricated electrical circuit. A possible configuration of the electrical circuit is shown. It is composed by 5 rows of 6 parallel heaters, that are placed in correspondence to the position of the wells (dashed red line) from the 96-well plate. Each heater is a resistor, shaped as a serpentine (enlargement) to maximize its resistance and thus the heat produced. A different voltage can be applied to each row to perform cell cultures at 5 different stirring conditions.

Photolithography techniques are employed to transfer the micro-circuit design from a transparency mask to the SiO_2 layer. The micro-circuit is made of thin films: 200Å of titanium and 1800Å of platinum, deposited via electron-beam evaporation. Titanium is used as an adhesive layer, and platinum provides the robustness and linear resistance-temperature relationship needed for the micro-heater electrode components characterization.

Different configurations of the electrical circuit are feasible. Fig. 3 shows the micro-circuit used for the biological experiments in this paper. It includes five parallel rows, which have six resistors each, connected in parallel. A different voltage can be applied to each row to produce five different stirring conditions.

3.2.1.3 Heater characterization

The micro-fabricated resistors, in the electrical circuit above, function as resistive heaters. They are put in direct contact with the base of each well. A constant voltage, *V*, is applied to the ends of each resistor that dissipates a heat flow rate, *P*, given, according to Ohm's law, by:

$$P = \frac{V^2}{R} \tag{3.1}$$

where *R* is the resistance of each resistor.

In order to minimize the necessary external power, the resistors are designed to maximize their resistance. The resistance of an individual heater is given by:

$$R = \frac{\rho \cdot L}{w \cdot t} \tag{3.2}$$

where ρ is platinum resistivity (105 nΩ·m at 20°C), *L* is the length of the resistor, *w* the width, and *t* the thickness. To increase heater resistance, its length is maximized with a serpentine structure (*L*=28.11 mm), and the width minimized enough to create the winds in the serpentine within the resolution limits of a transparency mask (w=40±5 μm). The heater thickness is t=1800 Å. The theoretical resistance of the heater, calculated by (3.2), is R=410±10 Ω at 20°C, in accordance to that experimentally measured. As shown in Fig. 3, the serpentine heater is designed rod-shaped, such that the ratio between the lens width and the parallel chord of the circular well is kept at the constant value of 0.1.

The temperature-dependence of platinum resistivity is linear for the narrow operating temperature ranges used. The change in the resistance of each heater with temperature is calculated by:

$$\Delta R = R_0 \cdot a \cdot (T - T_0) \tag{3.3}$$

where R_0 is the resistance at the reference temperature, T_0; $\Delta R=R-R_0$, R is the resistance at temperature T; a is the temperature coefficient of resistance, which is determined experimentally to be 0.0033 $^oC^{-1}$.

3.2.1.4 Numerical model

A numerical model is developed to investigate thermoconvective flow in the well. The physical system simulated includes three subdomains: the silicon wafer, with a heater on its surface whose thickness is neglected, the polystyrene well bottom, and the liquid inside the well. Because of the symmetrical geometry of the system, only one quarter of an individual well is simulated.

An energy balance at steady-state is applied to each subdomain:

$$k\ \nabla^2 T = <\rho>\ c_P\ u \cdot \nabla T \tag{3.4}$$

where T is the temperature, u is the velocity (different from zero only for the liquid in the well); k is the thermal conductivity, $<\rho>$ the density at the average temperature in the well, and c_P the heat capacity at constant pressure of silicon, polystyrene and medium, whose properties are approximated with those of water.

In the subdomain that includes the liquid in the well, the energy balance is coupled, at steady-state, with the continuity equation for an incompressible fluid:

$$\nabla \cdot u = 0\ , \tag{3.5}$$

and the Navier-Stokes equation:

$$0 = -\nabla p + \mu\ \nabla^2 u + \rho(T)\ g\ , \tag{3.6}$$

where p is the pressure, μ medium dynamic viscosity, approximated with that of water, g is the gravitational acceleration. In the gravity term medium density, ρ, is considered dependent on temperature, according to Boussinesq approximation.

The boundary conditions for the model are insulation and symmetry in all the external boundaries, except the bottom surface of the silicon wafer, where temperature is fixed at the cooler temperature, T_C. Continuity is assumed in all internal boundaries. The temperature of the resistive heater is fixed at T_H.

The model is solved using the software COMSOL Multiphysics V3.4 (COMSOL, Inc. Stockholm, Sweden). The parameter values used are summarized in Tab. I.

Table I. Parameter values. * from Ito *et al*. (2001). ** from volume in Hunt *et al*. (2003) under the assumption of cell spherical shape. § from COMSOL material library. Medium properties are approximated with water properties.

	Medium	Polystyrene	Silicon
Thermal conductivity, [W/(m K)]	0.598§	0.13§	1.05§
Heat capacity, [J/(kg K)]	4186§	1200§	840§
Density, [kg/m3]	998§	1050§	2600§
Dynamic viscosity, [Pa s]	10^{-3} §		
Volume expansivity, [1/K]	$2.07 \cdot 10^{-4}$ §		
Cell density, [kg/m3]	1065*		
Cell radius, [m]	$4.03 \cdot 10^{-6}$ **		

3.2.1.5 Micro-particle image velocimetry (μPIV)

The fluid velocity in a convectively-stirred well is experimentally measured by micro-particle image velocimetry (μPIV) technique, as described in detail in Meinhart *et al*. (1999) and Santiago et at. (1998). Briefly, a well from a 96-well plate (Sigma-Aldrich) is filled with deionized water for a working volume of 76 μl,

and seeded with 1-μm diameter fluorescent polystyrene beads (Duke Scientific, Fremont, CA).

A Solo-PIV Nd:YAG Laser (New Wave Research Inc, Fremont, CA) is used to illuminate at 532 nm the flow-tracing particles, which are imaged with an epifluorescent microscope (Nikon E600FN) through a 10x lens (NA=0.25). The particle images are recorded with a cooled CCD camera with a time delay of 1 s between exposures. The captured images pairs are analyzed to determine the in-plane velocity field, $u(x, y)$. All measurements are taken at a room temperature of 22°C.

3.2.2 Cell culture

3.2.2.1 Cell isolation and culture conditions

Cord blood (CB) units are obtained from Bone Marrow Stem Cell Transplant Laboratory (Pediatric Oncohaematology Department, Padua, Italy), after informed consent. Cord blood is eluted with 20 ml PBS 1X (Gibco, Invitrogen, Milan, Italy) and mononuclear cells are isolated by density-gradient centrifugation (2000 rpm, 30 min), layering on equal volume of Ficoll (GE Healthcare). Mononuclear cells are counted by hematocytometer, and analyzed by flow cytometry as a negative control.

$CD34^+$ cells are isolated by superparamagnetic microbeads (CD34 antibody, QBEND-10, Abcam, Cambridge, UK) selection using high-gradient magnetic field and mini-MACS columns (Miltenyi Biotech, Glodbach, Germany). A fraction of $CD34^+$-cells of more than 70% is obtained, as verified by flow cytometry (FACS Calibur, Becton Dickinson) after counterstaining with CD34-phycoerythrin antibody (AC136 clone, Miltenyi Biotec).

The selected cells are suspended in Iscove's Modified Dulbecco's Medium (Gibco), 10% scomplemented (56°C, 30 min), with 10% FBS (Gibco), 1% Penicillin/Streptomycin (Gibco), and supplemented with the following human citokynes (PeproTech Inc, Rocky Hill, NJ): hSCF (50 ng/ml), hTPO (10 ng/ml), hIL-6 (10 ng/ml), hFL (50 ng/ml), according to the protocol in Gunetti *et al* (2008). $CD34^+$ cells are seeded into 30 wells of a 96-well plate of the micro-liter bioreactor array, in correspondence to the heaters in the silicon wafer below, and in 6 separated wells as a static culture control. Cell seeding density is 10^4 cell/ml. The voltages applied to the resistors in each row are summarized in Table II.

3.2.2.2 Cell viability, cell count and flow cytometry analyses

At day 4 and 7 cell count is performed by hematocytometer. The medium removed at day 4 is substituted with fresh medium to restore the original volume.

At day 7 cells are suspended with 40 μl PBS 1X and incubated at 4°C for 15 min with 8 μl anti-CD34-PE antibody (GIBCO, Invitrogen), and 5 μl of 7-amino-actinomicyn D (7-AAD). Labelled cells are then suspended in 1 ml PBS 1X, centrifuged (1200 rpm, 5 min), and suspended in 200 μl PBS 1X for flow cytometer acquisition.

3.3 Results and discussion

3.3.1 Numerical simulations and μPIV data

Numerical simulations are performed to assist in bioreactor design, and to define feasible experimental conditions for HSC culture in the device. Experiments of

μPIV are carried out to validate numerical simulation results for the fluid velocity in the well.

The bioreactor has a working volume for cell culture of 250 μl (8-mm height), but for μPIV experiments the working volume is reduced to 76 μl (2.4-mm height), because the larger working volume created significant background glow and impaired discrete particle visibility on the measurement plane. The numerical model is modified accordingly.

Comparing the μPIV measurements to the reduced-height model yields insight to the accuracy and predictability of the model to the experimental thermoconvective stirring conditions used in biological experiments.

The temperature and velocity fields are calculated by the numerical model for a temperature difference, ΔT, between the heater and the cooler of 0.5°C. The results are shown in Fig. 4 A and B, respectively.

A first set of μPIV data investigated the velocity field as a function of fluid height, z. Measurements are taken in the region of expected fastest in-plane velocity to improve data accuracy, and averaged in the (x,y)-plane. The region of interest is shaded in Fig. 4 B.

The relationship between ΔT, used as an input in the numerical model, and the voltage applied to the ends of the resistive heater, V, used for μPIV measurements, is shown in Fig. 4 C. A ΔT of 0.5°C corresponds to a V of 10 V. The comparison of the numerically-simulated in-plane velocity with that experimentally measured is shown in Fig. 4 D, as a function of the distance from the well bottom. The excellent match between the two results confirms the reliability of the numerical model in simulating the experimental conditions.

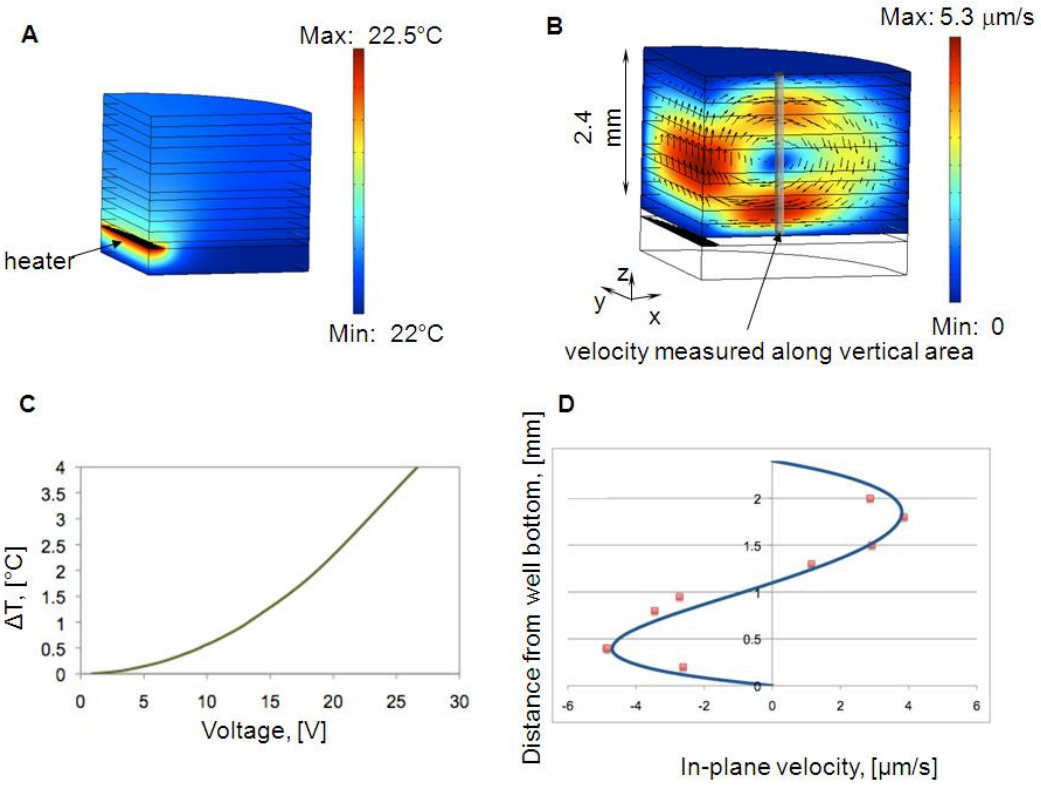

Figure 4. Comparison between the numerical simulation results and the experimental μPIV data. Numerical simulation results of the temperature (A) and the velocity field (B) in a quarter of a well filled with 76 μl of deionized water, for $T_C = 22°C$ and for a $\Delta T = T_H - T_C$ (see Fig. 1) of 0.5°C at the bottom of the well. In (B) the region of interest for the μPIV measurements is indicated. Numerical simulation results and experimental μPIV data are compared considering the relationship between *V* and *ΔT* shown in (C). Comparison of μPIV measurements (bullet points), for a voltage, *V*, of 10 V applied to the ends of the heater, with simulation results (line) in terms of in-plane velocity vs. vertical coordinate (D).

A second set of μPIV experiments evaluates the in-plane fluid velocity dependence on the voltage applied to the ends of the resistive heater.

Velocity measurements are taken at a distance from the well bottom, z, of 400μm, in the region of interest shown in Fig. 4 B, with increasing voltages applied to the heater. Fig. 5 shows the μPIV experimental data as well as the numerical model

results. The in-plane velocity from the two cases matches well, and the model is reliable also in simulating different voltages applied.

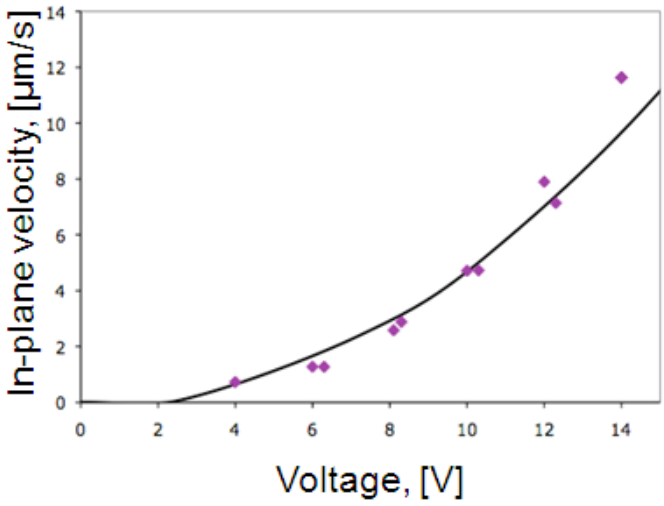

Figure 5. Comparison between the numerical simulation results and the experimental µPIV data. Maximum velocity in the well from µPIV experiments and from numerical simulations as a function of voltage, *V*, applied to the ends of the heater, for a well filled with 76 µl of deionized water. Simulation results are expressed in terms of *V*, considering the relationship between *V* and ΔT shown in Fig. 4C. µPIV data are related to the region of interest shown in Fig. 4B at z=400µm from the well bottom.

3.3.2 Theoretical considerations

In this section the effect of the maximum temperature difference at the bottom of the well, ΔT, and the well height, h, on different mixing conditions and mass transport regimes are analyzed.

Fig. 6 shows how an increase in ΔT produces an increase in the convective flow, represented by the maximum upward velocity, $v_{max,fluid}$, of the medium, normalized by the average cell terminal falling velocity, $v_{0,cell}$. Depending on medium height inside the well, proportional to medium volume for the same base

area, a given ΔT produces a different $v_{max,fluid}$. As shown in Fig. 6, this difference is not very significant in the range of volumes of a 96-well plate (a medium volume range of 76-250 µl is shown), thus a possible imprecision in the filling volume has negligible effect on the convective flow generated.

The cells in culture moves as a whole with the medium, but at the same time they settle with a terminal falling velocity given by Stokes' equation:

$$v_{0,cell} = \frac{2(\rho_{cell} - \rho)R_{cell}^2 g}{9\mu} \tag{3.7}$$

where ρ and μ are medium density and viscosity respectively; g is the acceleration of gravity; ρ_{cell} is cell density, and R_{cell} is cell radius.

The condition for cell suspension in the medium is represented by $v_{max,fluid} / v_{0,cell} > 1$. Because of the distribution of cell density and radius (Hunt *et al*, 2003) in a cell population, the transition between cell suspension and not-suspension culture conditions is not sharp. In Fig. 6 a region is highlighted where for increasing values of $v_{0,cell}$, cells of increasing dimension start being suspended.

In the zone where there is no cell suspension, the transport of molecules of gases, growth factors, and metabolites can be either diffusion-driven or convection-driven, depending on the magnitude of medium convective flow. A first insight of the dominant mass transport mechanism is achievable by analyzing Péclet dimensionless group, Pe, which is the ratio of convection rate to diffusion rate, given by $Pe = L \cdot v / D$. Where v is a characteristic velocity of the fluid, $v_{max,fluid}$ is used in this analysis; L is a characteristic length of the system; and D is the diffusivity of the molecule of interest in the medium. When $Pe < 1$ diffusion prevails, conversely when $Pe > 1$ convective transport is dominant.

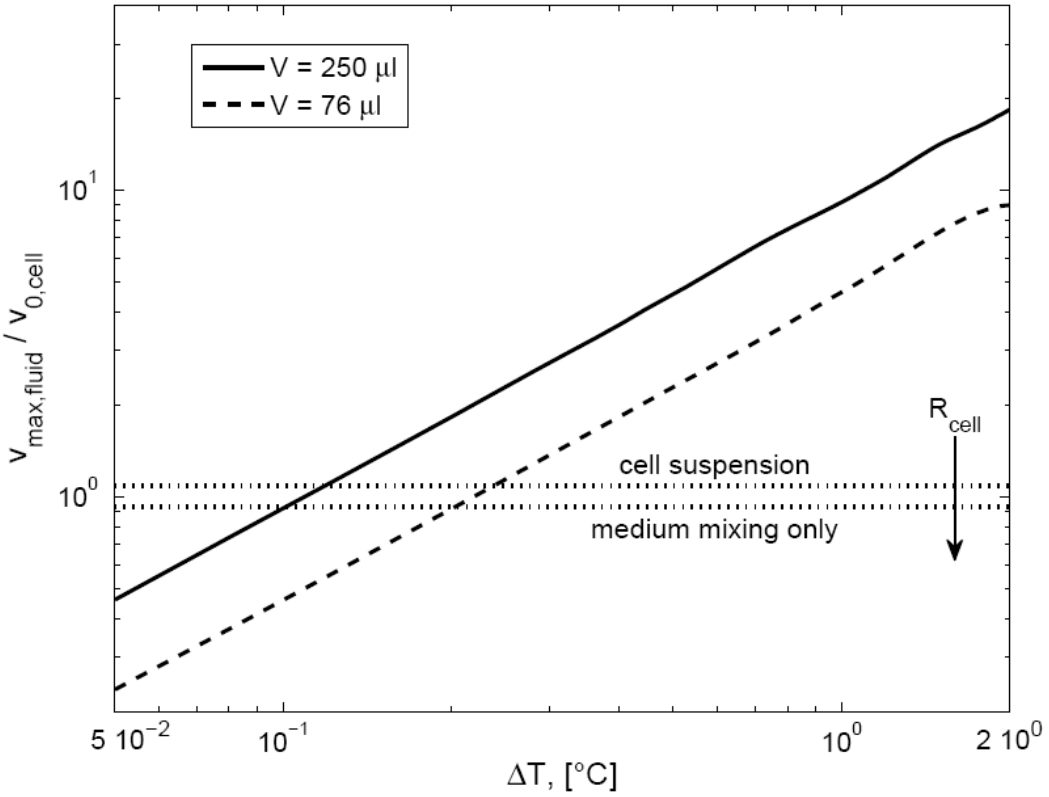

Figure 6. Simulation results. Numerical simulation results for the dependence of the ratio $v_{max,\,fluid} / v_{0,cell}$ from ΔT at the bottom of the well. $v_{0,cell} = 2.58 \mu m / s$, calculated by (3.7). Two curves are plotted for a filling volume of 76 µl (used in µPIV measurements) and 250 µl (used in biological experiments), in dashed and solid lines respectively. The horizontal dotted lines include the region of transition between the condition of cell suspension and that of medium mixing only without cell suspension, dependent on cell radius, R_{cell}.

Pe depends on $v_{max,\,fluid}$, the characteristic length of the system, L, and the molecule diffusion coefficient in the medium, D. $v_{max,\,fluid}$ is fixed for a certain ΔT. D depends on the molecule of observation; thus, at the same ΔT condition, the transport of different growth factors can be regulated by different mechanisms. L is defined differently depending on which molecule is under consideration, either exogenous or endogenous. L equals the medium height in the well in the

first case, and the average cell-cell distance, which is cell concentration-, and thus time-, dependent, in the last case. We can conclude that generally endogenous factors require a higher mixing velocity to be homogenized.

It is important to notice that for cells, different from HSCs, that form agglomerates, the ΔT required for cell suspension could be not feasible, because of a higher cell terminal falling velocity, but a mixing effect can still be achieved producing different Pe numbers.

3.3.3 Experiments of HSC culture

3.3.3.1 Temperature effect on HSCs

In Dexter *et al*. (1977) pioneering work, they were able to maintain hematopoiesis *in vitro* for several months. HSC cultures were performed on a feeder layer composed by stromal cells that provided molecular signaling important for hematopoiesis. They reported better results performing cell culture at 33°C. This temperature does not seem harmful for HSCs, and positively affects HSC interaction with the stromal layer. HSC cultures are currently performed at 37°C (see, for example, Gunetti *et al*, 2008), because the feeder layer has been substituted by medium enriched in protein content.

Thus, a temperature difference of half degree, with respect to 37°C, sufficient for cell suspension (Fig. 6), can be considered having negligible effects on HSC culture.

3.3.3.2 Biological experiments

The culture of human cord blood-derived $CD34^+$ cells in the microliter-bioreactor array is examined at five different stirring conditions of medium, and compared to

cell culture in regular 96-well plate under static conditions. Six parallel bioreactor devices are used for repeated experiments. Cells are seeded at an initial cell concentration of 10^4 cell/ml, and allowed to expand for 7 days. Stirring is produced by the voltage, V, applied to the heaters shown in Tab. II, where ΔT from model simulations is also reported.

In these biological experiments cells are not suspended because of the low voltage applied (Fig. 6). They are used to preliminarily investigate the practical feasibility of cell culture in these conditions. It is necessary to verify the device stability in the biological incubator, which is a closed environment with high levels of humidity. It is checked that the natural heat dissipation of the incubator is sufficient to remove the heat generated by the thermoelectric cooler as long as it is used without ventilation. Furthermore, because of the small culture volume (250 μl) it is necessary to test the entity of medium evaporation during cell culture in mixed conditions. This is an important parameter because cell culture becomes more concentrated if volume decreases, it is detected an acceptable level of evaporation of about 10 μl/well in 7 days.

Cell viability results show a comparable percentage of dead cells after 7 days in culture at different stirring conditions (Tab. II). This confirms that a temperature of 37°C is not exceeded during the experiments, in accordance with numerical simulation results. No statistically significant effect on cell proliferation rate is observed for any of the agitation rates tested as compared to the static control both at day 4 and 7 (Tab. II).

The expression level of marker CD34, a common marker used to select HSCs from UCB, is analyzed by flow cytometry after a week in culture. In all the different stirring conditions the cell population results substantially CD34-positive (Tab. II). A Kolmogorov-Smirnov test is applied for quantification, by D-statistic, of the difference in CD34 expression between cells cultured under static conditions, and in the stirred bioreactors. Results shows that there is a linear increase in D-statistic values at increased voltages applied to the heaters (Tab. II). Thus there is a slight increase in CD34 expression with respect to static culture at increasing stirring rates, but further experiments at higher stirring conditions are needed to confirm this result.

Table II. Biological results. *V*, voltage applied to the ends of the heater. $\Delta T=T_H-T_C$, as shown in Fig. 1. $v_{max,fluid}$, maximum upward fluid velocity. Fold-expansion, cell density after 4 and 7 days in culture divided by initial cell density. Viability, results after 7 days in culture, drawn by flow cytometry analyses after 7-AAD staining. CD34 expression, results after 7 days in culture, drawn by flow cytometry analyses after CD34 staining. D-statistic results are derived by a Kolmogorov-Smirnov analysis of the data of each row, compared to data from control sample. Data for each row are based on 6 repeated experiments. *p < 0.001.

				fold-expansion		viability		CD34 expression	
	V, [V]	ΔT, [°C]	v_{max}, [μm/s]	4 day	7 day	% dead	D-statistic	% CD34+	D-statistic
Control	0.00	0.00	0.00	1.9±0.7	16.2±6.0	3.2		97.4	
Row 1	1.01	0.006	0.14	1.8±0.7	17.1±2.6	2.9	0.03	99.5	0.15*
Row 2	1.10	0.007	0.17	1.8±0.9	14.2±2.4	2.7	0.15*	99.5	0.16*
Row 3	1.18	0.008	0.19	2.1±0.7	14.1±2.5	2.5	0.10*	99.8	0.17*
Row 4	1.35	0.010	0.24	1.7±0.6	14.9±2.2	2.3	0.06*	99.8	0.21*
Row 5	1.60	0.015	0.34	1.6±0.7	15.2±3.6	2.6	0.02	99.8	0.22*

3.4 Conclusions

In this work a bioreactor array was developed to culture HSCs under stirred conditions at a microliter scale. Thermoconvective stirring is applied to a commonly-used multiwell plate. The system can be implemented to perform up to 96 parallel experiments.

Small-scale devices are required for a wide screening of different experimental conditions to optimize cell culture protocols. Because of the variability between different umbilical cord units and of the scarce number of cells a unit contains, it is important to have a system to perform HSC cultures under many different conditions using cells from the same umbilical cord unit. The advantage of having a stirred system, to perform this screening at a micro-liter scale, is helpful in the scale-up process, when bioreactors are used at a production scale.

Numerical simulations were used to analyze the temperature and velocity field inside the stirred well. The results were validated by experiments of particle tracking that confirmed the accuracy of the model in predicting the velocity in the well. They were performed both in different regions of the well, and for different voltages applied to the resistive heater under the well.

Numerical simulations were used to define the operative conditions for biological experiments. In particular the feasibility of having cells suspended without overheating the culture medium was analyzed, considering stem cell sensitivity to temperatures above 37°C.

Cell cultures were performed using HSCs from human umbilical cord blood in the device developed in this work. Operative conditions used gave a bland mixing without cell suspension. These preliminary experiments were useful for defining the feasibility of the culture process in this bioreactor array. Conditions that were tested are the possibility to remove the heat generated by the thermoelectric cooler

by exploiting the natural dissipations of the incubator, and the importance played by medium evaporation in such a small volume under stirring conditions.

The biological results show a comparable behavior between cells cultured under static conditions and in presence of a bland mixing. Furthermore the volume of the individual well results sufficient to perform flow cytometry analyses, important for characterizing the cellular outcome at the end of the culture in the bioreactor array.

In perspective, the system should be tested to find the optimal degree of mixing that keeps cells suspended, before being used for multiparametric studies of culture conditions for optimized protocols.

3.5 References

Dexter TM, Allen TD, Lajtha LG. 1977. Conditions controlling the proliferation of haemopoietic stem cells *in vitro*. J Cell Physiol 91(3):335-44.

Gunetti M, Ferrero I, Rustichelli D, Berger M, Gammaitoni L, Timeus F, Piacibello W, Aglietta M, Fagioli F. 2008. Refreezing of cord blood hematopoietic stem cells for allogenic transplantation: *in vitro* and *in vivo* validation of a clinical phase I/II protocol in European and Italian Good Manufacturing Practice conditions. Exp Hematol 36(2):235-43.

Hua JM, Erickson LE, Yiin TY, Glasgow LA. 1993. A review of the effects of shear and interfacial phenomena on cell viability. Crit Rev Biotechnol 13(4):305-328.

Hunt CJ, Armitage SE, Pegg DE. 2003. Cryopreservation of umbilical cord blood: 1. Osmotically inactive volume, hydraulic conductivity and permeability of $CD34^+$ cells to dimethyl sulphoxide. Cryobiology 46(1):61-75.

Ito Y, Shinomiya K. 2001. A new continuous-flow cell separation method based on cell density: principle, apparatus, and preliminary application to separation of human buffy coat. J Clin Apher 16(4):186-91.

LaIuppa JA, McAdams TA, Papoutsakis ET, Miller WM. 1997. Culture materials affect ex vivo expansion of hematopoietic progenitor cells. J Biomed Mater Res 36:347-59.

Meinhart CD, Wereley ST, Santiago JG. 1999. PIV measurements of a microchannel flow. Experiments in Fluids 27(5):414-419.

Santiago JG, Wereley ST, Meinhart CD, Beebe DJ, Adrian RJ. 1998. A particle image velocimetry system for microfluidics. Experiments in Fluids 25(4):316-319.

Verfaillie CM. 1992. Direct contact between human primitive hematopoietic progenitors and bone marrow stroma is not required for long-term *in vitro* hematopoiesis. Blood 79(11):2821-2826.

Chapter 4

Six-well stirred suspension bioreactor

In this chapter a six-well bioreactor system designed to perform stirred suspension cultures in a working volume of some milliliters is described. Experimental data obtained culturing human hematopoietic stem cells in the proposed device are presented, both at normal oxygen concentration and under hypoxic conditions. This bioreactor system is useful for process optimization purposes and for small-scale stem cell production (Fig. 1, Chapter 1).

4.1 Introduction

As already pointed out (Chapter 2), the most attractive feature of a stirred bioreactor is the reduction of spatial gradients in the working volume, and the possibility to perform cell culture under controlled and defined conditions in space and in time. For application to stem cells, essential design and operative requirements are sterility and biocompatibility of the materials used, temperature and pH control, low-shear mixing, and possibly cell suspension.

The bioreactor system developed in this work is composed by six 10-ml volume stirred wells. It is suitable both for process optimization and for stem cell production. In the first case, after a step of wide exploration of different experimental conditions (microliter scale), it is necessary to perform a more confined screening at a working volume that produces a sufficient cell number to perform a more accurate characterization of the cellular outcome. In the second case, stem cell production, a milliliter-scale bioreactor is promising in view of a personalized cell-based therapy, where stem cells are expanded *ad hoc* for a single patient (Kirouac *et al*, 2008). A cost-effective disposable version of the bioreactor system proposed is implementable for this purpose, as safety is a major clinical concern.

Because most of the currently available hematopoietic cell culture protocols were developed in conventional culture systems, like multiwells or flasks (Morgan *et al*, 1999), having a bioreactor that has a high degree of continuity with these systems makes straightforward the adaptation of these protocols. Besides, it helps understanding the effective role of mixing in stem cell culture, without the interference of other culture variables.

Considering the interdisciplinary of stem cell field, where for example biologists, biotechnologists, and engineers work together on *in vitro* stem cell culture, it is important to develop a robust device that can be handled even by users without a strong technical background, for a wide-spread use, and repeatability of the results obtained. Thus simplicity in a bioreactor for stem cell culture is not a secondary aspect.

The milliliter-scale bioreactor designed in this work is constituted by a lid with an integrated mechanical stirring system, which can be coupled to a standard

disposable six-well plate, and placed inside a biological incubator. Thus, it can take advantage of incubator temperature and pH control and avoid complex systems to control these parameters. Furthermore, it allows up to six experiments to be performed in parallel under stirred suspension conditions.

Physiological oxygen partial pressure is in the range of 2–9% for most adult cells. Several studies have revealed that oxygen tension affects differently the various subsets of hematopoietic cells (Simon *et al*, 2008). Thus a study of oxygen solubility in different types of media, with and without serum, is performed. The proposed bioreactor is then implemented to be suitable to perform hypoxia cell cultures.

Results of $CD34^+$-cell culture in the proposed bioreactor are presented, along with cellular outcome characterization by hematocytometer, flow cytometry, and colony-forming cell assays. $CD34^+$-cells were selected from human umbilical cord blood by either one or two immunomagnetic separation steps.

The bioreactor presented is a promising tool to perform accessible stem cell cultures under dynamic conditions, and to investigate the effect of convective mass transport on cell interaction with the local surrounding environment, also under hypoxia conditions.

4.2 Materials and methods

4.2.1 Bioreactor device

The bioreactor system (Fig. 1) is composed of two principal components: a conventional polystyrene six-well plate (Becton Dickinson, Milan, Italy), and a lid with an integrated stirring system. The whole system is put inside a biological incubator during the cell culture.

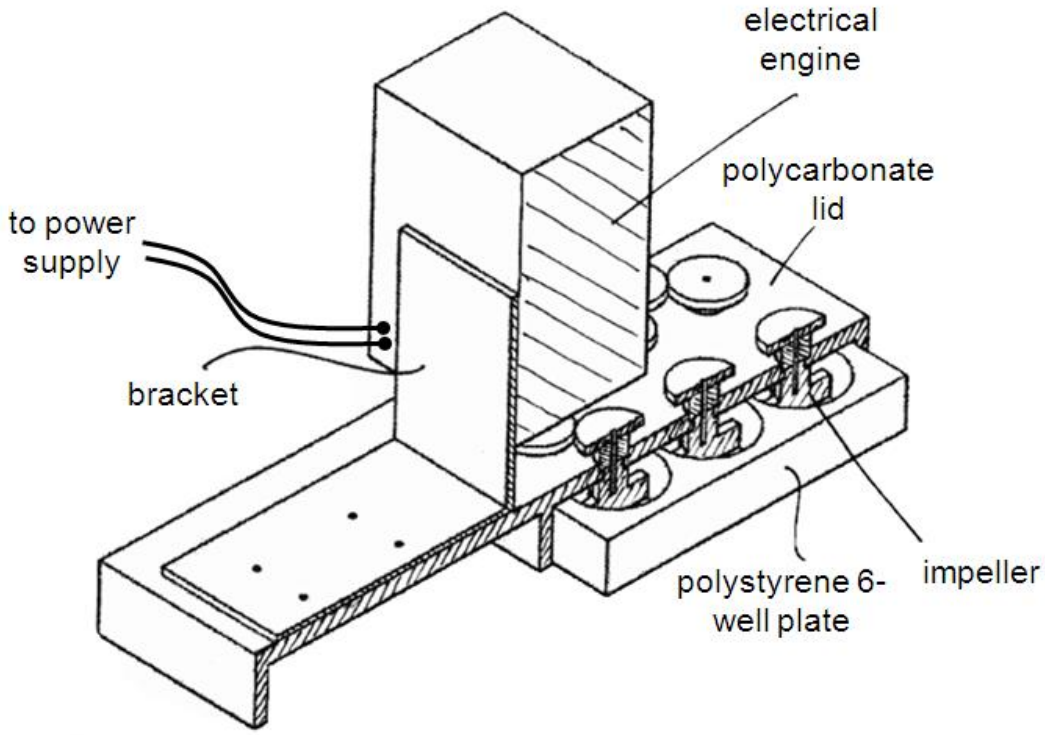

Figure 1. Section of the bioreactor system coupled with a 6-well plate.

The lid, made of polycarbonate, has a portion that fits the multiwell as a cover, and a portion that sustains an electrical engine (RS-Components, Milan, Italy).

The first part has six openings, in correspondence to the center of each well of the plate, for the passage of the stirrer shafts. A detailed view of the coupling between the opening and the stirrer is shown in Fig. 2 A.

The impeller, made of teflon polytetrafluoroethylene (PTFE), is shaped as a turbine with 45°-pitched blades (Fig. 2 B), and it is connected to a gear (RS-Components) by a screw of stainless steel. The motion is transmitted from the electrical engine to the impellers by a gear train, where the driving gear is directly fixed to the engine shaft.

The engine is closed into an airtight plastic box for protection from incubator humidity, and removably fixed to the lid by a bracket. Electrical wires connect the engine to a power supply (Kert, KAT4VD), which is the only component of the system that is placed outside of the incubator during cell culture.

The system is designed according to the guidelines in Brodkey *et al*. (1988).

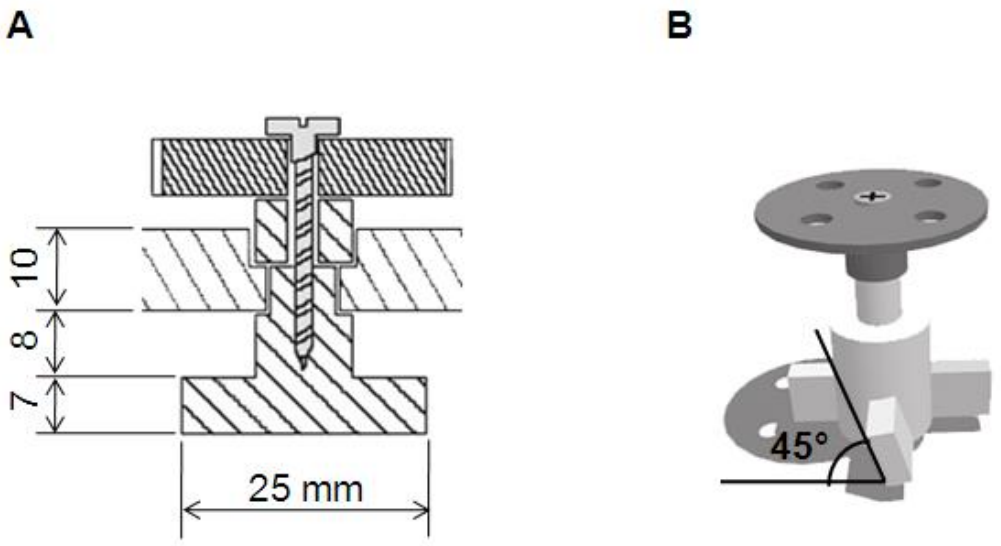

Figure 2. (A) Section of the impeller embedded in the polycarbonate lid. (B) Three-dimensional representation of the impeller, shaped as a turbine with 45°-pitched blades.

4.2.2 Study of oxygen solubility

4.2.2.1 Experimental setup

An experimental setup is developed to perform accurate measurements of oxygen solubility in different media. A 25-ml Schott Duran bottle (Zetalab Srl, Padua, Italy) is filled with 5 ml of medium. A definite-composition gas mixture is fed on medium surface with a flow rate of 100 ml/min. A fluorescent probe is put inside

the medium in proximity of the bottle bottom. The bottle top has a silicon part that is perforated for the probe, and the inlet and outlet gas tubing to pass through.

Briefly the main components of the experimental setup are a system to produce definite-composition mixtures, a system to ensure temperature control, and the system of detection itself.

Compressed nitrogen and oxygen cylinders with a purity of 99.999% (Air Liquide, Milan, Italy) are employed. Thermal mass flow meters EL-FLOW Series F-201C (Precision Fluid Controls Srl, Milan, Italy), equipped with HAM-LET filters of 7 μm (Precision Fluid Controls Srl), are used to produce mixtures with definite composition. Gases from flow meters are mixed in a 3-way coupling. All the connections are non-porous polyamide Rilsan tubing of 4-mm internal diameter, except a 250-μm diameter tube used to feed the gas mixture at medium surface.

Temperature control is accomplished by putting the 25-ml bottle, containing the medium, in a thermostatic bath, where temperature is controlled by PID thermoregulation with GTR2000 Circulator (Isco, Milan, Italy).

Fiber Optic Oxygen Sensor System (GHT Photonics, Padua, Italy) is used to detect oxygen solubility by fluorescence measurements.

4.2.2.2 Calibration

The oxygen probe is calibrated with water at three different temperatures (27, 37, 47°C). For each temperature, first 100% nitrogen is fed until equilibrium is reached. Then mixtures of nitrogen with oxygen at different partial pressures (0.04, 0.08, 0.12, 0.16, 0.20 atm) are used, allowing the system to reach equilibrium. All measurements are repeated three times. Calibration is obtained by comparing the data to those in Benson and Krause (1976) to convert fluorescence intensity data to oxygen solubilities.

4.2.2.3 Oxygen solubility measurements

Oxygen solubility in Iscove's Modified Dulbecco's Medium (IMDM), with and without 10% Fetal Bovine Serum (FBS), is experimentally measured at three different temperatures (27, 37, 47°C) and partial pressures (0.04, 0.08, 0.12, 0.16, 0.20 atm), following the same procedure used for calibration with water.

Analogous measurements are performed also for Dubecco's Modified Eagle's Medium (DMEM), with and without 10% FBS, a type of medium commonly used for stem cell cultures, even if not used in the biological experiments presented in this work.

4.2.3 Cell culture

4.2.3.1 Cell isolation and culture conditions

Cord blood (CB) units are obtained from Bone Marrow Stem Cell Transplant Laboratory (Pediatric Oncohaematology Department, Padua, Italy), after informed consent. The blood from five or six units is used for each experiment.

Cord blood is eluted with 20 ml PBS 1X (Gibco, Invitrogen, Milan, Italy) and mononuclear cells are isolated by density-gradient centrifugation (2000 rpm, 30 min), layering on equal volume of Ficoll (GE Healthcare). Mononuclear cells are counted by hematocytometer, and analyzed by flow cytometry as a negative control.

$CD34^+$ cells are isolated by superparamagnetic microbeads (CD34 antibody, QBEND-10, Abcam, Cambridge, UK) selection using high-gradient magnetic field and mini-MACS columns (Miltenyi Biotech, Glodbach, Germany). The magnetic separation step is repeated twice. A fraction of $CD34^+$-cells of more than 70% was obtained after one column passage, and of more than 90% after two column

passages, verified by flow cytometry (FACS Calibur, Becton Dickinson) after counterstaining with CD34-phycoerythrin antibody (AC136 clone, Miltenyi Biotec).

The selected cells are suspended in Iscove's Modified Dulbecco's Medium (Gibco), 10% scomplemented (56°C, 30 min), with 10% FBS (Gibco), 1% Penicillin/Streptomycin (Gibco), and supplemented with the following human citokynes (PeproTech Inc, Rocky Hill, NJ): hSCF (50 ng/ml), hTPO (10 ng/ml), hIL-6 (10 ng/ml), hFL (50 ng/ml), according to the protocol in Gunetti *et al* (2008). CD34+ cells are seeded in a 6-well plate (Becton Dickinson) filled with 10 ml of medium each, and cultured for up to 13 days both under normal oxygen conditions and in hypoxia. Impeller speed is 15 rpm in all the experiments. Hypoxia cell cultures are performed by feeding to the system a gas mixture of 5% CO_2, 5% O_2, and N_2, from a gas cylinder.

4.2.3.2 Cell analyses

In experiments at normal oxygen concentration and hypoxia, cell count and viability is detected by hematocytometer.

Flow cytometry analyses are performed at day 0, 5.5, and 12.5. After suspension in 40 µl PBS 1X, cells are stained by incubation at 4°C for 15 min with a panel of monoclonal antibodies: 8 µl of PE-conjugated CD34 (AC136 clone, Miltenyi Biotec), 7 µl of APC-conjugated CD117 (104D2 clone, Biolegend, Milan, Italy), and 5 µl of FITC-conjugated CD38 (HIT2 clone, Biolegend), CD41 (HIP 8 clone, Biolegend), CD61 (monoclonal antibody, Immunotech, Czech Republic). Cells are also incubated with 5 µl 7-amino-actinomicyn D, 7-AAD (Becton Dickinson), to analyze only viable cells. Labelled cells are then suspended in 1 ml PBS 1X,

centrifuged (1200 rpm, 5 min) and suspended in 200 µl PBS 1X for flow cytometry acquisition.

Colony-forming cell (CFC) assays are performed seeding 1000 cells from each well in a 24-well plate and grown in a semisolid medium (400 µl of Methylcellulose-MethoCult® GF H4434, StemCell Technologies, Grenoble, France) for two weeks. The hematopoietic progenitor cell colonies are then counted: burst-forming unit- erythroid (BFU-E), colony-forming unit granulocyte-macrophage (CFU-GM).

4.3 Results and discussion

4.3.1 Bioreactor design

The bioreactor is designed to keep cells suspended in conditions that respond to the essential requirements for a stem cell culture: biocompatibility of materials, maintenance of sterility, and low shear stress.

All the materials either in contact or in proximity to the cell culture are biocompatible: polystyrene from the 6-well plate, PTFE from the impellers, and polycarbonate from the lid (LaIuppa *et al*, 1997).

The system ensures cell culture sterility as the six-well plate is disposable, and the lid, after engine removal, is autoclavable at 121°C. Furthermore, as shown in Fig. 1 B, the openings on the lid for the stirrer shaft passage are shaped so that entering gases pass through a tortuous path that blocks the suspended solids responsible of carrying contamination agents.

The impeller is shaped as a turbine with 45°-pitched blades to produce an axial flow pattern that favors cell suspension from the bottom of the well, where cells otherwise settle. The impeller Reynolds number, *Re*, is defined as $Re = D^2 N \rho / \mu$,

where D is the impeller diameter (25 mm), N is the impeller rotational speed, ρ and μ the medium density and dynamic viscosity respectively. A stirring rate of 15 rpm is chosen for the experiments, to avoid dead zones in the well and to keep the shear on the cells at low values. In this condition, approximating medium properties with those of water, $Re \approx 10^2$ and the flow is in the transitional regime between laminar and turbulent. To verify the maximum shear stress on the cells at this impeller rate, an approximate calculation of the shear, τ, at well bottom is performed by:

$$\tau = \mu \frac{\partial v_x}{\partial y} \approx \mu \frac{v_{tip}}{\delta} \tag{4.1}$$

where v_{tip} is the velocity of the impeller tip (0.02 m/s), and δ is the distance of the impeller from the well bottom ($5.5\,\text{mm}$). The approximate maximum shear stress in the well is $3.6 \cdot 10^{-3}$ Pa, which is orders of magnitude lower than the critical shear stress that is harmful for the cells (Hua *et al*, 1993).

The bioreactor is also implemented to perform hypoxia cell cultures. All the different components of the bioreactor are sealed to avoid gas leak, and the lid is provided with an inlet and an outlet. The system is then fed with a gas mixture of 5% O_2, 5% CO_2, and N_2, from a cylinder, after a humidification step.

4.3.2 Oxygen solubility

Accurate measurements of oxygen dissolved in different media, at thermodynamic equilibrium, are performed at 27, 37, and 47°C. Results for experiments at 37°C are shown in Fig. 3 for water, DMEM, DMEM supplemented with 10% FBS, IMDM, and IMDM with 10% FBS. A linear fitting, according to Henry's law, is in excellent agreement with the experimental data in all cases. From these data

Henry's constants at 37°C are determined, which are reported in Tab. I, along with the constants at 27 and 47°C.

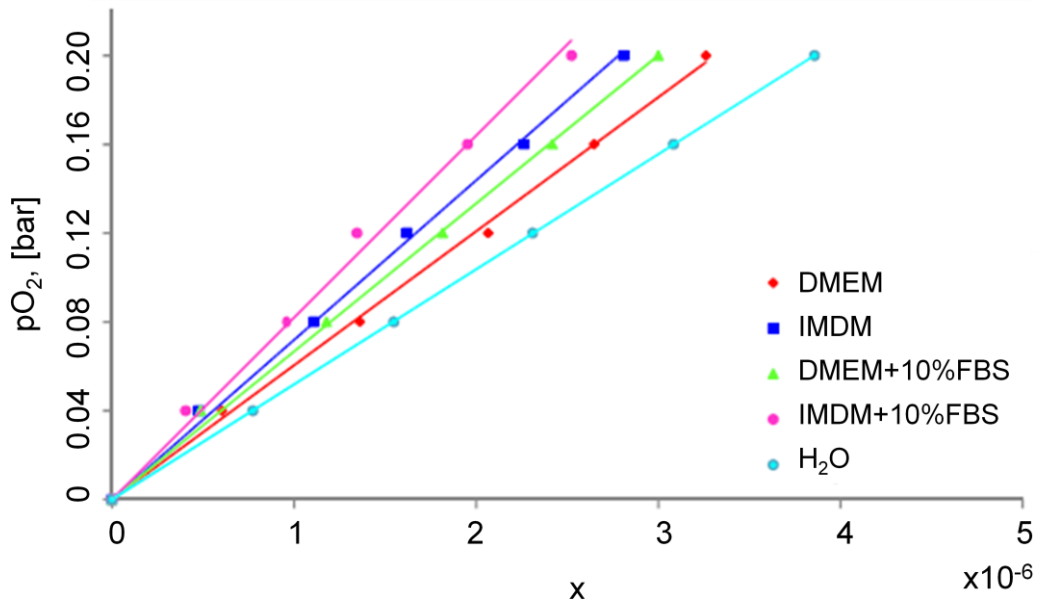

Figure 3. Thermodynamic data of oxygen solubility at 37°C. Experimental data and linear fitting of oxygen partial pressure as a function of mol fraction in the liquid phase, in different media (see legend).

As shown in Tab. I, Henry's constant increases from water to DMEM, and from DMEM to IMDM, because the high concentration of salts, glucose and other solutes in the medium causes a phenomenon of salting-out that reduces oxygen solubility, IMDM is in fact a more protein-rich medium than DMEM.

It is more important to notice the strong impact that 10% FBS supplementation have on oxygen solubility. At 0.2 bar of oxygen partial pressure, serum decreases solubility by 9.4% in DMEM, and by 12.2% in IMDM. The effect of serum on hematopoietic cell cultures involves many complex interactions (Sandstrom *et al*, 1994), and it is often difficult to discern which serum components and properties contribute to a particular effect. As oxygen has a significant influence on

hematopoietic cell behavior (Nielsen, 1999), one of the aspects to take into account, when considering serum effects on the cells, is the decreased solubility of oxygen in culture medium.

Table I. Henry's constant. Experimentally-derived Henry's constants for different media at temperature of 27, 37, and 47°C.

H_{O2}, [bar]	T = 27°C	T = 37°C	T = 47°C
H_2O	45071	51848	57835
DMEM	52401	60411	64148
DMEM+FBS	56788	66675	72533
IMDM	60048	71807	76991
IMDM+FBS	67446	81732	84482

4.3.3 Cell culture

The bioreactor system is used to culture $CD34^+$ cord blood cells. CD34 is a marker that is associated to stem cell behavior in cord blood, and is commonly used to isolate cells before seeding. First, preliminary experiments, whose results are not shown here, are used to optimize the design of the system, for example impeller geometry, and to choose the proper operative conditions, like working volume and mixing rate. Then cell cultures are performed, both under normal oxygen conditions and in hypoxia. Each type of experiment is repeated 2-4 times (as indicated in figure captions) to account for variability.

4.3.3.1 Experiments at 20% oxygen partial pressure

CD34 is a surface marker commonly used to select hematopoietic stem cells from the whole pool of umbilical cord blood cells (Jaatinen *et al*, 2007). The first two experiments are performed to compare the different proliferation rate of $CD34^+$ cells isolated by either a single- or a double-step magnetic separation. Because of the efficiency in the separation steps, the fraction of $CD34^+$ cells in the two case is higher than 70% and 90% respectively, as detected by flow cytometry measurements immediately after selection (Fig. 4).

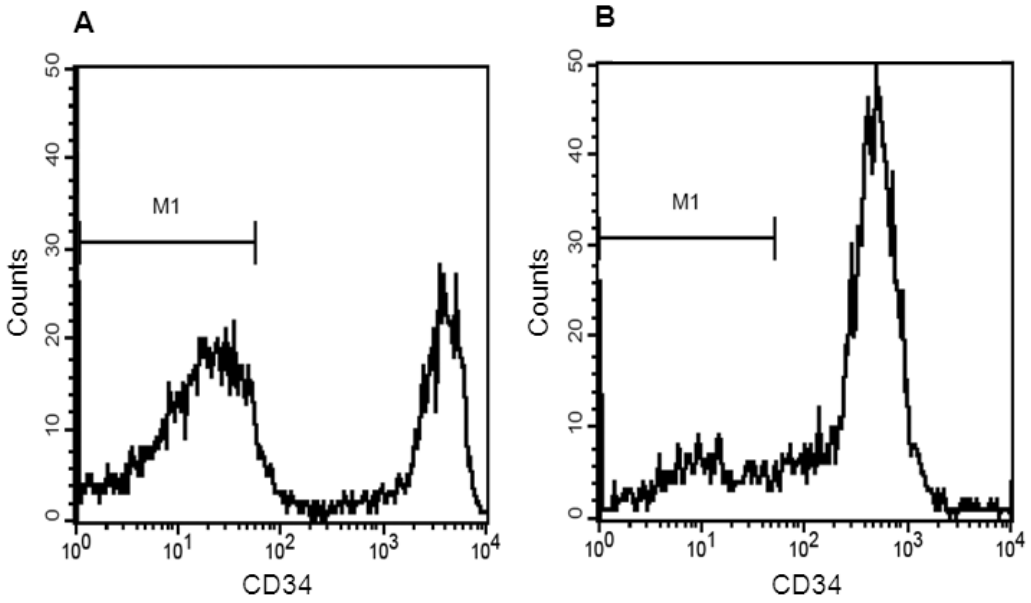

Figure 4. Results from flow cytometry measurements of CD34 marker at pO2=20%. Experimental measurement of CD34 marker on the surface of cells isolated by a single- (A), and a double-step magnetic separation (B).

Isolated cells are then cultured in the stirred bioreactor and under static conditions as a control. The two experiments are performed at different initial cell densities

because of the scarce number of cells available in the case of a double-step selection.

In Fig. 5 the fold expansion, which is the cell density normalized by its initial value, is shown for the two experiments. The initial drop in cell concentration shown for the double-selection case is the normal cell response at the beginning of a cell culture because of the adaptation process to the environment.

In both cases, single- and double-selection, stirring increases the proliferation rate, but this effect was enhanced in the single-step selected cell culture, because of a higher seeding density that makes material transport a more relevant concern.

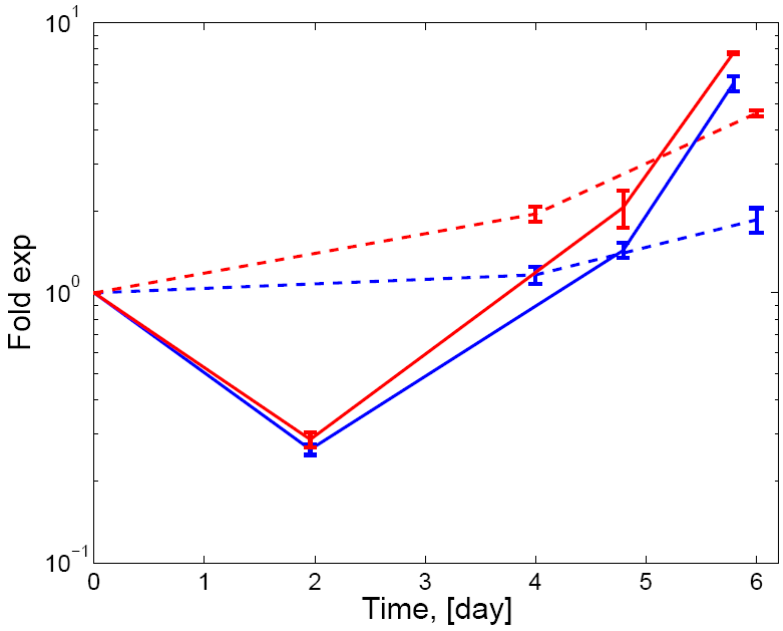

Figure 5. Growth curve of cells cultured under static and dynamic conditions at pO2=20%. Hematocytometer measurements of fold expansion of cells isolated by one (dashed), and by two magnetic separation steps (solid) cultured under static conditions (blue) and in bioreactor (red). Initial cell density is 54000 cell/ml for single-step selected cells, and 10000 cell/ml for double-step selected cells. Mean and standard deviation data for three repeated experiments for single-step selected cells, and two repeated experiments for double-step selected cells.

Even if starting from a lower cell density, double-selected cells have a higher division rate. This confirms that the cells mainly contributing to the population proliferation are the $CD34^+$ cell fraction. Thus, next experiments will all be performed seeding cells isolated by an immunomagnetic double-selection.

A second set of experiments at normal oxygen concentration is performed for a cell culture period of 13 days both under static conditions and in the bioreactor system. Fig. 6 A and B report the data of cell count and viability measurements performed by hematocytometer. Results are comparable for cells cultured under static and dynamic conditions. The lack of difference in cell behavior between the two conditions is attributed to the lower cell seeding density in these experiments (3600 cell/ml).

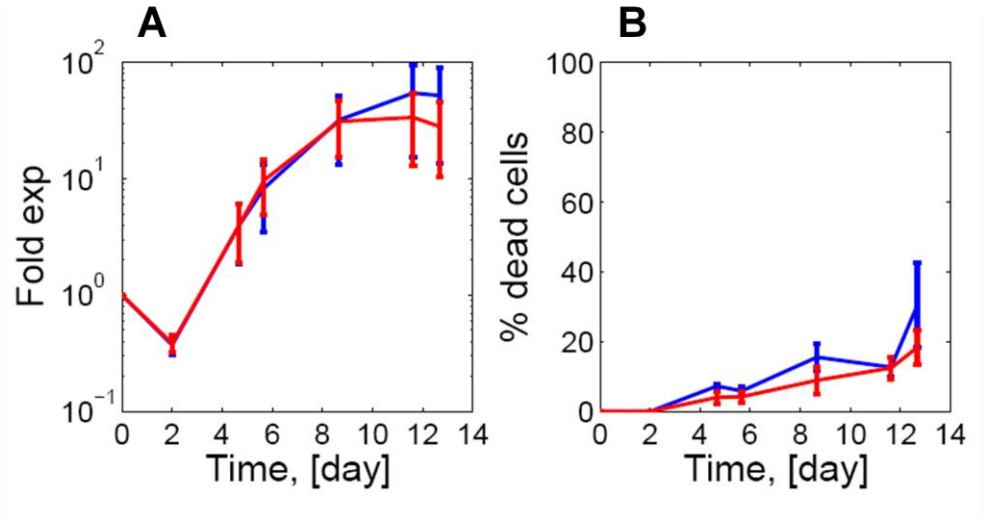

Figure 6. Growth curve and viability of cells cultured under static and dynamic conditions at pO2=20%. Hematocytometer measurements of fold expansion (A) and percentage of dead cells (B), cultured under static conditions (blue) and in bioreactor (red). Initial cell density is 3600 cell/ml. Mean and standard deviation data for three repeated experiments.

Fig. 7 shows the results from flow cytometry analyses taken after 5.5 and 12.5 days of static cell culture. Markers CD34, CD38, CD41, CD61, and CD117 were analyzed. Human hematopoietic stem cells are $CD34^{+}$, $CD117^{+}$, $CD38^{-}$, $CD41^{-}$, $CD61^{-}$ (Iwasaki *et al*, 2007), but during *in vitro* culture they change their marker profile. For example, as shown in Fig. 7, they become more $CD34^{-}$ and $CD38^{+}$, this can be attributed either to cell differentiation or to aberrant changes that occur because of unsuitable culture conditions.

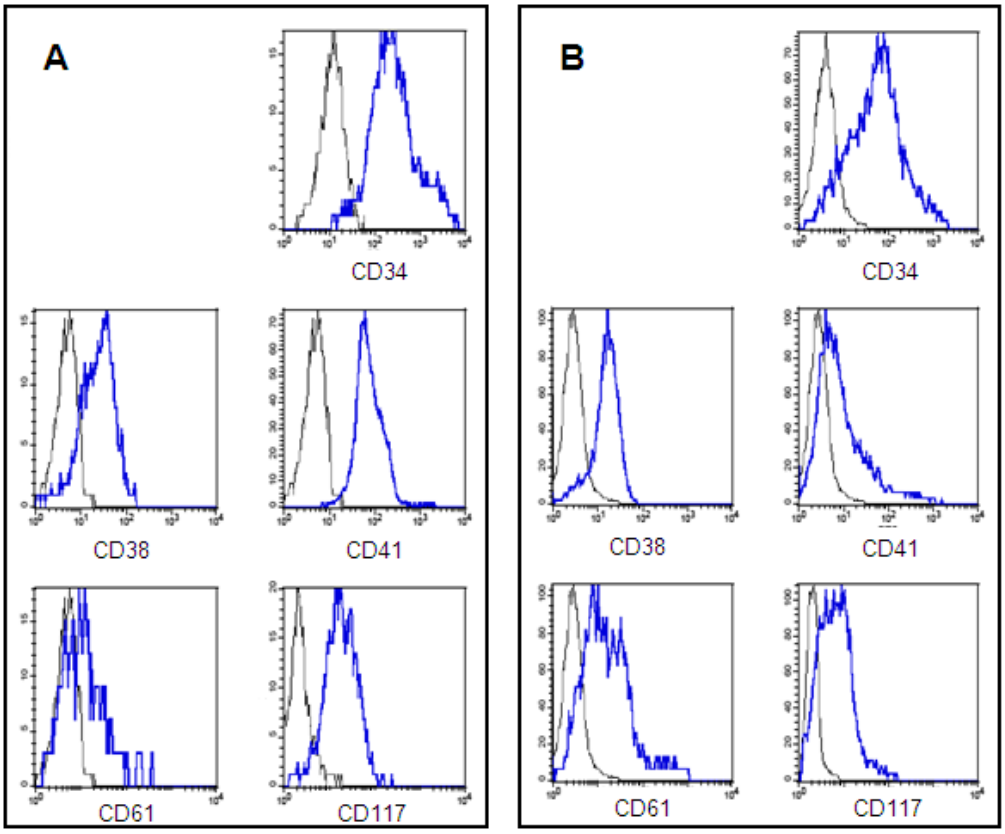

Figure 7. Flow cytometry measurements of cells cultured under static conditions at pO2=20%. Profile of markers CD34, CD38, CD41, CD61, and CD117 in the cell population cultured in static conditions (blue) at day 5.5 (A) and 12.5 (B). Initial cell density is 3600 cell/ml. Black curves refer to the negative control without fluorescent staining.

A protocol optimization to maintain cell phenotype stable during culture is currently not available, and research is in progress in this field. Flow cytometry analyses taken after 5.5 and 12.5 days of cell culture in bioreactor did not show remarkable differences with respect to results in Fig. 7 reported for static culture.

Colony-forming cell assays are commonly used to detect the multipotency of a hematopoietic cell population after *in vitro* culture. Cells differentiation potential is not clearly identifiable by markers or morphology, thus is defined retrospectively.

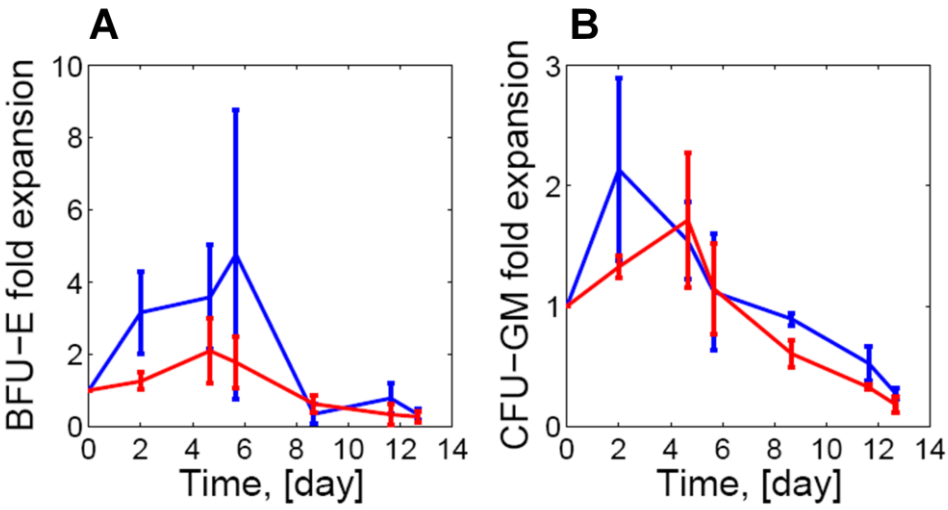

Figure 8. Fold expansion of BFU-E and CFU-GM of cells cultured under static and dynamic conditions at pO2=20%. Colony-forming cell (CFC) assays to detect fold expansion of BFU-E (A) and CFU-GM (B), cultured under static conditions (blue) and in bioreactor (red). Initial cell density is 3600 cell/ml. Mean and standard deviation data for three repeated experiments.

Briefly, a fraction of cells taken from the culture are seeded on a semisolid material, methylcellulose, that induces differentiation. By evaluating the phenotype of the colonies formed after two weeks by the daughter cells, the original multipotency is detected (Broxmeyer *et al*, 2006). In Fig. 8 results are shown of the percentage of burst-forming units-erythroid (BFU-E) and colony-forming units-granulocytes/macrophages (CFU-GM) colonies, cells taken from both the static

and dynamic cultures are able to produce. The decrease in the number of colonies formed in both cases, static and dynamic, demonstrates a loss of differentiative potential that is attributable to a culture protocol not adequate to maintain a stable cell phenotype.

4.3.3.2 Experiments at 5% oxygen partial pressure

Experiments of $CD34^+$ cell culture are performed under hypoxia conditions, with an oxygen partial pressure of 5%. Cells are seeded at a density of 3600 cell/ml both in static conditions and in the bioreactor. Fig. 9 presents the data of cell count and viability.

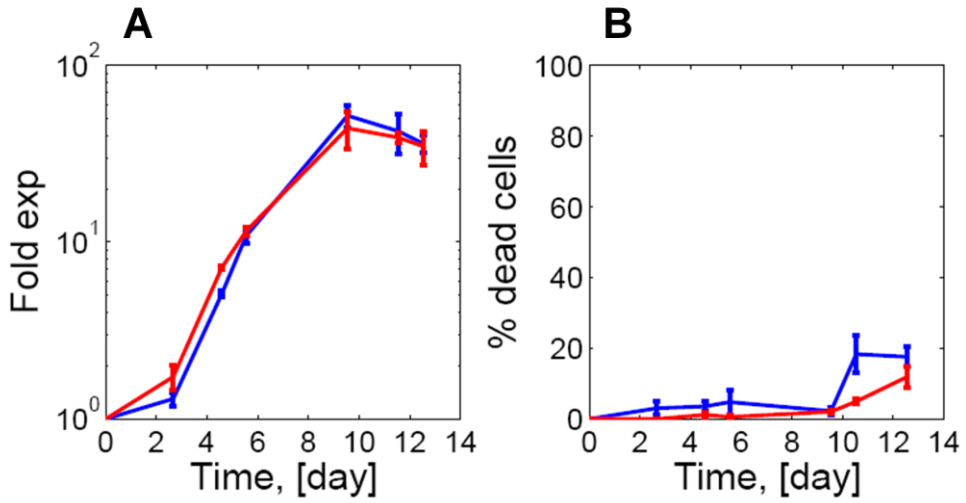

Figure 9. Growth curve and viability of cells cultured under static and dynamic conditions at pO2=5%. Hematocytometer measurements of fold expansion (A) and percentage of dead cells (B), cultured under static conditions (blue) and in bioreactor (red). Initial cell density is 3600 cell/ml. Mean and standard deviation data for four repeated experiments.

Comparing results in Fig. 9 A to Fig. 6 A, where cells are cultured in the same conditions but for oxygen tension, the overall proliferation rate after 12.5 days is similar. However, in hypoxia conditions there is no decrease in cell density in the first two days of culture, prove that conditions requires less time for the cells to

adapt to the new environment. As shown in Fig. 9 B cell death is less significant than in normoxic conditions (Fig. 6 B). Comparing the results in Fig. 9, static conditions and bioreactor culture do not show relevant differences. The low cell seeding density can again explain this comparable behavior, which is confirmed also in flow cytometry (Fig. 10) and colony-forming cell assay (Fig. 11) data.

Fig.10 illustrates flow cytometry results after a static culture of 5.5 and 12.5 days.

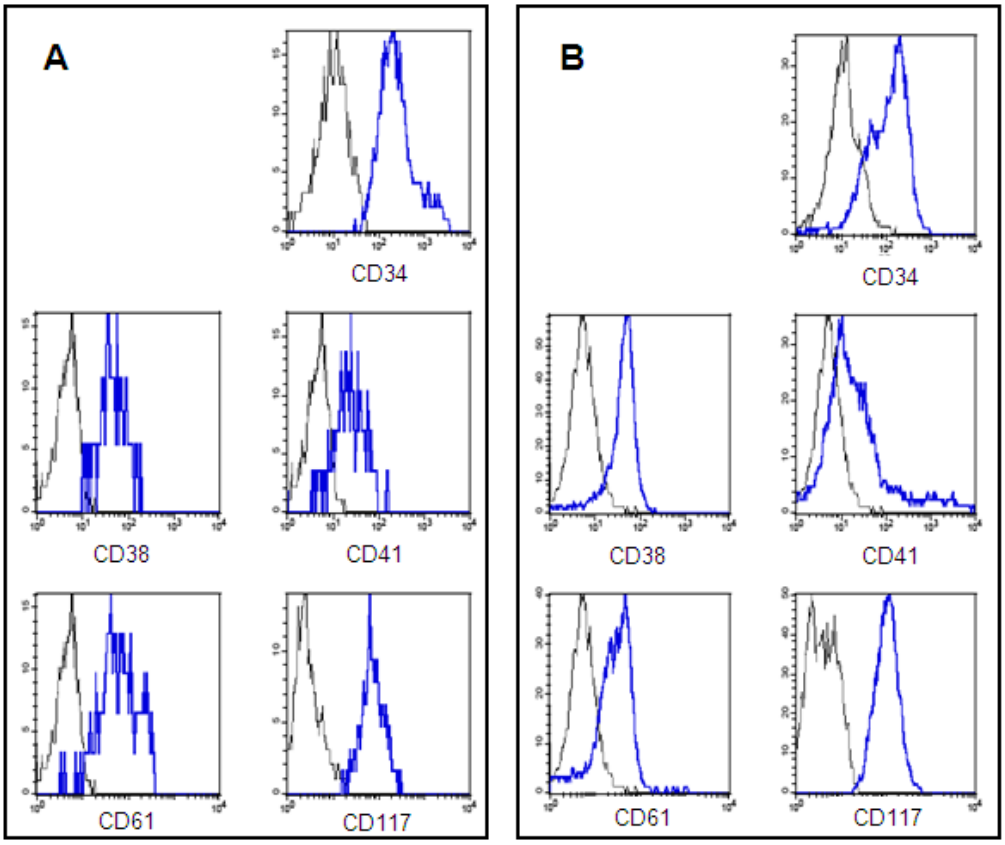

Figure 10. Flow cytometry measurements of cells cultured under static conditions at pO2=5%. Profile of markers CD34, CD38, CD41, CD61, and CD117 in the cell population cultured in static conditions (blue) at day 5.5 (A) and 12.5 (B). Initial cell density is 3600 cell/ml. Black curves refer to the negative control without fluorescent staining.

A comparison with data obtained at 5% oxygen partial pressure (Fig. 7), shows some immunophenotypic differences: at day 5.5, cells cultured in hypoxia have higher expression of CD38, CD61, and CD117, whereas a decreased expression of CD41; at day 12.5, they have comparable profiles of CD34 and CD38, and increased expression of CD41, CD61, CD117. More biological understanding is needed to comprehend the implication of these different profiles.

Fig. 11 shows the results from colony-forming cell assays, the trend of BFU-E fold expansion seems comparable to that reported in Fig. 8 A for normoxic conditions, whereas that of CFU-GM fold expansion shows an opposite trend. This result needs further confirmation, seen the high variability detected in these measurements among the four repeated experiments.

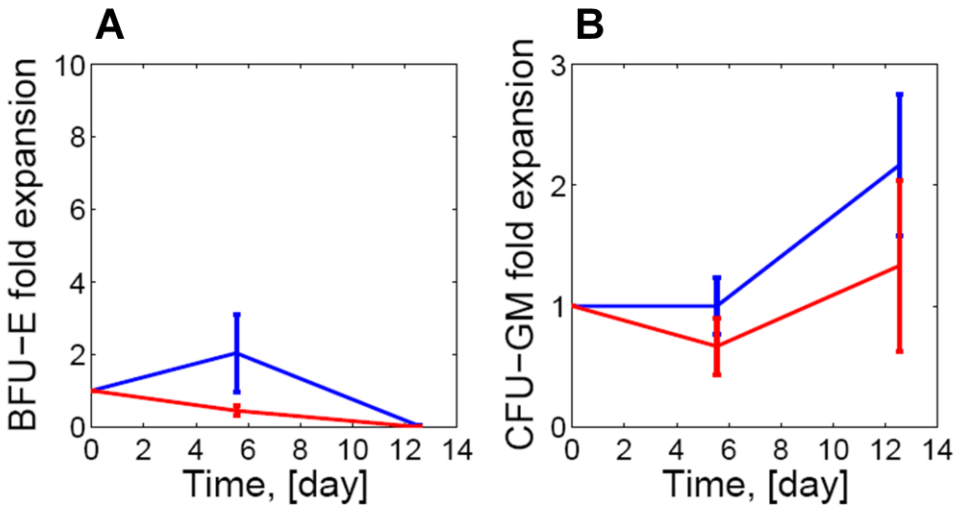

Figure 11. Fold expansion of BFU-E and CFU-GM of cells cultured under static and dynamic conditions at pO2=5%. Colony-forming cell (CFC) assays to detect fold expansion of BFU-E (A) and CFU-GM (B), cultured under static conditions (blue) and in bioreactor (red). Initial cell density is 3600 cell/ml. Mean and standard deviation data for four repeated experiments.

4.4 Conclusions

In this work a stirred bioreactor system was developed for hematopoietic stem cell culture. It is a lid with an integrated stirring system that has dimensions compatible with conventional disposable six-well plates. It was designed as simple, user-friendly, and robust as possible, and requires a little bit more than handling a lid for use. Only essential features for stem cell culture were included, such as biocompatibility of materials, sterility, low-shear mixing with cell suspension. It was possible to reduce system complexity by exploiting temperature and pH control of the biological incubator, where the bioreactor is placed during cell culture.

In this device cell culture is performed under mixing conditions, which is the only difference respect to conventional culture systems, such as multiwell or flasks, where medium is stagnant. Thus it allows the use of already developed protocols of hematopoietic stem cell culture, looking exclusively at the effect of mixing. Any introduced difference with respect to this reference culture system may impact cellular outcome in a still unknown way, considering that our understanding of stem cell behavior is still underway.

Besides the bioreactor allows up to six parallel cell cultures under identical conditions. This is particularly interesting when cell culture is performed for long periods of time with demi-populations (Gammaitoni *et al*, 2004), where at fixed intervals of time cell culture from one well is split in two wells and diluted, to decrease cell density, and then re-cultured.

A slightly more complex version of the bioreactor allows cultures to be performed under hypoxia conditions, as oxygen tension seems to play a key role in regulating hematopoietic stem cell behavior. In this work, the oxygen solubility in different types of media was studied, in order to understand the actual cell concentration

present during cell culture. This is important for example when comparing different amounts of serum added to the culture medium, as serum strongly affects oxygen solubility.

The bioreactor system was tested for up to 13-day cultures of human hematopoietic stem cells from umbilical cord blood, both under normal oxygen conditions and in hypoxia. Experiments at high cell density showed an increase in cell proliferation rate under dynamic conditions with respect to static conditions, whereas at low cell densities no remarkable difference was noticed. This can be a confirmation of the comparable behavior of the bioreactor culture system with respect to the static culture under conditions where mass transport is not limiting. However, the absence of differences could also be attributable to unknown cell feedback regulatory mechanisms that can possibly hide variations in cell behavior at the conditions under study in this work. More biological insight in biological mechanisms is needed to understand concentration-dependent cell behavior.

4.5 References

Benson BB, Krause D. 1976. Empirical laws for dilute aqueous solutions of nonpolar gases. J Chem Phys 64:689-709.

Brodkey RS, Hershey HC. 1988. Transport phenomena: a unified approach. Singapore: McGraw-Hill Inc. 847 p.

Broxmeyer HE, Srour E, Orschell C, Ingram DA, Cooper S, Plett PA, Mead LE, Yoder MC. 2006. Cord blood stem and progenitor cells. Meth Enzymol 419:439-473.

Gammaitoni L, Weisel KC, Gunetti M, Wu KD, Bruno S, Pinelli S, Bonati A, Aglietta M, Moore MA, Piacibello W. 2004. Elevated telomerase activity and

minimal telomere loss in cord blood long-term cultures with extensive stem cell replication. Blood 103(12):4440-8.

Gunetti M, Ferrero I, Rustichelli D, Berger M, Gammaitoni L, Timeus F, Piacibello W, Aglietta M, Fagioli F. 2008. Refreezing of cord blood hematopoietic stem cells for allogenic transplantation: *in vitro* and *in vivo* validation of a clinical phase I/II protocol in European and Italian Good Manufacturing Practice conditions. Exp Hematol 36(2):235-43.

Hua JM, Erickson LE, Yiin TY, Glasgow LA. 1993. A review of the effects of shear and interfacial phenomena on cell viability. Crit Rev Biotechnol 13(4):305-328.

Iwasaki H, Akashi K. 2007. Hematopoietic developmental pathways: on cellular basis. Oncogene 26:6687-6696.

Jaatinen T, Laine J. 2007. Isolation of hematopoietic stem cells from human cord blood. Curr Protoc Stem Cell Biol. John Wiley & Sons Inc.

LaIuppa JA, McAdams TA, Papoutsakis ET, Miller WM. 1997. Culture materials affect ex vivo expansion of hematopoietic progenitor cells. J Biomed Mater Res 36:347-59.

Kirouac DC, Zandstra PW. 2008. The systematic production of cells for cell therapies. Cell Stem Cell 3:369-381.

Morgan J.R. and Yarmush M.L. Tissue engineering methods and protocols. Humanda Press 1999

Nielsen LK. 1999. Bioreactors for hematopoietic cell culture. Annu Rev Biomed Eng 01:129-152.

Sandstrom CE, Miller WM, Papoutsakis ET. 1994. Serum-free media for cultures of primitive and mature hematopoietic cells. Biotechnol Bioeng 43(8):706-33.

Simon MC, Keith B. 2008. The role of oxygen availability in embryonic development and stem cell function. Molec Cell Biol 9:285-296.

Chapter 5

Cell population modeling describes intrinsic heterogeneity

In this chapter a theoretical study of the intrinsic heterogeneity of a stem cell population is presented. The analysis is performed by a computational approach based on a population balance model in the absence of the environmental extrinsic heterogeneity sources described in Chapter 2.

5.1 Introduction

In this work, a theoretical study of the intrinsic heterogeneity of a cell population under homogeneous environmental conditions is performed. HSCs have a number of different type of receptors on their surface to be sensitive to a variety of stimuli from the stem cell local environment in which they reside (Metcalf *et al*, 1971). It is a difficult task to model contemporarily these different kinds of interactions at the population level. As increasing the complexity of the mathematical model by enhancing the detail level precludes a more general insight into the system (Stelling, 2004), the cell population is considered heterogeneous only in the

number of cell surface receptors and receptor-ligand complexes formed, and consideration of the intracellular pathways is kept at a minimum. A single receptor-ligand pair is considered, selected on the basis of the crucial role it covers in the first steps of HSC expansion, in fact this ligand is present in most of the expansion protocols: c-kit and Stem Cell Factor (SCF) (Sharma *et al*, 2006).

The model is in the form of a population balance equation (Ramkrishna, 2000), coupled with an equation for ligand consumption. At the single-cell level it accounts for the following processes: the reversible reaction between receptors and ligand molecules to form receptor-ligand complexes, the production and degradation of receptors, the degradation of complexes, and cell division. As an understanding of a HSC culture is the result of the combination of experimental and computational approaches (Kitano *et al*, 2002), the model is developed to connect the influence of an operative culture variable, ligand concentration, to a macroscopic measurable quantity, receptor distribution in the population. First simulations reproduce the cell population behavior in ideal culture conditions where ligand concentration is kept constant. Then a simulation is performed to describe the heterogeneity evolution in culture when ligand is added all at once at the beginning of the cell culture, as happens in most of the conventional culture protocols. Finally some general considerations are drawn on the mechanisms that generate the intrinsic heterogeneity in the cell population, and on the conditions to reduce heterogeneity for optimized protocols.

5.2 Theoretical framework

The intrinsic heterogeneity of a cell population is related to many different phenomena. In this work, we consider only heterogeneity in the number of surface cell receptors, and receptor-ligand complexes produced in presence of ligand in

culture medium, because of the importance of receptor-ligand interactions in cell response to the environment. A multiscale approach is used, the bottom-up processes examined are:

- single-cell signaling related to production and consumption of receptors and complexes;
- ligand-dependent cell proliferation at population level;
- overall consumption of ligand in the cell culture system.

Fig. 1 A shows a graphical representation of the processes considered at the single-cell level. Receptors are produced by a cell at constant rate, and internalized and degraded at a rate proportional to their number on cell surface. Ligand, as a dimer, reacts reversibly with two receptor molecules forming one complex molecule. Complex molecules are internalized at a rate proportional to their number on cell surface. The number of complex molecules in a cell is strictly related to downstream intracellular processes. In particular its effect in enhancing cell proliferation rate is considered (Fig. 1 B). Cell division has an important impact in producing heterogeneity in the cell population. First, receptors and complexes are split between the two daughters when a mother cell divides, and thus the two cells formed are different from the mother that have produced them (Fig. 1 B). Furthermore, cells divide at different rates because of the different number of complexes they have, consequently different generations of cells are present in culture at the same time (Fig. 1 C). The overall mass balance of ligand in the cell culture system is performed, taking into consideration that ligand is consumed by each cell in the population at different rates, according to the number of receptors on its surface.

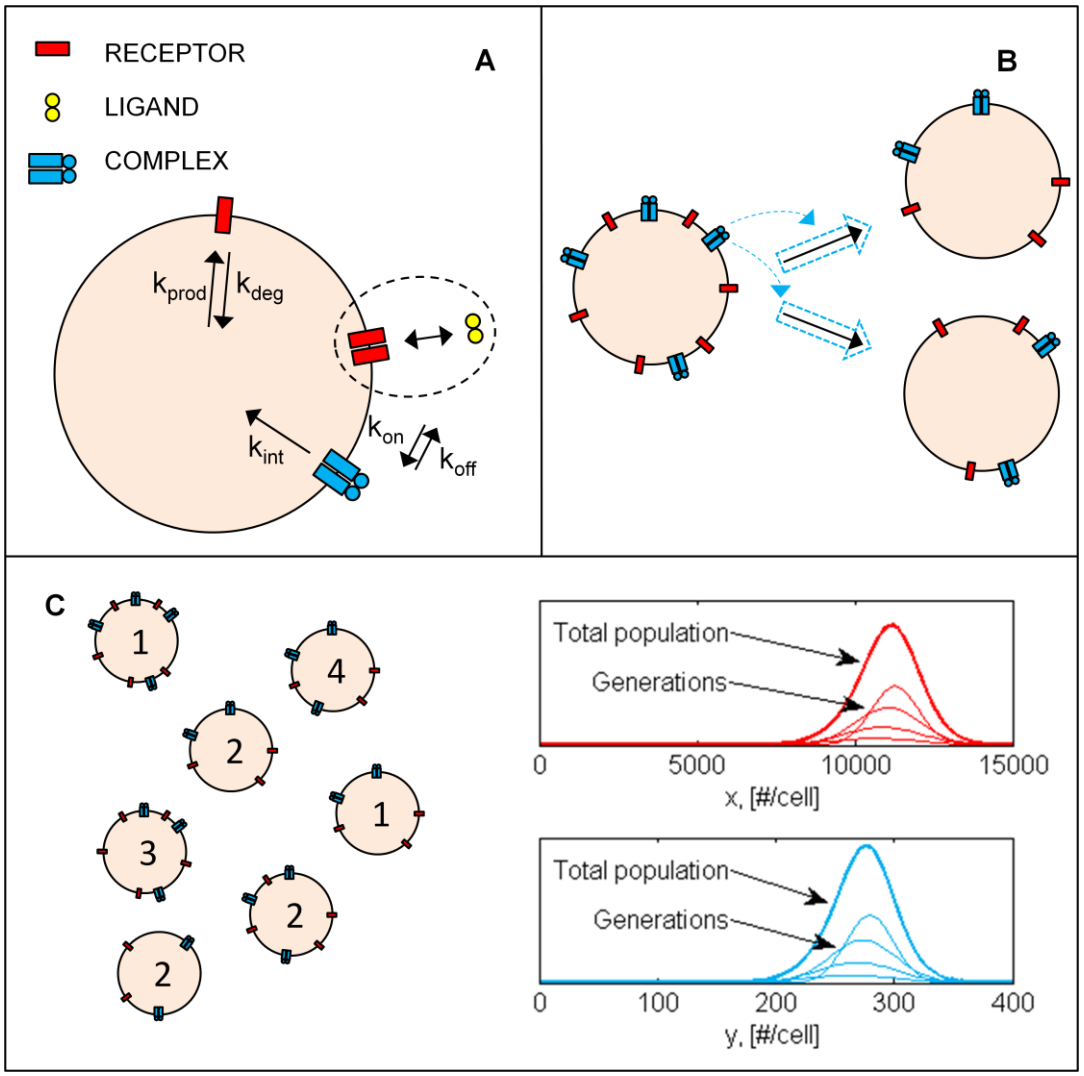

Figure 1. Schematic representation of the mechanisms taken into account in the mathematical model. (A) At the single cell level, receptors are produced and degraded; ligand is present as a dimer in the extra-cellular space and reacts with two receptor molecules to form a complex; the complex is degraded. (B) At cell division, receptors and complexes are split equally between the two daughter cells; the complex enhances the proliferation rate. (C) The population is composed by cells belonging to different generations (exemplified by the numbers inside the cells). Model simulates the distribution of the number of receptors/cell (red) and of the number of complexes/cell (blue) for the total population (thick line) and for each cell generation (thin line).

The combination of these phenomena leads to a population of cells that has distributed properties as for the number of receptors and complexes. The mathematical model developed can be used to understand the relative importance of different contributions that lead to the intrinsic cell population heterogeneity.

The model is analyzed for two different experimental situations:

- cell culture performed in batch mode, where all the ligand is added at the beginning of the experiment;
- cell culture performed at constant ligand concentration.

These two cases represent, respectively, the more common actual methodology used in biological experiments of HSC culture, and the ideal case in presence of a perfect control system that add exactly the L amount that is consumed by the cells.

5.3 Mathematical model

5.3.1 General population balance model

A population balance equation (PBE) (Ramkrishna, 2000) is a conservation equation that accounts for various ways in which cells of a specific state can either form in or disappear from the system, like by cell division and cell growth. The complete formulation of the mathematical model developed in this work is given by the bivariate PBE:

$$\frac{\partial W(x,y,t)}{\partial t} + \frac{\partial}{\partial x}\, r_x(x,y)\cdot W(x,y,t) \; + \frac{\partial}{\partial y}\, r_y(x,y)\cdot W(x,y,t) \;= \\ -\mu(y)\cdot W(x,y,t) + 2\int_y^{\infty}\int_x^{\infty} \mu(y')\cdot p(x,y \mid x',y')\cdot W(x',y',t)\,dx'\,dy' \,, \tag{5.1}$$

where the independent variables are: x, number of receptors per cell; y, number of complexes per cell; and t, time. x and y are approximated as continuous variables. $W(x,y,t)$ is the joint probability density function in x and y multiplied by the cell density; in particular, $W(x,y,t)dxdy$ represents the number of cells per unit culture volume having number of receptors between x and $x+dx$, and number of complexes between y and $y+dy$, at time t.

$r_x(x,y)$ is the rate of variation of receptor number at the single-cell level, whereas $r_y(x,y)$ that of the number of complexes. $\mu(y)$ is the cell division rate; in the case of a perfectly homogeneous population (same number of complexes in all the cells), it is equivalent to the commonly used specific growth rate, $<\mu>$:

$$<\mu>=\frac{1}{N_{cell}}\frac{dN_{cell}}{dt}\ , \tag{5.2}$$

where N_{cell} is the cell density.

$p(x,y\,|\,x',y')dxdy$, the partitioning function, represents the probability that a mother cell with status $[x',x'+dx']$ and $[y',y'+dy']$ will produce upon division a daughter cell with status $[x,x+dx]$ and $[y,y+dy]$. Because of the conservation of the number of receptors and complexes at cell division, it must be satisfied the equality $p(x,y\,|\,x',y')=p(x'-x,y'-y\,|\,x',y')$.

The first term on the rhs of Eq. (5.1) accounts for mother cells disappearing after cell division, while the second term for the two daughter cells introduced by the same process.

The PBE is coupled with the equation for ligand consumption, given by:

$$\frac{dN_{L2}}{dt}=-\frac{k_{on}}{2}N_{L2}N_x+k_{off}N_y\ , \tag{5.3}$$

where N_{L2} is the number of ligand dimer molecules per unit volume of culture; k_{on} and k_{off} are model parameters; N_x and N_y are the total number of receptors

and complexes, respectively, per unit volume of culture, derived as first moments of $W(x,y,t)$:

$$N_x = \int_0^\infty \int_0^\infty x \cdot W(x,y,t)dxdy \ . \tag{5.4}$$

An analogous expression holds for N_y.

5.3.2 Single-cell process kinetics

The mathematical expressions of r_x and r_y depend on the rates of different phenomena: the reversible receptor-ligand reaction:

$$2R + L_2 \underset{k_{off}}{\overset{k_{on}}{\rightleftarrows}} (RL)_2 \ , \tag{5.5}$$

the receptor synthesis and degradation:

$$\xrightarrow{k_{prod}} R \xrightarrow{k_{deg}} \ , \tag{5.6}$$

and the complex internalization:

$$(RL)_2 \xrightarrow{k_{int}} \ . \tag{5.7}$$

The final balances are given by:

$$r_x = \frac{dx}{dt} = -k_{on} N_{L2} x + 2k_{off} y + k_{prod} - k_{deg} x \ , \tag{5.8}$$

and

$$r_y = \frac{dy}{dt} = \frac{k_{on}}{2} N_{L2} x - k_{off} y - k_{int} y \ . \tag{5.9}$$

Cell division rate, μ, is composed of a basal rate in absence of ligand, and a second term proportional to the number of complex molecules present in the cell:

$$\mu = k_{div} + k_{div2} y \ . \tag{5.10}$$

Receptors and complexes are assumed to be split equally between the two daughter cells. Thus, the partitioning function, p, is given by:

$$p = \delta\left(x - \frac{x'}{2}, y - \frac{y'}{2} \right) . \tag{5.11}$$

5.3.3 PBE model by generations

As previously pointed out, an important source of heterogeneity in the cell population is introduced at cell division. Thus a system of PBEs can be used to track the temporal evolution of cells belonging to different generations:

$$\begin{cases} \dfrac{\partial W^{(1)}}{\partial t} + \dfrac{\partial}{\partial x}\left[r_x W^{(1)} \right] + \dfrac{\partial}{\partial y}\left[r_y W^{(1)} \right] = -\mu W^{(1)} \\ \dfrac{\partial W^{(q)}}{\partial t} + \dfrac{\partial}{\partial x}\left[r_x W^{(q)} \right] + \dfrac{\partial}{\partial y}\left[r_y W^{(q)} \right] = -\mu W^{(q)} + 2\int_{y}^{\infty}\int_{x}^{\infty} \mu p W^{(q-1)} dx' dy' \end{cases} \tag{5.12}$$

where superscript $q = 2,...,Q$ is the number of the generation, and Q is the total number of generations present during the culture period. The mother cells disappearing from $(q-1)$-generation are introduced in the q-generation PBE as daughter cells. The equations for each generation are similar except for the first generation, the oldest present in culture, whose equation does not show the

daughter-entrance term. Eqs. (5.12) are coupled with Eq. (5.3) for ligand consumption.

Cells in each generation, before dividing, tend to a steady-state, dependent on ligand concentration, that is calculated by solving the coupled Eqs. (5.8) and (5.9), given by:

$$x_{ss} = \frac{(k_{int} + k_{off})k_{prod}}{(k_{int} + k_{off})k_{\deg} + k_{int}k_{on}N_{L2}} \ , \tag{5.13}$$

and

$$y_{ss} = \frac{k_{on}k_{prod}N_{L2} / 2}{(k_{int} + k_{off})k_{\deg} + k_{int}k_{on}N_{L2}} \ , \tag{5.14}$$

where subscript ss stands for steady-state.

5.4 Simulation and analysis

5.4.1 Numerical solution and parameter estimation

A numerical solution of the mathematical model given by Eqs. (5.3) and (5.12) has been developed in this work. Briefly, each $W^{(q)}$ is approximated by a bivariate normal distribution with time-dependent parameters. The Method of Moments (Ramkrishna, 2000) is then applied to convert the model to a set of ordinary differential equations, as described in detail in Appendix 5.8.1. All model simulations in this work are performed using the ode113 solver in Matlab. Specific parameter values used for the kinetic expressions are summarized in Tab. I, whereas their derivation is provided in Appendix 5.8.2.

Table I. Parameter values used for all the simulations, if not otherwise specified.
* indicates references for data directly available
** indicates references for data adapted from literature

Parameter	Value	Unit	Reference
k_{on}	$2.8 \cdot 10^{-16}$	ml/molecule/s	Yee *et al*. (1993)
k_{off}	$3.36 \cdot 10^{-4}$	1/s	Lev *et al*. (1992)
k_{int}	$1.5 \cdot 10^{-3}$	1/s	Yee *et al*. (1993)
k_{prod}	2	molecule/cell/s	Lauffenburger *et al* (1993)
k_{deg}	10^{-4}	1/s	Lauffenburger *et al* (1993)
k_{div}	$3.7 \cdot 10^{-6}$	1/s	Ko *et al*. (2007)
k_{div2}	$7 \cdot 10^{-9}$	cell/molecule/s	Piacibello *et al*. (1997)

5.4.2 Model output

A preliminary simulation is performed to generate the initial conditions for all the simulations shown in the Results section. At the beginning the population is considered containing all cells in the first generation, with mean number of receptors equal to x_{ss}, mean number of complexes equal to y_{ss}, and null standard deviation of both receptors and complexes. This first simulation is run for a time interval of 3 days in absence of ligand. The final distributions of receptors and complexes are used as input for the subsequent simulations, where the initial cell density is fixed at 10^6 cell/ml.

The proposed model can simulate the temporal evolution of the distributions of receptors and complexes per cell for each generation. The results will be summarized in the form of the following statistics: the mean number of receptors and complexes per cell, $< x >$ and $< y >$, both for the total population and for each cell generation; the coefficient of variation (which is the standard deviation

divided by the mean), CV_x and CV_y, of the number of receptors and complexes per cell, both for the total population and for each cell generation; the standard error of the mean for the generations with respect to the mean values of the total population normalized by the mean, $SEM_x / < x >$ and $SEM_y / < y >$:

$$SEM_x = \left(\frac{\sum_{q=1}^{Q} < x >^{(q)} - < x > ^2}{Q} \right)^{1/2} , \tag{5.15}$$

where $< x >^{(q)}$ is the mean number of receptors in the q-generation. An analogous expression holds for SEM_y. Simulations are performed for the two cell culture conditions of constant ligand concentration, and with ligand added all at once at $t = 0$, thus progressively decreasing in concentration.

5.5 Results

5.5.1 Simulations at constant ligand concentration

First a simulation is computed at constant ligand concentration. As it is shown in Fig. 2 A (dashed line), it is necessary to continuously add ligand to keep the concentration constant, because of single-cell ligand consumption, coupled with the increase of cell density. The cell density in culture, N_{cell}, increases exponentially (Fig. 2 B). On the contrary, each cell generation, after its entrance, first increases in cell number, and then decreases and disappears. Thus, the cell population has a time-dependent composition in terms of fraction of cells belonging to different generations. Cells in each generation appear with half the number of receptors and complexes of their mother cells, and then tend to the steady-state given by Eqs. (5.13) and (5.14). When a new generation enters, its mean properties, $< x >$ and

$< y >$, are quite different from those of the total population, but its contribution to the whole is limited by the few cells it contains (Fig. 2 C and E).

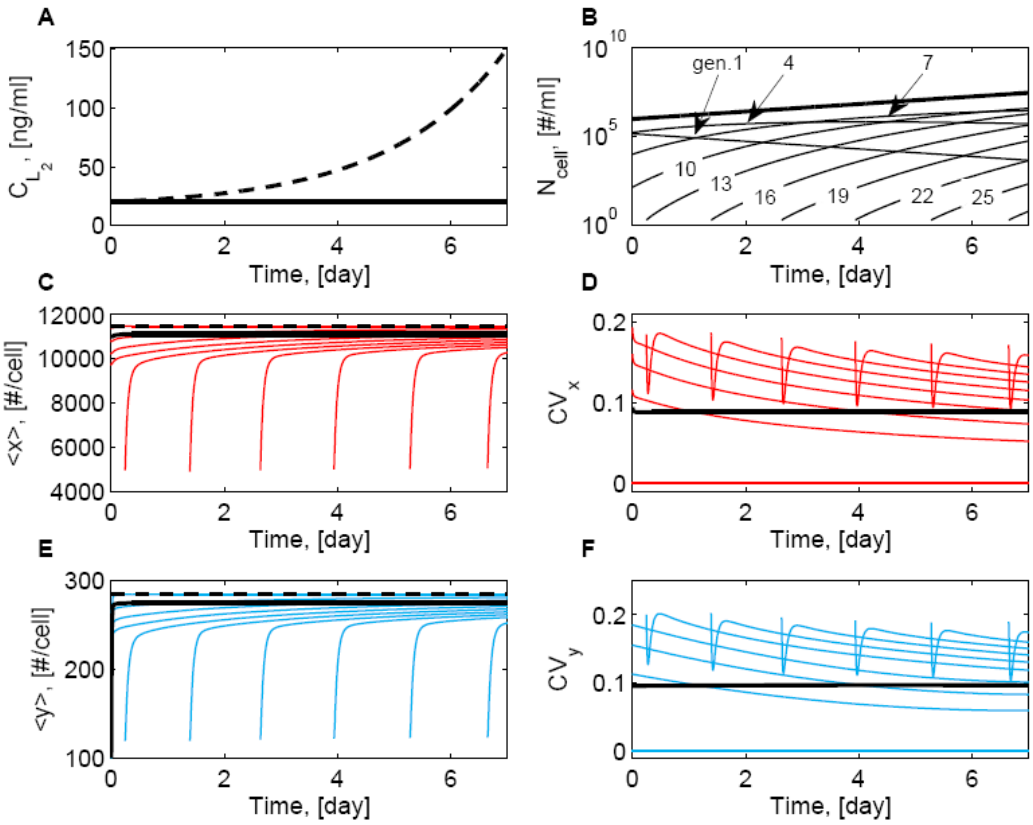

Figure 2. Results at constant ligand concentration (20 ng/ml). (A) Constant ligand concentration in culture (solid line), total amount of ligand added to keep concentration constant (dashed line). (B) Cell density of the total population (thick line), and of the generations indicated (thin lines) as a function of time. (C) Mean number of receptors/cell for the total population (black solid line), and for the same generations indicated in B (red lines), as a function of time. Steady-state of the number of receptors/cell (black dashed line) as a function of time. (D) Coefficient of variation of the number of receptors/cell for the total population (black line), and for the same generations indicated in B (red line). (E-F) Analogous to C-D for the number of complexes/cell.

The coefficients of variation for the number of receptors and complexes, CV_x and CV_y, quantitatively describe the heterogeneity in the cell population and inside each generation. They are calculated by the expression:

$$CV_x = \frac{\sigma_x}{< x >} \ , \tag{5.16}$$

where σ_x is the standard deviation of the number of receptors, either of the total population or of the single generations. An analogous expression holds for CV_y. Unlike standard deviations, coefficients of variation of different distributions can be compared as they are normalized by the respective mean. A part from the first generation that has practically null CV_x and CV_y, because all of its cells reach the steady-state, all next generations have a certain degree of heterogeneity because of cells from the previous generation continuously entering with a smaller number of receptors and complexes (Fig. 2 D and F).

Whereas the properties of each cell generation are time-dependent, the total population distribution of receptors and complexes exhibits a pseudo-steady-state. In Fig. 3 results are presented to show the dependence of this steady-state from different constant ligand concentrations. A higher ligand concentration produces an increase in $< y >$ (Fig. 3 G) that affects the proliferation rate, according to Eq. 10, increasing final cell density (Fig. 3 B). As the dependence of $< y >$ on ligand concentration is not linear this effect is more relevant at small values of C_{L2}. At the single generation level, an increase of ligand concentration causes a decrease of heterogeneity, CV_x and CV_y (Fig. 3 E and H), because of the reduction of time cells need to reach the steady-state, given by Eqs. (5.13) and (5.14).

The total population heterogeneity, CV_x and CV_y (Fig. 3 E and H), arises from three different sources:

- the cell population is composed of a distribution of different generations (Fig. 3 C);
- it has an inter-generational heterogeneity, because the mean properties of each generation, $< x >$ and $< y >$, differ from each other (Fig. 3 D and G);
- it has an intra-generational heterogeneity, as each generation is heterogeneous on its own (Fig. 3 E and H).

The first source of heterogeneity is negligible as long as different generations have the same properties. The relative importance of the second and third sources is dependent on the particular kinetics considered for the single-cell processes and for cell division. CV_x and CV_y are a measure of the global heterogeneity of the population, whereas SEM_x and SEM_y quantify only the inter-generational contribution.

5.5.2 Different ligand administration profiles

In the previous case of constant ligand concentration, ligand needs to be continuously added to the system. In the absence of a precise control, ligand concentration in culture is usually changing with time. In Fig. 4 and Fig. 5 results are presented that show a comparison between the case of constant ligand concentration, already analyzed, and that where ligand is added to the cell culture all at once at $t = 0$. The simulations cover a period of 7 days. To ensure a fair comparison, an equal amount of ligand is administered in the two cases for the whole period.

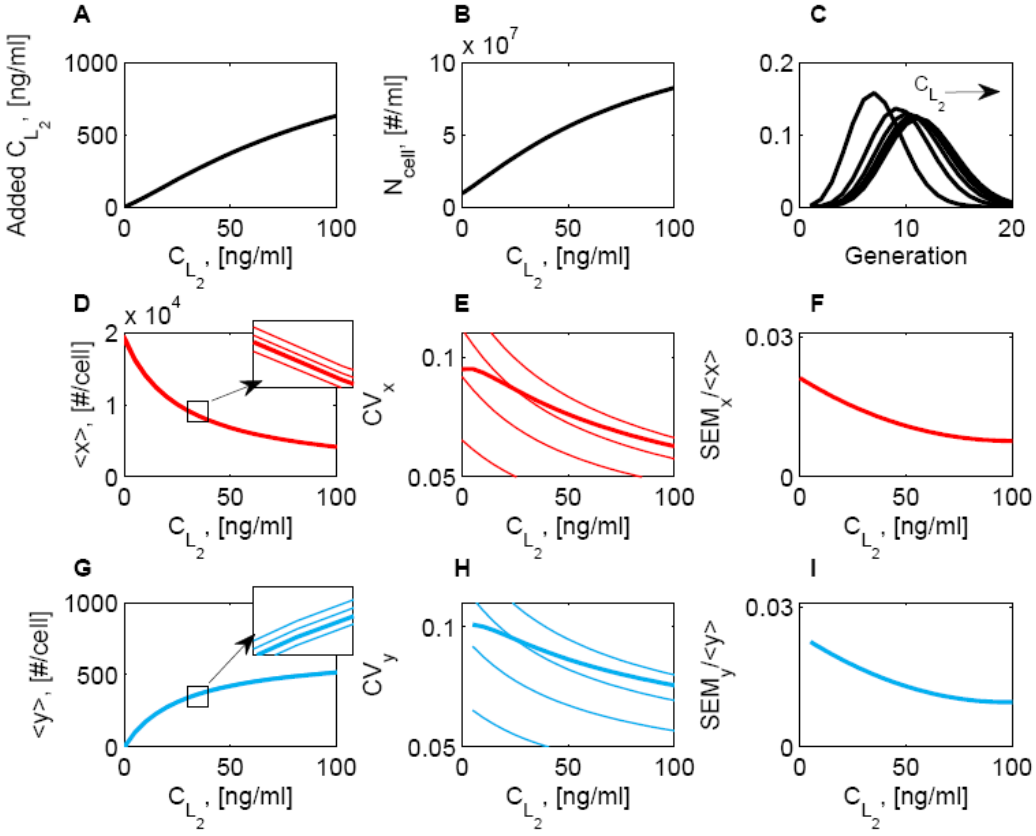

Figure 3. Results at 7 days for different constant ligand concentrations. (A) Total amount of ligand added to keep concentration constant. (B) Cell density of the total population. (C) Distribution of generations in the population for C_{L2} = 0, 15, 30, 45, 60 ng/ml. (D) Mean number of receptors/cell for the total population (thick line) and for generations 4, 7, 10, 13 (thin line). (E) Coefficient of variation of the number of receptors/cell for the total population (thick line) and for generations 4, 7, 10, 13 (thin line). (F) Normalized standard error of the mean of number of receptors/cell, considering only the generations that contribute to 98% of the total population cell number. (G-I) Analogous to D-F for the number of complexes/cell.

When ligand is added at the beginning, its concentration decreases with time (Fig. 4 A). The cell density is increased in this case, because division rate is influenced by complex formation in the presence of ligand (Fig. 4 B). This effect is reduced as soon as ligand is depleted in culture. The mean number of receptors per cell, $< x >$, increases at decreasing ligand concentrations because more receptors are unbound

(Fig. 4 C). At zero ligand concentration, $< x >$ reaches a steady-state that represents the dynamic equilibrium between receptor production and degradation. Conversely $< y >$ decreases at increasing ligand concentrations until no complexes are formed any more (Fig. 4 E). Both CV_x and CV_y grow (Fig. 4 D and F). The final heterogeneity is smaller in the constant ligand case as long as ligand is depleted at the end of the 7-day period in the second case. Whereas CV_x presents a steady state once $< x >$ remains constant, CV_y grows very rapidly (Fig. 4 E) because the mean $< y >$ becomes null (Fig. 4 E).

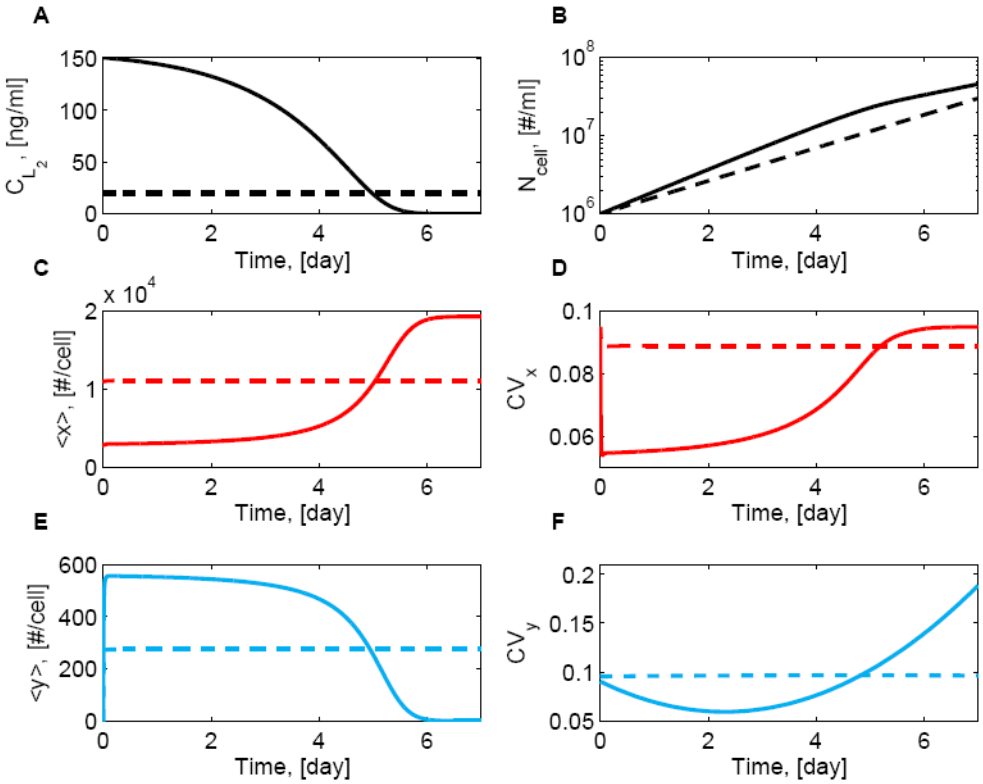

Figure 4. Comparison of results at the constant ligand concentration of 20 ng/ml (dashed lines), and for an equal amount of ligand added at t=0 (solid lines). (A) Ligand concentration in culture. (B) Cell density of the total population. (C) Mean number of receptors/cell for the total population. (D) Coefficient of variation of the number of receptors/cell for the total population. (E-F) Analogous to C-D for the number of complexes/cell.

Fig. 5 is analogous to Fig. 3. But, while in Fig. 3 C_{L2} is the actual ligand concentration in culture, in Fig. 5 it refers to the total amount added in 7 days. The concentration $C_{L2}{}^{*}$ instead refers to the actual ligand concentration in culture after 7 days (Fig. 5 A).

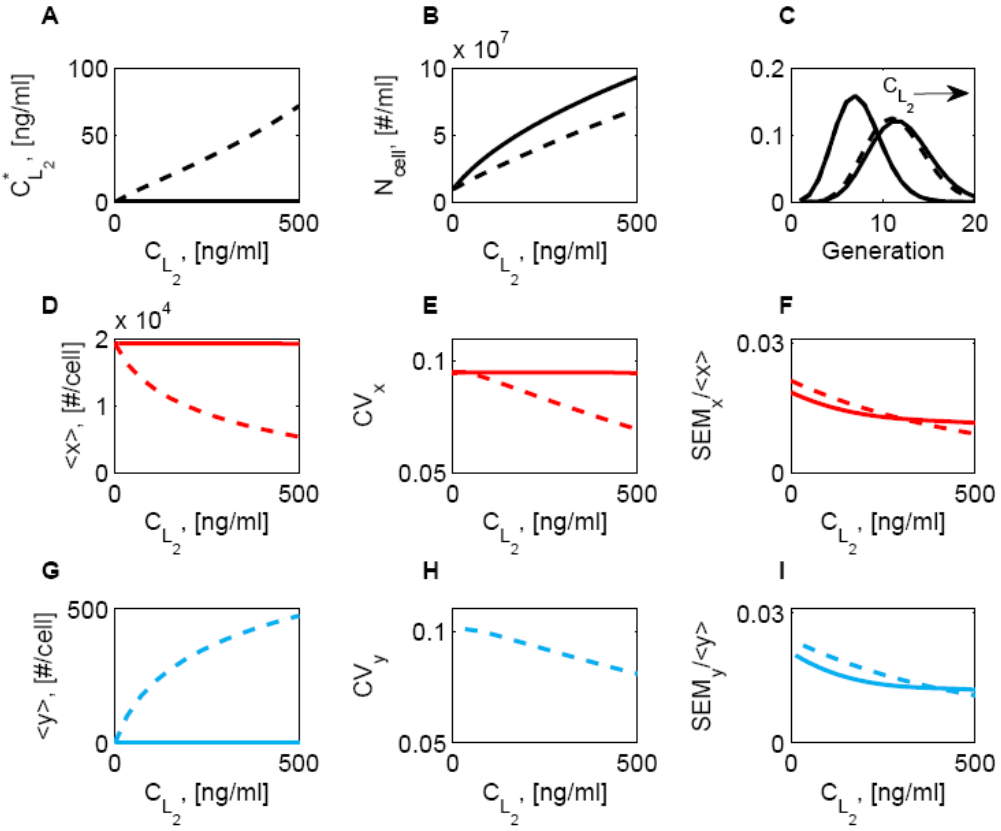

Figure 5. Results at 7 days for different total amounts of ligand added for the two cases: ligand constant (dashed lines) and ligand added at t = 0 (solid lines). Abscissas always refer to the total amount of ligand added in 7 days. (A) Ligand concentration in culture. (B) Cell density of the total population. (C) Distribution of generations in the population for C_{L2} = 0 and 500 ng/ml. (D) Mean number of receptors/cell for the total population. (E) Coefficient of variation of the number of receptors/cell for the total population. (F) Normalized standard error of the mean of number of receptors/cell, considering only the generations that contribute to 98% of the total population cell number. (G-I) Analogous to D-F for the number of complexes/cell.

The proliferation rate is highly enhanced when ligand is added since the beginning (Fig. 5 B), but the cell population composition in terms of fraction of cells for each generation is almost not affected (Fig. 5 C). The increased proliferation rate is thus not related to a higher number of generations in culture, but to an increase of the proliferation rate of the first generations, because they experienced a very high ligand concentration in the first period of culture. In the case of ligand added at $t = 0$, the simulation results show that population properties are almost invariant to changes of ligand total amount (Fig. 5 D-I). This can be explained considering that a higher amount of ligand increases the proliferation rate, thus in any case after 7 days almost all the ligand is depleted, and population heterogeneity increased (Fig. 5 E and H).

5.5.3 Dimensionless analysis of cell population heterogeneity

A dimensionless analysis is performed to understand the fundamental mechanisms that play a crucial role in determining intrinsic heterogeneity in a cell population. To determine how close to the steady-state cells in each generation arrive before dividing, two characteristic times are calculated. The characteristic time of cell division, τ_{div}, is given by the average doubling time of the cell population:

$$\tau_{div} = \frac{\log(2)}{k_{div} + k_{div2} y_{ss}} \ , \tag{5.17}$$

where y_{ss} is calculated for different ligand concentrations. The characteristic time for a newborn cell to reach the steady-state, τ_{ss}, is calculated by solving the system of Eqs. (5.8) and (5.9), with the initial condition of a cell having $x = x_{ss} / 2$ and $y = y_{ss} / 2$, for different ligand concentrations. τ_{ss} represents the time needed to reach 99% the number of receptors and complexes of the steady-state. Fig. 6 A shows the relationship between the ligand concentration and the

characteristic time ratio for the single-cell kinetics considered in this work. Fig. 6 B and C show the dependence of population heterogeneity in the number of receptors and complexes, CV_x and CV_y, from the ratio τ_{div} / τ_{ss}. CV_x and CV_y are calculated by solving Eqs. (5.12) at different constant ligand concentrations. The distinct curves are obtained for different sets of parameters. In particular, one parameter was doubled at a time.

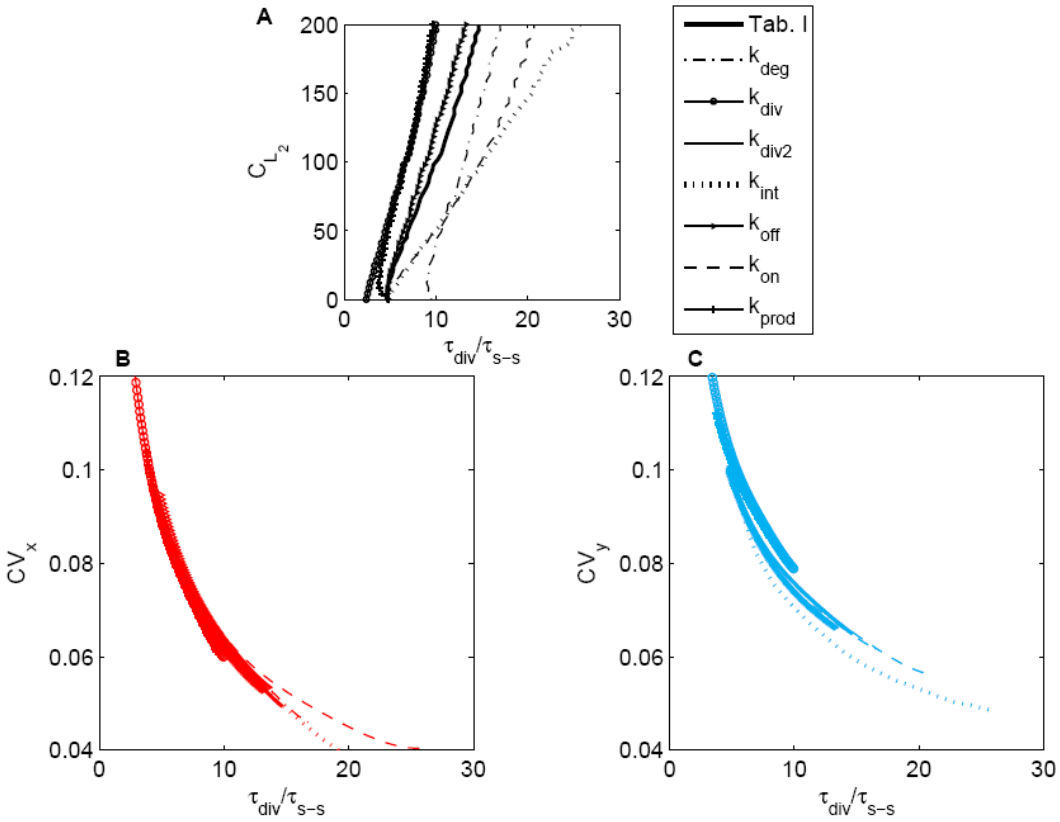

Figure 6. Dimensionless analysis of intrinsic heterogeneity. Different types of lines refer to results obtained by doubling the parameter indicated by the legend. (A) Relationship between the ratio of the characteristic times and ligand concentration. (B) Coefficient of variation of the number of receptors/cell for the total population as a function of the ratio of the characteristic times. (C) Analogous to B for the number of complexes/cell.

Intrinsic heterogeneity shows a dependence on the characteristic time ratio. In particular a reduction of cell population heterogeneity is achieved when cells proliferate more slowly, for higher τ_{div}. This dependence is insensitive to arbitrary parameter changes in the model (Fig. 6 B and C). Thus the ratio τ_{div} / τ_{ss} is a dimensionless number that can be used to characterize intrinsic heterogeneity in the case presented in this work, calculated for ligand concentration kept constant in culture. If ligand concentration changes slowly in culture, with a characteristic time much larger than τ_{div} and τ_{ss}, then results in Fig. 6 A and B are a good approximation, even in that conditions. This is useful to understand the efficiency in ligand concentration control that is necessary to reduce cell population intrinsic heterogeneity.

Because of their generality, Fig. 6 B and C could be considered as operative diagrams for protocol optimization, once it is known the relationship between τ_{div} / τ_{ss} and ligand concentration, which is dependent on the particular kinetics of the system under study.

5.6 Conclusions

Expansion of HSCs *in vitro* is required for a wider use of UCB as a source of stem cells for cell therapy (Hofmeister *et al*, 2006). The control of the phenotype of cells from the culture is necessary for a safe clinical application (Kirouac *et al*, 2008). Heterogeneity in the expanded cell population needs to be reduced, as small fractions of different cells can contribute negatively to the clinical response to the therapy (Bryder *et al*, 2006). It is widely recognized that heterogeneity in a cell population arises because of spatial gradients in metabolite and growth factor concentrations over the culture volume. Dynamic culture systems, like bioreactors, are convenient means to reduce these spatial inhomogeneities (Blanch *et al*, 1997).

But even in perfect mixing conditions, a cell population presents a certain degree of intrinsic heterogeneity.

In this work, a theoretical study was performed to understand the sources of intrinsic heterogeneity under perfectly homogeneous culture conditions. The heterogeneity considered was that in the number of receptors and complexes per cell. The focus on receptor-ligand mechanism was motivated by the importance it has in the cell interaction with the environment. Furthermore it connects an operative variable in cell culture, ligand concentration, to a measurable single-cell property, receptor number. In particular, the mathematical model developed focuses on c-kit-SCF pair.

First, intrinsic heterogeneity was studied in the ideal case of constant ligand concentration representing the ideal condition to have a constant quality of cell culture outcome. Even in this case, intrinsic heterogeneity is generated at cell division, because of the partitioning of receptors and complexes molecules from a mother cell to the two daughters. The overall population presents steady distributions of receptors and complexes, whereas the different generations of cells that it contains have time-dependent properties. Working at different ligand concentrations produces a cellular outcome with different properties. The effect of a change in ligand concentration resulted more pronounced at low ligand concentrations because of the nonlinear dependence of the different processes from ligand concentration.

To study the importance of ligand administration kinetics, a case was studied where the ligand is added all at once at the beginning of culture. Cell population properties become time-dependent in this case also for the total population, thus the time duration of cell culture becomes an additional parameter to consider. A comparison was performed between the ideal case of constant ligand concentration

and the case where an equal amount of ligand is added all at once at the beginning. The final cellular outcome has a different heterogeneity in the two cases. In particular cell population heterogeneity increases very rapidly as soon as ligand concentration falls under a certain threshold in the second case. On the overall, it seems important not to completely deplete ligand concentration in culture to maintain reasonable values of heterogeneity. The same comparison was performed for different amounts of ligand added in the same span of time. Heterogeneity remains higher in the condition with ligand added at the beginning, because the higher proliferation rate causes ligand to be depleted in 7 days, even when starting at very high initial ligand concentrations. In the range of ligand concentrations normally used (20-100 ng/ml), keeping ligand concentration constant helps in reducing population heterogeneity.

The intrinsic heterogeneity is not avoidable as long as cells are dividing, but working close to constant ligand conditions can effectively reduce it. The choice of optimal ligand concentration to minimize population heterogeneity is dependent on the relative rates of cell division and single-cell steady-state achievement, Fig. 6 summarizes this result. Fig. 6 B and C can be considered as operative diagrams, as they have a much wider applicability than the model presented here. In fact, besides being invariant to the model parameters used, it accounts also for different mathematical forms of single-cell kinetics, r_x and r_y, as long as the cells tend to one stable steady-state, and do not interact with each other. Other simple expression of the division rate, μ, can be also included in Fig. 6 B and C, but a deeper analysis should be performed in this case. Given the relationship between ligand concentration in culture and the characteristic time ratio, which is dependent on the specific kinetics considered, it is possible to estimate cell population

heterogeneity from Fig. 6 B and C, in the ideal case when external environmental sources of heterogeneity are neglected.

5.7 References

Blanch HW, Clark DS. 1997. Biochemical engineering. New York: Marcel Dekker Inc. 702 p.

Bryder D, Rossi DJ, Weissman IL. 2006. Hematopoietic stem cells - The paradigmatic tissue-specific stem cell. Am J Pathol 169(2):338-346.

Hofmeister CC, Zhang J, Knight KL, Le P, Stiff PJ. 2007. Ex vivo expansion of umbilical cord blood stem cells for transplantation: growing knowledge from the hematopoietic niche. Bone Marrow Transplantation 39:11-23.

Kirouac DC, Zandstra PW. 2008. The systematic production of cells for cell therapies. Cell Stem Cell 3:369-381.

Kitano H. 2002. Computational systems biology. Nature 420:206-210.

Ko KH, Odell R, Nordon RE. 2007. Analysis of cell differentiation by division tracking cytornetry. Cytometry part A 71A(10):773-782.

Lauffenburger DA, Linderman JJ. 1993. Receptors. Model for binding, trafficking and signaling. New York:Oxford University Press.

Lev S, Yarden Y, Givol D. 1992. Dimerization and activation of the kit receptor by monovalent and bivalent binding of the Stem Cell Factor. J Biol Chem 267(22):15970-15977.

Metcalf D, Moore, MAS. 1971. Hematopoietic Cells. Amsterdam: North Holland.

Piacibello W, Sanavio F, Garetto L, Severino A, Bergandi D, Ferrario J, Fagioli F, Berger M, Aglietta M. 1997. Hematopoietic stem cells from cord blood

extensive amplification and self-renewal of human primitive hematopoietic stem cells from cord blood. Blood 89: 2644-2653.

Ramkrishna D. 2000. Population balances theory and applications to particulate systems in engineering. San Diego:Academic Press.

Sharma S, Gurudutta GU, Satija NK, Pati S, Afrin F, Gupta P, Verma YK, Singh VK, Tripathi RP. 2006. Stem cell c-KIT and HOXB4 genes: Critical roles and mechanisms in self-renewal, proliferation, and differentiation. Stem Cells Dev 15(6):755-78.

Stelling J. 2004. Mathematical models in microbial systems biology. Curr Opin Microbiol 7:513-518.

Yee NS, Langen H, Besmer P. 1993. Mechanism of kit ligand, phorbol ester, and calcium-induced down-regulation of c-kit receptors in mast cells. J Biol Chem 268(19):14189-14201.

5.8 Appendices

5.8.1 Model solution method

Each generation was approximated by a bivariate normal distribution given by:

$$W^{(q)} = \frac{N_{cell}^{(q)}}{2\pi\sqrt{\sigma_{xx}^{(q)}\sigma_{yy}^{(q)}}\sqrt{1-\rho^{(q)2}}}\exp\left[-\frac{z^{(q)}}{2(1-\rho^{(q)2})}\right], \qquad (5.18)$$

where:

$$z^{(q)} = \frac{(x-\mu_x^{(q)})^2}{\sigma_{xx}^{(q)}} - \frac{2\rho^{(q)}(x-\mu_x^{(q)})(y-\mu_y^{(q)})}{\sqrt{\sigma_{xx}^{(q)}\sigma_{yy}^{(q)}}} + \frac{(y-\mu_y^{(q)})^2}{\sigma_{yy}^{(q)}}, \qquad (5.19)$$

and:

$$\rho^{(q)} = \frac{\sigma_{xy}^{(q)}}{\sqrt{\sigma_{xx}^{(q)}\sigma_{yy}^{(q)}}}. \qquad (5.20)$$

There are 6 unknowns for each generation: $N_{cell}^{(q)}(t)$, $\mu_x^{(q)}(t)$, $\mu_y^{(q)}(t)$, $\sigma_{xy}^{(q)}(t)$, $\sigma_{xx}^{(q)}(t)$, $\sigma_{yy}^{(q)}(t)$, and one for ligand concentration, $N_{L2}(t)$. Thus, $(6Q+1)$ equations are needed to solve the model: $6Q$ equations of moments and one equation from N_{L2} balance.

The following moments were chosen for solving the system: $M_{00}^{(q)}$, $M_{10}^{(q)}$, $M_{01}^{(q)}$, $M_{20}^{(q)}$, $M_{02}^{(q)}$, $M_{21}^{(q)}$. The general (i,j)-moment is given by:

$$M_{i,j}^{(q)}(t) = \int_0^\infty \int_0^\infty x^i y^j W^{(q)}(x,y,t)dxdy \ . \tag{5.21}$$

The general equation for the (i,j)-moment applied to Eq. (5.12) is:

$$\begin{aligned} \frac{dM_{i,j}^{(q)}}{dt} = i\ & -k_{on}N_{L2}M_{i,j}^{(q)} + 2k_{off}M_{i-1,j+1}^{(q)} + k_{prod}M_{i-1,j}^{(q)} - k_{deg}M_{i,j}^{(q)} \ + \\ j\ & k_{on}N_{L2}M_{i+1,j-1}^{(q)}/2 - (k_{off}+k_{int})M_{i,j}^{(q)} \ + \\ -\ & k_{div}M_{i,j}^{(q)} + k_{div2}M_{i,j+1}^{(q)} \ + \\ +2^{1-i-j}\ & k_{div}M_{i,j}^{(q-1)} + k_{div2}M_{i,j+1}^{(q-1)} \end{aligned} \tag{5.22}$$

Eq. (5.3) in terms of moments becomes:

$$\frac{dN_{L2}}{dt} = -\frac{k_{on}}{2}N_{L2}\sum_{q=1}^{Q}M_{10}^{(q)} + k_{off}\sum_{q=1}^{Q}M_{01}^{(q)} \tag{5.23}$$

This solution method by generations was verified comparing the results to those obtained by solving Eq. (5.1) by the Direct Quadrature Method of Moments (Zucca *et al*, 2007). Results were obtained running the two programs with parameter values in Tab. I, and initial conditions consisting of a homogeneous cell population with $N_{cell}=10^4$ cell/ml, $<x>=x_{ss}$, $<y>=y_{ss}$, at a ligand concentration equal to 50 ng/ml for 7 days. The Direct Quadrature Method of Moments (DQMOM) was applied with two nodes, choosing the equations of the following moments: M_{00}, M_{10}, M_{01}, M_{20}, M_{02}, M_{21}, coupled with Eq. (5.3). The deviation between the two solution methods results in the range of numerical uncertainty.

5.8.2 Parameter derivations

Model parameters were obtained from data in the literature for the system c-kit and SCF, when available, and are summarized in Tab. I. The kinetic constant of the direct receptor-ligand reaction, k_{on}, is equal to $2.8 \cdot 10^{-16}$ ml/molecule/s, derived from Yee *et al*. (1993). The kinetic constant of the reverse receptor-ligand reaction, k_{off}, is calculated by $k_{off} = k_{on} K_{eq}$, where K_{eq} is the dissociation constant for the reaction, having a value of 2 nM (Lev at al., 1992).

The rate constant of complex internalization for the system, k_{int}, is $1.5 \cdot 10^{-3}$ s^{-1} as reported in Yee *et al*. (1993). C-kit production rate constant, k_{prod}, was not available for the system under consideration. Its value was fixed to 2 s^{-1}, similar to the value of Epidermal Growth Factor Receptor (EGF-R) synthesis rate from Lauffenburger and Linderman (1993), as c-kit and EGF-R belong to the same family of tyrosine-kinase receptors. The same assumption was used for the internalization rate constant of free receptors, k_{deg}, whose value was fixed to 10^{-4} s^{-1}.

The doubling time of hematopoietic cells cultured in presence of 100 ng/ml of SCF, as described in Ko *et al*. (2007), is $t_{d1} = 26$ h. In absence of SCF the proliferation rate is highly decreased (McNiece *et al*, 1995), and it was assumed a double doubling time in this case, $t_{d2} = 52$ h, this value is consistent with the data reported in Piacibello *et al*. (1997). From these data, values of k_{div} and k_{div2} were derived according to $k_{div} = \log(2) / t_{d2}$, and $k_{div2} = (\log(2) / t_{d1} - k_{div}) / y_{ss}$.

Chapter 6

Conclusions

This work aimed at rationally understanding biological and physical phenomena in hematopoietic process of cell expansion *in vitro,* and their related technological implications. A particular focus was on the development of strategies to improve the final product quality, i.e. the stem cell clinical therapeutic potential. In particular, the importance of stem cell quality in terms of distributed properties in the population was investigated.

Methodologies to produce experimental data on a population level were gained and used during this PhD program. Experimental data highlighted the importance of a rational understanding of which operative parameters from different culture conditions affect cell behavior. In fact, the complexity and the competition between different biological and physical phenomena hide the different sources of heterogeneity, in terms of marker expression.

In this thesis the concepts of intrinsic and extrinsic heterogeneity were introduced, along with those of intra-generational and inter-generational heterogeneity when thinking to the whole population. These aspects can be investigated from both an experimental and a computational approach.

A bioreactor array was designed to culture HSCs under stirred conditions at a microliter scale. Small-scale devices are required for a wide screening of different experimental conditions to optimize cell culture protocols. Because of the variability between different umbilical cord units and of the scarce number of cells a unit contains, it is important to have a system to perform HSC cultures under many different conditions using cells from the same umbilical cord unit. Besides, the advantage of having a stirred system, to perform this screening at a micro-liter scale, is helpful in the scale-up process, when bioreactors are used at a production scale. In perspective, the system developed in this work should be used for multiparametric studies of culture conditions for optimized protocols.

A six-well stirred bioreactor was developed with a very simple design to perform cultures under mixing conditions. Mixing in this system is the only difference respect to conventional culture systems, such as multiwell or flasks, where medium is stagnant. Thus, this bioreactor allows the use of already developed protocols for hematopoietic stem cell culture, looking exclusively at the effect of mixing. Considering the interdisciplinary of stem cell field, it is important to develop a robust device that can be handled even by users without a strong technical background, for a wide-spread use, and repeatability of the results obtained. Thus simplicity in a bioreactor for stem cell culture is not a secondary aspect, and it was considered during the design of this system.

A theoretical study was performed to understand the sources of intrinsic heterogeneity under perfectly homogeneous culture conditions. The heterogeneity

considered was that in the number of receptors and complexes per cell. The focus on receptor-ligand mechanism was motivated by the importance it has in the cell interaction with the environment. Furthermore it connects an operative variable in cell culture, ligand concentration, to a measurable single-cell property, receptor number. The intrinsic heterogeneity is not avoidable as long as cells are dividing, but optimal protocols for ligand administration can be developed to reduce it.

On the overall, the most important conclusion from this work is that we cannot completely eliminate heterogeneity, but to design safe manufacturing processes we need to be aware of the sources that generate it and of the variability in the system.

Appendix A

Flow cytometric cell cycle analysis of muscle precursor cells cultured within 3D scaffolds in a perfusion bioreactor

*Marina Flaibani, Camilla Luni, Elisa Sbalchiero, Nicola Elvassore**

Department of Chemical Engineering, University of Padova, I-35131 Padova, Italy

(*)To whom correspondence should be addressed

E-mail: nicola.elvassore@unipd.it

phone: +39 (049) 8275469; fax: +39 (049) 8275461

A.1 Abstract

It has been widely demonstrated that perfusion bioreactors improve *in vitro* three-dimensional (3D) cultures in terms of high cell density and uniformity of cell distribution; however, the studies reported in literature were primarily based on qualitative analysis (histology, immunofluorescent staining) or on quantitative data averaged on the whole population (DNA assay, PCR). Studies on the behavior, in terms of cell cycle, of a cell population growing in 3D scaffolds in static or dynamic conditions are still absent. In this work, a perfusion bioreactor suitable to culture C_2C_{12} muscle precursor cells within 3D porous collagen scaffolds was designed and developed and a method based on flow cytometric analyses for analyzing the cell cycle in the cell population was established. Cells were extracted by enzymatic digestion of the collagen scaffolds after 4, 7, and 10 days of culture, and flow cytometric live/dead and cell cycle analyses were performed with Propidium Iodide. A live/dead assay was used for validating the method for cell extraction and staining. Moreover, to investigate spatial heterogeneity of the cell population under perfusion conditions, two stacked scaffolds in the 3D domain, of which only the upstream layer was seeded, were analyzed separately. All results were compared with those obtained from static 3D cultures. The live/dead assay revealed the presence of less than 20% of dead cells, which did not affect the cell cycle analysis. Cell cycle analyses highlighted the increment of cell fractions in proliferating phases ($S/G_2/M$) owing to medium perfusion in long-term cultures. After 7–10 days, the percentage of proliferating cells was 8–12% for dynamic cultures and 3–5% for the static controls. A higher fraction of proliferating cells was detected in the downstream scaffold. From a general perspective, this method provided data with a small standard deviation and detected the differences between

static and dynamic cultures and between upper and lower scaffolds. Our methodology can be extended to other cell types to investigate the influence of 3D culture conditions on the expression of other relevant cell markers.

A.2 Introduction

Tissue engineering has been presented as a potential strategy in the field of regenerative medicine and, more recently, in the field of *in vitro* applications for developing models for physiology studies or drug testing(Khetani *et al*, 2006). Both applications require the *in vitro* development of three dimensional, high cell density grafts. Growing mammalian tissues *in vitro* is considered extremely challenging because of their need for important nutrients and their sensitivity to nitrogenated wastes (Freshney *et al*, 2000); a highly controlled environment and a culture method, capable of generating an *in vivo*-like microenvironment, are therefore indispensable (Martin *et al*, 2004; Gomes *et al*, 2006; Wang *et al*, 2003).

The different requirements in terms of nutrient supply and waste disposal in different tissues can be satisfied by using bioreactor systems capable of meeting those needs by modulating mass transfer (Martin *et al*, 2005). A bioreactor can be defined as "a device that reproduces the physiological environment (including biochemical and mechanical functions) specific to the tissue that is to be regenerated" (Bilodeau *et al*, 2006). Medium perfusion through cellularized 3D scaffolds enables the reduction of internal mass-transfer limitations (Bancroft *et al*, 2003); in particular, efficient oxygen transport is fundamental while culturing cells with high oxygen uptake rates, i.e. muscle cells. Mass-transfer improvement leads to an enhancement in cell numbers, which in turn improves the uniformity of cell distribution (Gomes *et al*, 2006; Vunjak-Novakovic *et al*, 2006; Radisic *et al*, 2006) and – in the case of stem cell cultures – can influence their differentiation

(Bilodeau *et al*, 2006; Janssen *et al*, 2006). These general effects of medium flow are well known, but the mechanism by which it influences single cell behavior is not yet clear, e.g., the enhancement in cell numbers can be attributed to an effect on the cell cycle increasing cell proliferation or to other factors such as cell viability. In addition, it is not well understood whether the proliferation rate (or the cell viability) is uniform within the cell population inside the 3D-domain of the perfused scaffold. Studies on *in vitro* 3D cultures are mainly focused on investigating cell number (DNA assay), viability (MTT test), morphology (scanning electron microscopy, histologies), and gene and protein expression (immunofluorescence staining, PCR). As some of these analytical methods do not provide quantitative information on a statistically relevant number of cells, and others only give mean values averaged on the whole population, different analytical techniques are needed to answer the questions posed earlier. Among the different experimental techniques available, flow cytometry is a powerful tool widely applied in 2D cultures to obtain quantitative information on cell size, viability, DNA content, and protein expression (Ormerod, 2000). Instead of supplying averaged values, this tool provides information on the distribution of these variables within the cell population. Flow cytometry has recently been applied to study dynamic cultures in suspension (Alam *et al*, 2004; Dang *et al*, 2004) and, in only a few cases, to investigate 3D cultures of adherent cells (Braccini *et al*, 2005; Schmidt *et al*, 2006). In these studies, the cells were extracted from the scaffold after detachment from trypsin (or analogue) and marked for phenotypic characterization. For our current research, we developed protocols to perform flow cytometric analyses of adherent cells cultured on 3D collagen scaffolds in a perfusion bioreactor with a particular focus on skeletal muscle cells. We analyzed the cell cycle to describe the fraction of cells in the duplication phases within a

culture, because no other method of analysis can furnish the same detailed information about cell cycles. Initially, live/dead cell fraction measurement was performed to verify the presence of a high percentage of living cells in the culture and to obtain repeatable data with flow cytometry after enzymatic scaffold degradation. To evaluate the uniformity of cell viability and cell cycle within the 3D-domain in the perfused scaffold, we analyzed two scaffold domains separately: the top one seeded with cells from the outset and the bottom one, without cells. Data on the live/dead cell fraction and its distribution within the cell population enabled us to investigate the presence and extension of areas with nonviable cells that could falsify cell cycle data. The cell cycle is a complex and highly ordered process that results in the duplication and transmission of genetic information from the parent cell to the duplicated cells.[13] The cell cycle can be divided into mitosis (M phase) and a period of cell growth termed interphase, which can be subdivided into the DNA synthesis period (S phase), and the pre- and post-DNA gap phases (G_1 and G_2 phases, respectively) (Alberts *et al*, 2002). Following the M phase, two possible outcomes occur for the new cells: the immediate start of another round of growth and division or the end of the active cell cycle that enters a state of quiescence termed G_0. A cell in the G_0 phase may perform normal cellular functions, but it is not preparing for division. Normal quiescent cells maintain the capability to re-enter the cell cycle, but need appropriate signals (Alberts *et al*, 2002). The percentage of cells in S/G_2/M phases is linked both to the frequency with which cells enter the duplication process and the proliferation rate. Data on the influence of medium perfusion on cell viability and/or on cell cycle can help explain how a bioreactor enhances cell numbers and uniformity of cell distribution. For this reason, we developed protocols to perform Propidium Iodide (PI) assays on adherent cells cultured on 3D scaffolds for investigating both the live/dead

fraction and the proliferation rate taking care to reduce data variability in order to measure any significant differences between them. Analogous protocols can be identified so that flow cytometry may be of value in a wide range of applications in investigating 3D cultures of any type of adherent cells, analyzing not only cell size, cell viability, and DNA content, but also protein expression, as it does for 2D cultures (Ormerod *et al*, 2000).

A.3 Materials and methods

A.3.1 Cell culture

The murine skeletal muscle cell line C_2C_{12} (ATCC, Manassas VA, USA) was grown in Dulbecco's modified Eagle medium (DMEM, Sigma-Aldrich, Milano, Italy) supplemented with 10% fetal bovine serum (FBS, Gibco-Invitrogen, Milano, Italy) and 1% penicillin-streptomycin solution (1000 U/ml, Invitrogen, Milano, Italy) on standard 100 mm Petri Tissue Culture dishes, in a 95% humidified and 5% CO_2 atmosphere at 37°C and maintained at low confluence. The medium was regularly changed every other day.

A.3.2 Dynamic culture system

Our dynamic culture system was designed with 8 independent units, each composed of a culture chamber and a gas exchanger (Fig. 1). The culture chambers were designed with two distinct platforms made of polycarbonate (PC), each chamber containing a15 ml medium hold up, which also served as a culture medium reservoir. Medium perfusion was ensured by an 8-channel peristaltic pump (Masterflex® L/S Variable-Speed Modular Driver, Ismatec® Minicartridge Pump Heads, General Control, Milan, Italy). The scaffolds were placed inside a 5 mm

diameter hole created on a polydimethylsiloxane (PDMS) disk; the disk prevented the scaffolds from floating and ensured medium perfusion from the top to the bottom, thus avoiding fluid shortcutting and channeling (insert in Fig. 1A).

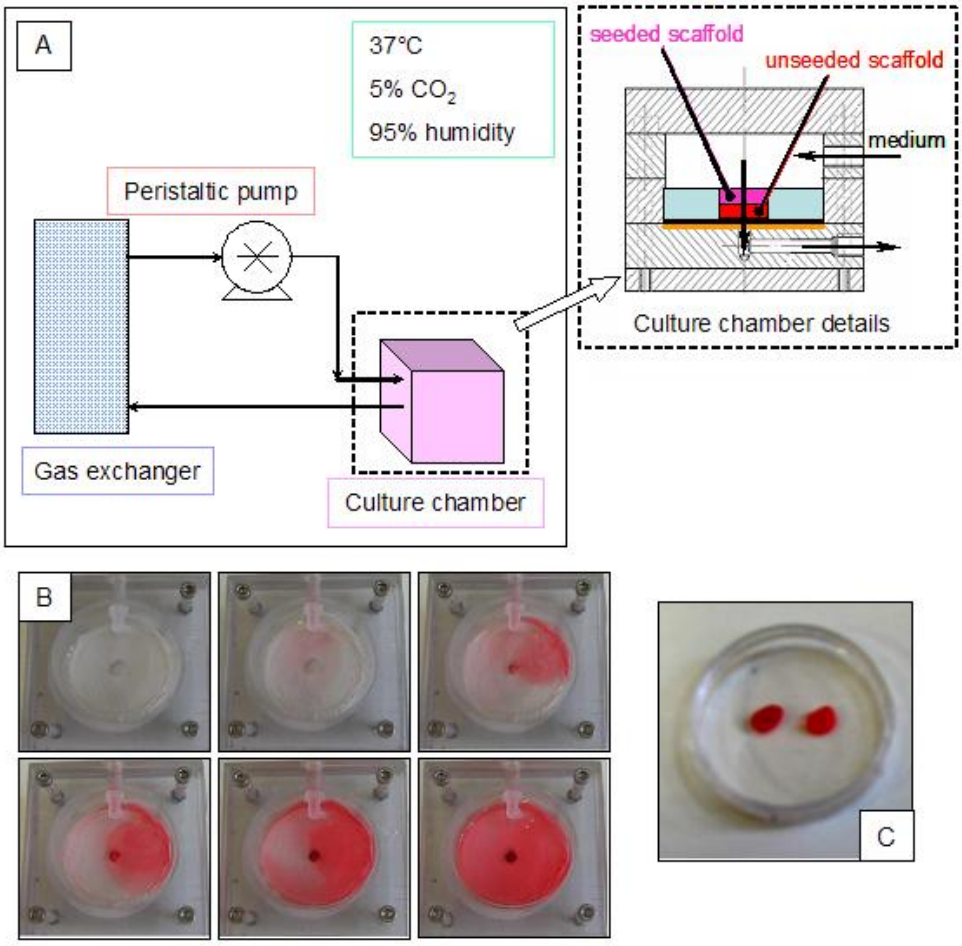

Figure 1. Dynamic culture system. The perfusion system is composed of a peristaltic pump, a gas exchanger and a culture chamber that also acts as a medium culture reservoir (A). On the right, an enlargement shows in more detail the culture chamber with two stacked scaffolds (the seeded one in purple and the unseeded one in red) placed in the PDMS punched disk (light blue). The medium flows from the top to the bottom (as indicated by the arrows). Between the PDMS disk and the medium outlet there is a nylon mesh (orange) to equalize medium flow. Images taken every minute (B) of the flow dynamic test performed by a step of colored tracer confirmed the absence of shortcuttings and stagnant regions. The scaffolds extracted after 5 minutes of flow dynamic testing were uniformly colored (C).

Between the PDMS disk and the medium outlet, a 100 μm mesh nylon netting was inserted to give mechanical support and induce equalization of the flow. To visualize the flow pattern developed in our bioreactors, we performed dynamic experiments introducing a step disturbance of a colored tracer in the system (Fig. 1B shows pictures taken each minute); the scaffold samples were then extracted and analyzed (Fig. 1C).

The gas exchanger unit was constructed with a gas permeable, non-porous silicon membrane (Platinum Cured Silicone Tubing, Vetrotecnica, Padua, Italy) and designed to ensure adequate oxygen and carbon dioxide concentrations, i.e. pH value in the culture medium.

Pharmed® tubing (General Control, Milan, Italy) was used to connect the culture chambers to the gas exchanger and the peristaltic pump. All connections were made with Luer® fittings (General Control, Milan, Italy).

The dynamic system was assembled and sterilized in an autoclave at 121°C for 20 min.

A.3.3 Cell seeding

The scaffold was a highly porous collagen sponge (Avitene® UltrafoamTM Collagen Hemostat. Davol inc., Craston, USA) shaped in disks of 7 mm in diameter and 3 mm in thickness. Previous research demonstrated how this material could be successfully used as a substrate for *in vitro* cell adhesion and growth 18, 19. The scaffold was cut larger than the hole in the silicon holder; as sponge shrinkage after wetting was taken into consideration, a larger scaffold was needed to ensure the formation of shortcutting or channeling.

The dry scaffolds were pre-treated with a culture medium inside standard 35 mm Petri dishes and incubated for 1 hour to allow protein deposition onto the matrix. The excess medium was then removed through absorption using sterile gauzes.

Confluent plates of C_2C_{12} were detached using trypsin/EDTA (Invitrogen, Milan, Italy), pelleted by centrifugation for 5 minutes at 250 g and counted with a hemocytometer. At day 0, either $5 \cdot 10^5$ or $1 \cdot 10^6$ cells were suspended in $10 \cdot 10^{-3}$ ml of culture medium and seeded on a scaffold placed in a 35 mm Petri dish. The scaffold was incubated for 4 hours and $5 \cdot 10^{-3}$ ml of medium was added on top of it every 30 minutes; before overnight incubation, 2 ml of medium was added in the Petri dish. Each seeded scaffold was then coupled with an identical but unseeded scaffold.

A.3.4 Static culture

On day 1, PDMS (Sylgard 184 distributed by Dow Corning, USA) punched disks were placed in 35 mm Petri dishes and two stacked collagen scaffolds − the unseeded scaffold on the bottom and the seeded scaffold on the top − were placed into the 5 mm diameter hole in the center of each silicon disk within the culture chamber (Fig. 1B). Three ml of culture medium was added and the cultures were kept at 37°C in a humidified atmosphere with 5% CO_2 for 4, 7, and 10 days changing the medium every three days.

A.3.5 Dynamic culture

On day 1, the culture chambers were filled with 9 ml of culture medium and the pump was operated for 30 minutes to fill the tubing. The 7 ml of culture medium remaining outside the tubing was subsequently removed, and two stacked collagen

scaffolds, unseeded at the bottom and seeded at the top, were placed into the PDMS punched disk inside each culture chamber. 9 ml of culture medium was then added inside each unit. The medium was pumped at a flow rate of 0.5 ml/min chosen on the basis of previous experience on other perfusion bioreactors developed in our laboratory. The apparatus was maintained at 37°C in a humidified atmosphere with 5% CO_2 for 4, 7, and 10 days without any other external, operator intervention.

A.3.6 Collagen scaffold degradation

Enzymatic degradation of the scaffold material was necessary to analyze the cells by flow cytometry. Each cellularized scaffold was placed in a 1.5 ml Eppendorf tube. $10 \cdot 10^{-3}$ ml of DMEM with 2 mg/ml collagenase from *Clostridium hystoliticus* (Sigma-Aldrich, Milan, Italy) was then added and incubated for 1 hour at 37°C to allow complete collagen digestion. After which, 1 ml of culture medium was added to the scaffold. The suspension was filtered with a 0.05 mm filter to remove debris and centrifuged at 250 g for 5 min to pellet the cells, which were finally re-suspended in the culture medium.

A $50 \cdot 10^{-3}$ ml solution was taken, with tripan blue added, and used to count the cells in suspension in a Burker chamber.

The degradation protocol was preliminarily tested by exploiting solubilized collagen absorbance around 270 nm. Collagen samples were placed in 1.5 ml of PBS (Phosphate Buffered Saline, Invitrogen, Milan, Italy) and amounts of collagenase ranging between $5\text{-}20 \cdot 10^{-3}$ ml were added. The solution was analyzed by a UV-VIS spectrophotometer (UV 500 Spectronic Unicam, Cambridge, England) at different time points. The Collagenase quantity affected the degradation times while the peak of the spectra depended only on the collagen sample volume. According to a calibration curve (data not shown), we used

spectrophotometric analyses to provide preliminary verification that our protocol would lead to complete scaffold degradation.

A.3.7 Measurement of mitochondrial activity

Cellular viability was measured by the MTT test (Sigma-Aldrich, Milan, Italy): 300 µL of the dye solution containing 5 mg/ml of the tetrazolium salt MTT in PBS were diluted to a final volume of 3 ml with PBS and added to the samples, which were incubated for 3 hours at 37°C. After the removal of the dye solution, a 3 ml solubilization solution made of 10% DMSO (Dimethyl Sulfoxide, Sigma-Aldrich, Milan, Italy) and 90% Isopropanol (Acros, Milan, Italy) was added to dissolve the formazan crystals. The samples were again incubated at 37°C, enabling complete dissolution, and then centrifuged at 250 g for 5 minutes to precipitate wastes. Clear solutions were then processed for absorbance readings at 580 nm with an UV500 spectrophotometer, Spectronic Unicam (Cambridge, UK). The recorded optical density (OD) is a function of the mitochondrial activity and is related to cell number.

A.3.8 Histological analyses

Samples seeded with $5 \cdot 10^5$ cells and cultured for 4 days, were fixed in 4% Paraformaldehyde (PFA, Sigma-Aldrich, Milan, Italy) for at least 1 hour, rinsed three times with PBS for 10 min, and maintained at +4°C covered by a thin layer of PBS. Before sectioning, fixed tissue specimens were dehydrated and embedded in paraffin (Sigma-Aldrich, Milan, Italy). Sectioning was accomplished with a microtome and 7-µm thick sections of the cultured collagen matrices were analyzed both by Hematoxylin-Eosin (H-E) (Sigma-Aldrich, Milan, Italy) staining and

Masson's trichrome staining using phosphomolybdic acid (Sigma-Aldrich, Milan, Italy). Cell density and distribution within the scaffold were then assessed by microscope observations (inverted microscope Olympus IX51 Tokyo, Japan); images were captured and acquired using a JVC KY-F30 3-CC camera supported by Pinnacle, DVTools - Capture & Playback Application software.

A.3.9 Flow cytometry

Flow cytometric analyses were performed using a FACScan Flow Cytometer Becton Dickinson (BD Biosciences, Milan Italy) equipped with an argon-ion laser (488 nm). All data were acquired and analyzed using CellQuest Pro (Becton Dickinson) software, with the exception of the cellcycle related analyses, which were performed with the ModFit LT (Verity Software House, Inc.) software specific for the DNA histogram deconvolution. Each sample was run through the flow cytometer to record $1\text{-}3\cdot10^4$ events.

A.3.9.1 Live/Dead assay using Propidium Iodide (PI) nucleic acid stain

PI binds to DNA by intercalating between the bases with little or no sequence preference and with a stoichiometry of one dye per 4-5 base pairs of DNA. PI is membrane-impermeant and generally excluded from viable cells, so that cells showing a positive fluorescence can be identified as non-viable.

The flow cytometry protocol follows: after the scaffold digestion procedure, cells were suspended in 400 µL of PBS. 50 µL of the PI (Sigma-Aldrich, Milan, Italy) solution (400 µL/ml PI in distilled water) and 50 µL of the Ribonuclease (RNAse) (Sigma-Aldrich, Milan, Italy) solution (1 mg/ml RNAse in PBS) were added for staining. The suspension was incubated at 37°C for 30 min and then analyzed with

the flow cytometer detecting the forward (FSC) and side light scatter (SSC) and the fluorescence emission at 542/85 nm, acquired on a logarithmic scale.

A.3.9.2 Live/Dead® Viability/Cytotoxicity kit

The Live/Dead® Viability/Cytotoxicity kit (Invitrogen, Milan, Italy) provides a two-color fluorescence cell viability assay that is based on the simultaneous determination of live and dead cells by two different dyes. Live cells are distinguished by the presence of intracellular esterase activity by the enzymatic conversion of the virtually non-fluorescent cell-permeant calcein AM to the intensely fluorescent calcein. The polyanionic dye calcein is retained within live cells, producing an intense uniform green fluorescence. Ethidium homodimer (EthD-1) enters cells with damaged membranes and undergoes a 40-fold enhancement of fluorescence upon binding to nucleic acids, thereby producing a bright red fluorescence in dead cells.

The flow cytometry protocol follows: after the scaffold digestion procedure, the cells were suspended in 1 ml of culture medium; 2 µL of calcein AM working solution (50 µM) and 4 µL of ethidium homodimer-1 solution (2 mM) were added. The cells were incubated for 15-20 minutes at room temperature, protected from light. After the incubation period, the stained cells were analyzed by flow cytometer detecting the forward and side light scatter, the calcein fluorescence emission at 530/30 nm, and the ethidium homodimer-1 fluorescence emission at 585/42 nm, acquired on logarithmic scales.

A.3.9.3 Cell Cycle Analysis

The DNA content of the cells was detected after the staining with PI. This dye behaves as already described; but, in this case, fixing cells prior to the staining

protocol permeabilizes the cell membrane, so that the DNA content of all the cells is accessible to the dye.

The flow cytometry Protocol follows: before digestion, the scaffold was incubated in 70% ethanol at 4°C for 30 minutes to fix the cells. The scaffold was then washed twice with PBS and digested by collagenase; collected cells were then suspended in 400 µL of PBS. 50 µL of the PI solution (400 µL/ml PI in distilled water) and 50 µL of RNAse solution (1 mg/ml RNAse in PBS) were added. The suspension was incubated at 37°C for 30 min and then analyzed by flow cytometer detecting the forward and side light scatter and the fluorescence emission at 585/42 nm, acquired on linear scale.

A.3.10 Statistical analyses

All the quantitative results were obtained from three or more samples. Data were expressed as mean values ± their standard deviations (SD). All collected data were analyzed by ANOVA from multiple comparisons, and the statistical significance was accepted at $p<0.05$.

A.4 Results and discussion

Scientific literature agrees on the need for efficient dynamic culture systems for the *in vitro* realization of 3D high density grafts (Martin *et al*, 2005; Vunjak-Novakovic *et al*, 2006; Wendt *et al*, 2005). The reduction of the oxygen-transfer limitation (Bancroft *et al*, 2003) is fundamental for culturing cells with high oxygen uptake rates, i.e. skeletal muscle cells. Elevated number of cells, high cell viability, and uniformity of spatial distribution are the major advantages of dynamic culture systems (Radisic *et al*, 2006; Strehl *et al*, 2005), but it is not clear

how medium flow leads to these important improvements. The elevated cell numbers and the uniformity of cell density could be due to the activation of different mechanisms regulating, for example, the cell cycle or the cell viability. The commonly performed analyses on 3D cultures of adherent cells cannot provide useful information to assist in the investigation of the bioreactor effects on cell cycle. On the other hand, flow cytometry is a powerful technique widely applied to 2D cultures, for example, in collecting information on cell viability and DNA content. Flow cytometry can be used to identify the presence of one or more markers in the same population and obtain quantitative information on statistically significant samples (Ormerod, 2000). Furthermore, flow cytometry allows us to evaluate not only a marker's average value, but also to evaluate the distribution of a specific marker in a population. Flow cytometry has been used to study dynamic cultures in suspension (Alam *et al*, 2004; Dang *et al*, 2004) and, in only a few cases, to investigate 3D cultures of adherent cells (Braccini *et al*, 2005; Schmidt *et al*, 2006). In these studies the cells were extracted from the scaffold after detachment with trypsin (or analogue); however, with these methods the complete cell extraction from a 3D scaffold with highly interconnected pores present certain difficulties. Using a method of scaffold degradation, which does not damage the cells, e.g. enzymatic digestion, ensures that all the cells can be collected. Moreover, to our knowledge flow cytometry has never been applied to study the cell cycle within a population of cell grown in a 3D scaffold.

In this study, we first developed a new perfusion bioreactor and verified its functionality in supporting a uniform skeletal muscle cell culture within porous 3D scaffolds. We carried out different tests on the fluid-dynamic and on the cell growth for validating the bioreactor, in terms of reproducibility and repeatability of

the data. We then developed protocols to perform accurate flow cytrometric analyses of these cell populations. In particular, we tested our protocols with adherent C_2C_{12} cells cultured on 3D collagen scaffolds and stained with PI in order to investigate live/dead cell fraction. Finally, we applied PI flow cytometry for the measurement of the fraction of doubling cells.

A.4.1 Validation of bioreactor for cell culture

The dynamic cell culture method was validated by flow dynamic tests, cell count, histologies and MTT tests.

The uniformity of flow perfusion was assessed using a colored tracer; a step disturbance of the tracer gave a uniform color distribution in the culture chamber within 5 minutes, confirming the absence of stagnant regions (Fig. 1B). Moreover, the intense and uniform scaffold coloration gave additional evidence of the absence of shortcutting and channeling of the flowing solution (Fig. 1 B and C). The uniformity of the medium flow permitted accurate control of the cell microenvironment by means of an optimized dynamic culture protocol, which resulted in a low standard deviation of the obtained data.

The cell behavior is highly influenced by oxygen and metabolite concentrations, which can be far from uniform in a 3D culture inducing a position-dependent cell behavior. To better investigate the uniformity of cell behavior, we analyzed separately two scaffolds stacked in the same chamber and simulated one 6mm thick scaffold. An unseeded scaffold was placed at the bottom of the hole in the center of the PDMS disk and a seeded one was placed on top of the other (Fig. 1A).

Cell counts were performed on C_2C_{12} cells cultured in static and dynamic conditions for 4 days. Data obtained from cell counts showed an enhancement of cell numbers in dynamic cultures (Fig. 2 A and B) and confirmed the efficiency of

our perfusion bioreactor as a cell culture apparatus. In detail, the dynamic culture inside our bioreactor led to a doubling of the cell number in the seeded scaffolds (Fig. 2 A) and a tripling in the unseeded scaffolds (Fig. 2 B) when compared with static culture conditions. As expected, the positive influence of medium flow was much more evident in the lower scaffold, where static conditions maintain little control over metabolites and waste concentration. The effect was not dependent on the initial seeding density as the proportions were the same for the two cases of $5{\cdot}10^5$ and $1{\cdot}10^6$ seeded cells.

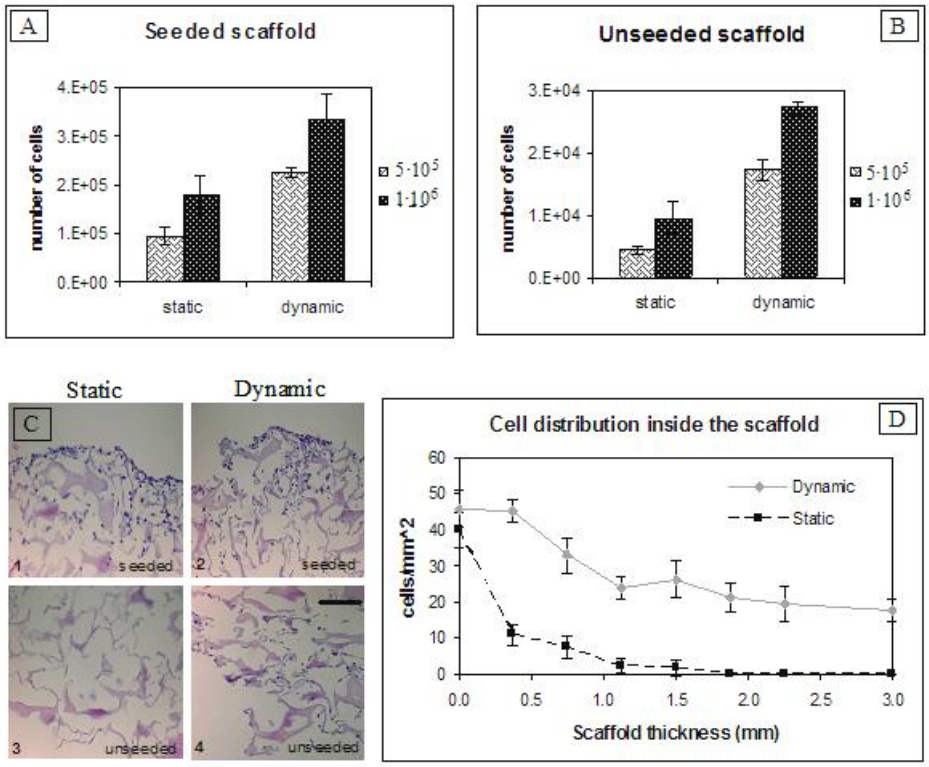

Figure 2. Number of cells counted in the seeded (A) and unseeded (B) scaffolds, cultured in static and dynamic conditions for 4 days, starting from either $5{\cdot}10^5$ or $1{\cdot}10^6$ seeded cells. Hematoxylin-Eosin histologies (C): images of the seeded surface (1, 2) and the opposite one (3, 4) of scaffolds seeded with $5{\cdot}10^5$ cells and cultured in static (1, 3) and dynamic conditions (2, 4) for 4 days (Magnification x200. Scale bar 100 μm). Plot of cell density vs. the distance from the seeded surface (D) obtained by analysis on histology images.

Histological analyses were performed on scaffolds seeded with $5 \cdot 10^5$ cells and cultured for 4 days. H-E and Masson's trichrome staining were performed, and representative examples of H-E microscope images are reported in Fig. 2 C. Staining of the scaffolds maintained in static conditions confirmed a high cell density in the seeded surface (Fig. 2 C_1) and the almost total absence of cells in the lower part (Fig. 2 C_3). On the contrary, cell culturing inside the bioreactor allowed not only a high density near the seeded surface (Fig. 2 C_2), but also the presence of a detectable number of cells in the opposite region (Fig. 2 C_4). A quantitative description of cell distribution is given in Fig. 2D where the cell density in different sections of the seeded scaffold, evaluated using images of H-E staining, is plotted as a function of the distance from the seeded surface. Static cultures resulted in a steep decrement of cell density down from 40 cells/cm^2 to almost zero within 1 mm in thickness. On the contrary, dynamic culture induced a smoother decrement in the upper part of the scaffold as the density reached a minimum of approximately 25 cells/cm^2 in 1 mm and then stabilized. High resistance to oxygen, metabolite, and waste diffusion in static cultures led to the presence of cells only within a thickness of 1 mm (Vunjak-Novakovic *et al*, 2006; Wendt *et al*, 2006).

With regards to long-term cultures, only the MTT test was performed. The optical absorbance was recorded after 4 and 7 days of culture both in static and dynamic conditions. The MTT semi-quantitative assay confirmed the importance of using a perfusion bioreactor for long-term cultures: after 7 days dynamic culture resulted in doubled cell viability ($p<0.01$) (data not shown).

We thus verified that this newly designed bioreactor allowed skeletal muscle cell growth and proliferation throughout the entire scaffold thickness, in line with data reported in literature (Radisic *et al*, 2006; Cimetta *et al*, 2007; Zhao *et al*, 2005).

Moreover, the system culture was robust and allowed repeatability data with small standard deviation.

A.4.2 Flow cytometric analysis

A.4.2.1 Validation of flow cytometry protocol

To collect the cells for flow cytometric analyses, the scaffold was degraded with the specific enzyme collagenase. Enzyme concentration and digestion time were optimized to minimize the damage of cell membranes and the presence of scaffold debris, as collagen particles with the dimension of a cell must be avoided as they would over-estimate the number of unmarked cells and, consequently, of the total cell number.

The degradation process was followed with UV-VIS spectrophotometry, as reported in the *Materials and Methods* section. This analysis permitted the identification of the optimal amount of collagenase and degradation time; however, the sensitivity of this technique is too low to ensure the absence of debris at the end. The presence of negligible debris had to be checked by flow cytometry. Both scaffolds - the upper, seeded one and lower, unseeded one - were analyzed and in every case the debris signal was located in the bottom-left corner of the side-forward scatter dot plot, as commonly happens for 2D cultures (Fig. 3 A and C). This dot-plot fashion made it possible to easily distinguish debris from the cell population (Fig. 3 C).

After the scaffold degradation, flow cytometric analysis was performed using PI to investigate both the percentage of living cells and the cell cycle. Fig. 3 shows the obtained dot plots and histograms. Each fluorescence signal detected by the flow-cytometer is characterized by a width correlated with the particle dimension and by

an area related with the total particle fluorescence. Dot plot of PI fluorescence area versus width in the case of cell cycle analysis (Fig. 3 E) allowed for the distinction between cells, debris, and aggregates.

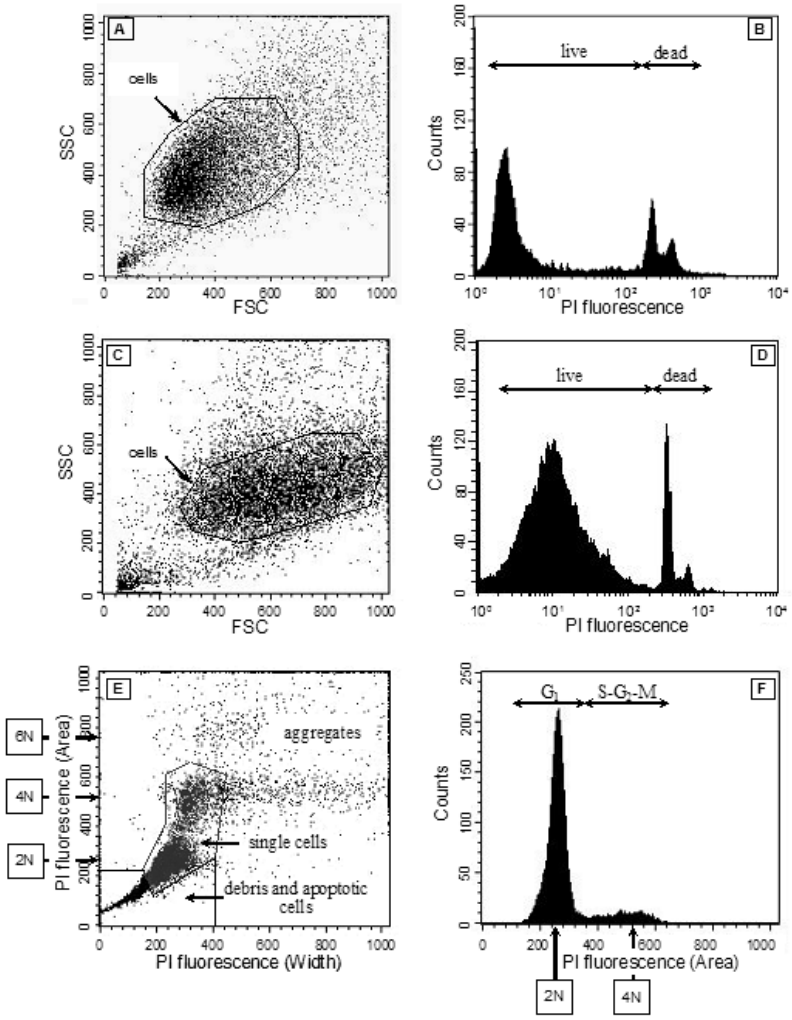

Figure 3. Examples of data collected by flow cytometry. Fig. (A) represents a dot plot showing forward (FSC) vs. side light scatter (SSC) of a population of C_2C_{12} cultured in Petri dish; dots related to single cells were selected by using a gate, as shown. Fig. (B) represents the histogram of the fluorescent intensity of the cell population gated in Fig. (A) and stained with PI for live/dead assay; live cells (low fluorescence) can be distinguished from non-viable cells (high fluorescence). Fig. (C) and (D) are equivalent graphs of (A) and (B) but refer to a population of C_2C_{12} cultured in the 3D collagen scaffold. Fig. (E) is an example of a dot plot showing

the area vs. width of the fluorescence signal emitted by a cell and detected by the flow-cytometer. This dot plot refers to cells cultured in 3D scaffold, fixed with ethanol and stained with PI: the area of the PI fluorescence signal is proportional to DNA content; the width of PI fluorescence signal is used to discriminate between single cells and aggregated cells with the same overall DNA content. Based on these two parameters, events were classified as debris and apoptotic cells (sub-G_1 DNA content), single cells, and aggregates. Fig. (F) represents a histogram of the single cell population stained with PI after fixation and gated as shown in Fig. (E); the peak at low fluorescence represents cells in G_1 (2N = diploid cells), at double fluorescence there is a small peak corresponding to cells in the G_2 and M phases (4N = tetraploid cells), intermediate fluorescence values represent cells in the S phase which are doubling their DNA.

The negligibility of the collagen debris was further verified for live/dead assays; in this case, PI marked only cells with damage on the cytoplasmatic membrane while living cells were not marked (Robinson *et al*, 1997). The histogram for PI fluorescence allows for identification of the marked dead cells (Fig. 3 B and D). Quantifying the living cells, instead, requires a correct gating in the side-forward dot plot to exclude collagen debris from the count. Inappropriate collagen degradation would lead to relevant error in estimating the number of living cells. To verify our protocol, we performed the analogue measurement with a live/dead kit as reported in the *Materials and Methods* section. This kit is widely used, and it has a double fluorescence with emission at 530/30 nm for living and 585/42 nm for dead cells. The double fluorescence reduces the risk of including scaffold debris in the statistical data analysis. This assay was performed on a 4-day static culture and the results were comparable with the ones obtained using PI (data not shown); for this reason, all other measurements were carried out only using PI.

The protocol for cell cycle analysis required a fixation step with 70% ethanol before scaffold digestion, and we verified that such a step had not reduced the collagenase efficiency.

Finally, we verified that the scaffold degradation protocol did not alter cell viability. Two cell populations were cultured on Petri dishes under the same static conditions; one was suspended in a collagenase solution, simulating the scaffold degradation protocol, while the other was used as a control. Both populations were then analyzed by flow cytometry after PI staining. Experimental viability data were drawn from the PI histogram as shown in Fig. 3 D; live/dead percentages of the two samples were comparable, confirming that the presence of collagenase had a negligible effect.

The flow cytometric protocols were developed and tested, as pointed out above, than applied to investigate the effect of dynamic cultures on C_2C_{12} viability and percentage of doubling cells.

A.4.2.2 Live/Dead Cell Fraction

The percentages of living cells for two time points (4 and 7 days) and for the two seeding densities were measured. In static cultures, the viability set between 70 and 85% was neither significantly dependent on the number of seeded cells nor on the culture period. After 7 days, the percentage of living cells for $1 \cdot 10^6$ seeded cells, set around 83% in both seeded and unseeded scaffolds, showed the spatial uniformity of this parameter. At the first time point, the analysis was not performed on the unseeded scaffold as the number of cells was not sufficient to proceed with the flow cytometry protocol. This observation is in agreement with the histological analyses (Fig. 2 C and D) and demonstrates the importance of medium perfusion in allowing cell growth in regions far from the seeded surface (Radisic *et al*, 2006).

The dynamic culture improved mass transport allowing a rapid enhancement of cell viability and led to 95±1% of living cells after 4 days. In the seeded scaffold the percentage decreased to a value of 87±3% after 7 days, slightly higher than that of

static cultures. At this time point, living cells in the unseeded scaffolds were 94±2%, a significantly higher percentage (p=0.002) than the one measured for the seeded scaffolds, and it was comparable to the data obtained after 4 days of dynamic culture. These data confirmed the ability of a perfusion bioreactor to maintain C_2C_{12} high viability during long term cultures. This information verifies that data on cell cycles are not influenced by non-viable cells.

A.4.2.3 Cell Cycle

The property of PI to bind stoichiometrically to DNA allowed us to distinguish between cells in the G_1 phase from cells in the S, G_2 and M phases (Fig. 3 E and F) (Anderson *et al*, 1998). The percentages of doubling cells (cells in the S, G_2 and M phases) were evaluated at three time points (4, 7 and, 10 days) in static and dynamic cultures, and resulting data are reported in Tab. 1. Data for the unseeded scaffold in static cultures at day 4 and 7 were not available due to an insufficient number of cells grown in this area.

Table 1. Percentage of cells in $S/G_2/M$ phases detected by flow cytometer after PI staining. The scaffolds were seeded with either $5{\cdot}10^5$ or $1{\cdot}10^6$ cells and cultured for 4, 7 and 10 days in static and dynamic conditions. The number of cells was not sufficient to perform flow cytometric analysis in unseeded scaffolds cultured in static conditions for 4 and 7 days (n.d. = not detectable).

	Static Culture		Dynamic Culture	
No. of Seeded Cells	Seeded Scaffold	Unseeded Scaffold	Seeded Scaffold	Unseeded Scaffold
4 days				
5×10^5	14.6 ± 0.7	n.d.	12.7 ± 1.2	16.4 ± 3.5
1×10^6	19.9 ± 2.9	n.d.	13.9 ± 2.2	23.6 ± 1.7
7 days				
5×10^5	4.3 ± 0.9	n.d.	7.4 ± 1.2	12.0 ± 1.2
1×10^6	5.3 ± 1.5	n.d.	9.6 ± 3.0	11.6 ± 0.8
10 days				
5×10^5	2.1 ± 1.5	4.3 ± 0.4	6.0 ± 0.2	6.7± 1.1
1×10^6	4.0 ± 1.1	3.7 ± 1.8	6.1 ± 1.7	7.0 ± 0.9

The percentage of doubling cells was greatly influenced by culture duration as the numbers decreased over time as shown in Fig. 4. The trend in decreasing cell numbers was observed in both dynamic and static conditions, as well as for the two different amounts of seeded cells, considering cell population ageing and increased cell density (Figallo *et al*, 2007). The fraction of non-viable cells was low, as reported in the previous paragraph, and did not alter the cell cycle data because it was distributed between the different phases with the same percentage of live cells.

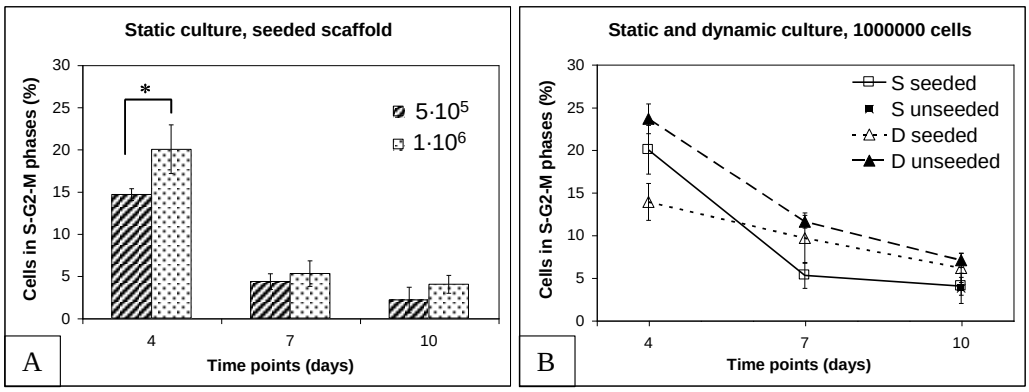

Figure 4. Data of cell cycle analysis by PI staining. The histogram (A) shows the comparison between the percentage of cells in the $S/G_2/M$ phases for scaffolds seeded with either $5{\cdot}10^5$ ( ) or $1{\cdot}10^6$ ( ) cells and cultured under static condition for 4, 7, and 10 days (∗ p=0.01). The plot (B) is related to cultures started with $1{\cdot}10^6$ cells and it shows the percentages of cells in the $S/G_2/M$ phases in the seeded (empty signs) and unseeded (full signs) scaffolds cultured under static (square) or dynamic (triangle) conditions for 4, 7, and 10 days.

The influence of the seeded density on the percentage of doubling cells was statistically significant (p=0.01) only at the first time point in the seeded scaffold of the static cultures and in the unseeded scaffold in dynamic cultures. In these cases $1{\cdot}10^6$ seeded cells led to a higher fraction of cells in $S/G_2/M$ phases as shown in Fig. 4 A for the case of static culture (an analogue histogram can be obtained for

dynamic cultures from data in Tab. 1). At the same time points, no significant differences were observed in the seeded scaffold dynamically cultured in the bioreactor. After 4 days these scaffolds had the highest cell density (Fig. 2 A), suggesting the presence of a critical cell density level above which the cell numbers do not affect cell cycle. This hypothesis provides an explanation for the flow cytometric data, and this could justify the absence of significant differences for long term cultures, but further investigation is needed in order to confirm these results.

Comparison between the time trends of static and dynamic conditions is reported in Fig. 4 B in the case of $1 \cdot 10^6$ seeded cells. This figure shows how dynamic cultures in our bioreactor allows a slower decrement of the percentage rate of doubling cells, thus keeping it higher than in static conditions in long term cultures by stimulating the cells to enter the $S/G_2/M$ phases. In static cultures, the fraction of doubling cells dropped from 15-20% at the first time point to 4-5% after 7 days, values similar to the minimum reached after 10 days. The decrement was smoother in dynamic cultures leading to a higher proliferation rate at 7 and 10 days in both the seeded ($p<0.01$ for $5 \cdot 10^5$ seeded cells) and unseeded scaffolds ($p<0.05$). Moreover, the unseeded scaffolds showed the highest percentage of cells in $S/G_2/M$ phases during the entire culture period, but the difference decreased over time.

A.5 Conclusions

In our research we focused on the development of new analysis protocols for obtaining quantitative information on a population of adherent cells cultured in a 3D scaffold. Researchers agree that cells adhered within 3D scaffolds need proper bioreactors to grow and proliferate and we suggest that the protocol we proposed in this study can help to obtain information for understanding the influences of

medium flow on cellular behavior. In particular, we focused our attention on flow cytometry techniques and their application for investigating the fraction of doubling cells within a population of skeletal muscle cells.

A critical step of protocol for flow cytometric analysis of culture in 3D-domain is the cell detachment and extraction from the scaffold. We performed the scaffold degradation; parameters of this step were optimized leading to the negligible presence of scaffold debris so that their signal could be easily distinguished from those of the cells. Furthermore, we verified that the digestion protocol did not alter the live/dead cell fraction and that the presence of dead cells has a negligible influence on the cell cycle data.

The data collected in this study using PI staining demonstrated the application of flow cytometry for investigating the effect of medium flow on C_2C_{12} cell cycles: the data has small standard deviation and, in some cases, the difference between static and dynamic cultures or between seeded and non-seeded scaffolds was statistically significant. In agreement with the literature, the medium perfusion through the collagen scaffold led to an improvement of mass transport inside the culture 3D-domain, especially in the lower scaffold, where the control of metabolite and waste concentration is in static conditions (Radisic *et al*, 2006; Cimetta *et al*, 2007; Wendt *et al*, 2005): both cell viability and the percentage of doubling cells had their highest values in the non-seeded scaffold when cultured in a bioreactor.

This research is relevant to a wide application of flow cytometry to *in vitro* 3D cultures of every type of adherent cells; analogous protocols can now be identified to achieve quantitative information on other parameters commonly investigated in 2D cultures, such as protein expression.

A.6 Acknowledgment

We would like to thank Christopher Cannizzaro and the Tissue Engineering Resource Center for the precious assistance provided during the bioreactor development. We would also like to thank Città della Speranza, the Regione Veneto (Azione Biotech II), the MIUR (Italian Ministry of University and Research), and the University of Padua for the financial support.

A.7 References

Alberts B, Johnson A, Lewis J, Raff M, Roberts K, Walter P. 2002. Molecular biology of the cell. 4th ed. Garland:New York.

Alam S, Sen A, Behie LA, Kallos MS. 2004. Cell Cycle Kinetics of Expanding Populations of Neural Stem and Progenitor Cells In Vitro. Biotech Bioeng 88(3):332-347.

Anderson HJ, de Jong G, Vincent I, Roderge M. 1998. Flow Cytometry of Mitotic Cells. Exp Cell Res 238:498-502.

Bancroft GN, Sikavitsas VI, Mikos AG. 2003. Design of a flow perfusion bioreactor system for bone tissue engineering applications. Tissue Eng 9:549-554.

Bilodeau K, Mantovani D. 2006. Bioreactors for Tissue Engineering: Focus on Mechanical Constraints. A Comparative Review. Tissue Eng 12(8):2367-2383.

Braccini A, Wendt D, Jaquiery C, Jakob M, Heberer M, Kenins L, Wodnar-Filipowicz A, Quarto R, Martin I. 2005. Three-Dimensional Perfusion Culture of Human Bone Marrow Cells and Generation of Osteoinductive Grafts. Stem Cells 23:1066–1072.

Cannizzaro C, Tandon N, Figallo E, Park H, Gerecht S, Radisic M, Elvassore N, Vunjak-Novakovic G. 2007. Practical aspects of cardiac tissue engineering with electrical stimulation. Methods Mol Med. 140:291-307.

Cimetta E, Flaibani M, Mella M, Serena E, Boldrin L, De Coppi P, Elvassore N. 2007. Enhancement of viability of muscle precursor cells on 3D scaffold in a perfusion bioreactor. Int J Artif Org 30:415-428.

Dang SM, Gerecht-Nir S, Chen J, Itskovitz-Eldor J, Zandstra PW. 2004. Controlled, Scalable Embryonic Stem Cell Differentiation Culture. Stem Cells 22: 275-282.

Figallo E, Flaibani M, Zavan B, Abatangelo G, Elvassore N. 2007. Micropatterned Biopolymer 3D Scaffold for Static and Dynamic Culture of Human Fibroblasts. Biotechnol Prog 23(1):210-216.

Freshney R. 2000. Culture of animal cells—a manual of basic techniques. 4th ed. Wiley-Liss:New York.

Gomes ME, Bossano CM, Johnston CM, Reis RL, Mikos AG. 2006. In Vitro Localization of Bone Growth Factors in Constructs of Biodegradable Scaffolds Seeded with Marrow Stromal Cells and Cultured in Flow Perfusion Bioreactor. Tissue Eng 12(1):177-188.

Janssen FW, Oostra J, van Oorschot A, van Blitterswijk CA. 2006. A perfusion bioreactor system capable of producing clinically relevant volumes of tissue-engineered bone: In vivo bone formation showing proof of concept. Biomaterials 27:315-323.

Khetani SR, Bhatia SN. 2006. Engineering tissues for in vitro applications. Current Opinion in Biotechnology 17:524–531.

Martin I, Wendt D, Heberer M. 2004. The role of bioreactors in tissue engineering. Trends Biotechnol 22(2):80-86.

Martin Y, Vermette P. 2005. Bioreactors for tissue mass culture: Design, characterization, and recent advances. Biomaterials 26:7481–7503.

Ormerod M. 2000. Flow cytometry-a practical approach. Oxford University Press.

Radisic M, Cannizzaro C, Vunjak-Novakovic G. 2006. Scaffolds and fluid flow in cardiac tissue engineering. Fluid Dynamics and Material Processing 2(1):1-15.

Robinson J, Darzynkiewicz Z, Dean P, Dressler L, Rabinovich P, Stewart C, Tanke H, Wheeless L. 1997. Current Protocols in Cytometry. John Wiley & Sons, Inc: New York.

Schmidt D, Asmis LM, Odermatt B, Kelm J, Breymann C, Gössi M, Genoni M, Zund G, Hoerstrup SP. 2006. Engineered Living Blood Vessels: Functional Endothelia Generated From Human Umbilical Cord-Derived Progenitors. Ann Thorac Surg 82:1465–71.

Strehl R, Tallheden T, Sjogren-Jansson E, Minuth WW, Lindahl A. 2005. Long-term maintenance of human articular cartilage in culture for biomaterial testing. Biomaterials 26:4540-4549.

Vunjak-Novakovic G, Radisic M, Obradovic B. 2006. Cardiac tissue engineering: effects of bioreactor flow environment on tissue constructs. J Chem Tech Biotech 81(4):485-490.

Wang Y, Uemura T, Dong J, Kojima H, Tanaka J, Tateishi T. 2003. Application of Perfusion Culture System Improves in Vitro and in Vivo Osteogenesis of Bone Marrow-Derived Osteoblastic Cells in Porous Ceramic Materials. Tissue Eng 9(6):1205-1214.

Wendt D, Jakob M, Martin I. 2005. Bioreactor-based engineering of osteochondral grafts: from model systems to tissue manufacturing. Journal of Biosci and Bioeng 100(5):489-494.

Wendt D, Stroebel S, Jakob M, John GT, Martin I. 2006. Uniform tissues engineered by seeding and culturing cells in 3D scaffolds under perfusion at defined oxygen tensions. Biorheol 43(3-4):481-488.

Zhao F, Ma T. 2005. Perfusion Bioreactor System for Human Mesenchymal Stem Cell Tissue Engineering: Dynamic Cell Seeding and Construct Development. Biotech Bioeng 91:482-493.

Appendix B

Population balance model of a muscle stem cell culture

C. Luni[1], M. Strumendo[1], L. Boldrin[2], P. De Coppi[2] and N. Elvassore[1,]*

[1]Dip. di Principi e Impianti di Ingegneria Chimica, Università di Padova, Italy.

[2]Dip. di Oncoematologia Pediatrica, Università di Padova, Italy.

*Corresponding author:

Nicola Elvassore

Department of Chemical Engineering

University of Padova

Via Marzolo, 9

35131 Padova (PD)

Italy

nicola.elvassore@unipd.it

Telephone: +390498275469 - FAX: +390498275461

B.1 Abstract

Stem cell is becoming an important cell source in now emerging fields such as tissue engineering, regenerative medicine, or cell therapy. In particular, muscle stem cells and muscle precursor cells derived from skeletal muscle are of enormous importance for their potential in muscle regeneration and gene transfer. Prediction and control of a stem cell population growth are essential to design and optimize in vitro cultures. In this work, the expansion of satellite stem cells, a muscle precursor cell, is modeled by a population balance equation (PBE). Two biological phenomena are considered: cell growth and division. Both phenomena take into account the contact inhibition that occurs at high cell density due to a complex network of molecular signals: an original approach based on cell radial distribution function is proposed. The PBE, solved using the method of moments, gives the temporal evolution of cell number density as a function of volume. Model parameters are fitted to experimental data, consisting of measurements by a Coulter Counter® at different time points. Satellite stem cells are isolated by single muscle fibers of adult rat and cultured on plastic dishes. A sensitivity analysis highlights the importance of single processes, such as proliferation, growth, and contact inhibition. The model is validated by the experimental results and is capable of predicting the number density evolution of satellite cell cultures with different initial cell seeding densities. In addition, the temporal evolution of cell number densities for each cell generation is simulated.

B.2 Introduction

Stem cells are becoming an important cell source in now emerging fields such as tissue engineering, regenerative medicine or cell therapy. They are characterized by two properties: multipotency and self-renewal ability. Firstly described by Mauro (1961), satellite cells, derived from skeletal muscle myofibers, are able of self-renewal but are committed to muscle phenotype. Nonetheless, it is now recognized their important role in muscle regeneration (Seale and Rudnicki, 2000; Chargé and Rudnicki, 2004). Their progeny, myoblasts, fuse to form multinucleated myotubes sharing their nuclei. This feature suggests that satellite cells can be used as a powerful vector for gene transfer by in vivo satellite cell delivery (Negroni, et al., 2006). However, their therapeutic use will require a means to expand in vitro the cell population from a biopsy, and some complications still need to be solved to define a robust clinical procedure. As biological experiments are highly costly and time-consuming due to the complexity of biological mechanisms, the use of quasi trial-and-error experiments may require a large number of experiments to optimize the operational activities (Viswanathan and Zandstra, 2003; Davey and Zandstra, 2004).

An accurate modeling of stem cell cultures may be used to pursue this goal. The first step in stem cell modeling is to elaborate a mathematical framework to rationally describe experimental observations; then, the prototype model may be used for a priori experimental design (Sidoli, et al., 2004). Viswanathan and Zandstra (2003) recently reviewed different types of models developed to characterize and predict the behavior of stem cells such as haematopoietic, intestinal crypt, neural and embryonic stem cells. They can be classified in stochastic models, where cell processes occur randomly because of cell-

autonomous properties, and deterministic models, where cells give precise responses to exogenous stimuli. Models that attempt to combine both approaches were recently proposed (Viswanathan, et al., 2005). In particular, Deasy et al. (2002) developed a model, applied to muscle-derived stem cells, to calculate the cell mitotic fraction from the cell cycle time and population growth data.

Mantzaris (2005) reviewed many possible sources of heterogeneity in a cell culture, difficult to be all taken into account within a mathematical framework. Some models describe bulk responses of stem cell populations, whereas other models consider a detailed characterization of a single cell without the ability of describing a cell property distribution within a population.

Instead, a PBE approach is a mathematical tool able to rationally describe not only average properties but also distributed properties within an ensemble of cells, i.e. within a whole cell population. In fact, in this kind of model, cell properties are defined at single-cell level. Since the first paper by Eakman, et al. (1966), several papers were devoted to PBE models of microbial cell populations (for references on this topic see Ramkrishna, 2000), few papers to PBEs of mammalian cells (Pisu, et al., 2004), but, so far, no works reported the use of PBEs for describing stem cell cultures.

In this work, we developed a PBE model to rationally describe the expansion of satellite stem cells in culture. The values of model parameters were obtained from experimental data and they were used to predict the cell number density and the volume distribution as a function of time.

The model was also enhanced to simulate the temporal evolution of cell number densities for each cell generation. Due to telomere shortening, there is a maximum number of generations that satellite cells can achieve before reaching a non-proliferative state called cellular senescence (Wernig et al., 2005). In this context,

the model can be effectively used to predict the myogenic potential of a population of satellite cells by keeping track of which generation cells belong to.

B.3 Materials and methods

B.3.1 Satellite cells isolation

Satellite cells derived from primary culture are used in the experiments. Myofibers are isolated as previously described (Rosenblatt, et al., 1995). Briefly, *flexor digitorum brevis* (FDB) muscles of Winstar rat (Charles River, Monza, Italy) are digested for 3 h at 37°C in 0.2% (weight/vol) collagenase type I (Sigma-Aldrich, Milano, Italy) diluted in Dulbecco's modified Eagles medium (DMEM, Sigma-Aldrich). Following muscle digestion, single fibers are selected at the inverted microscope (Olympus IX71, Tokyo, Japan) and plated on deep plastic dishes (Falcon, BD Biosciences, San Diego, California, USA), pre-coated with rat collagen (Sigma-Aldrich). Myofibers are incubated at 37.5°C, 5% CO_2 in a humidified tissue culture incubator. At the third day in culture, the proliferating medium, consisting of DMEM containing 20% (vol/vol) of foetal bovine serum (Gibco-Invitrogen, Milano, Italy), 10% (vol/vol) of horse serum (Gibco-Invitrogen) and 0.5% (vol/vol) of chicken embryo extract (MP-Biomedicals, Verona, Italy), is added to the dishes. Medium is changed every 2 days. At 70-80% confluence, cells are trypsinized and seeded for the experiments.

B.3.2 Experiments and analysis

Two sets of experiments are performed in order to define model parameters and to check model reliability. In the first set, cells are seeded at $N_0 = 500\,\text{cell/cm}^2$

density on 7 plastic dishes (10 cm^2 area) and cultured in identical conditions with proliferating medium which is changed every 48 hours. Every 24 hours, cells from one plastic dish are detached with trypsin (Gibco-Invitrogen) and counted by Z1™ Series Coulter Counter® Cell and Particle Counter (Beckman Coulter, Milano, Italy) which provides the cell number density as a function of volume. This procedure is adopted for a one-week culture period and this experiment is repeated twice to detect variability.

In the second set of experiments, cells are seeded on plastic dishes at different densities: $N_0 = 100, 500, 1000\,\text{cell/cm}^2$. The measurements of the cell number density as a function of volume are carried out as reported above.

B.4 Mathematical modeling

B.4.1 Process description

We assume that the state of a cell in the culture is defined by its volume. The choice of cell volume as the internal variable is motivated by flow cytometric studies: we stained a satellite population by propidium iodide (Sigma-Aldrich, Milano, Italy) and we analyzed it by a FACScan™ flow cytometer (Becton Dickinson, Milano, Italy). It was observed that cells at the beginning of the S-phase had a larger forward scatter (FSC) intensity, which is related to cell volume, than cells in G_1-phase. This result suggests that, for skeletal muscle stem cell cultures, cell volume can be assumed to be the driving force to enter the division phase.

Cells are approximated by round disks adherent on the surface of a Petri dish, assumed to be a two-dimensional system. $W(V,t)dV$ represents the number of

cells per unit plastic dish surface that at time t have volume between V and $V + dV$.

The biological process we reproduce by our model is schematically illustrated in Figure 1. In the model we neglect the lag phase occurring in the first two days after seeding, when cells adapt themselves to the new environment. The model initial conditions refer to experimental data at the beginning of the third day in culture. The initial cell population is heterogeneous in terms of cell volume. Cell growth increases cell volume deterministically, whereas cell division can occur at different cell volumes following a statistical distribution. Cell division can be asymmetric, which implies a different lifetime for each daughter cell. All these phenomena increase population heterogeneity. As soon as a critical cell density is attained ($\eta = \eta_{\max}$, where η is the cell packing factor), contact inhibition decreases cell division and growth rates. It is assumed that no significant cell death occurs as resulting from experimental observation.

The PBE model is formulated as follows:

$$\frac{\partial W(V,t)}{\partial t} + \frac{\partial}{\partial V}\left[r(V,N(t))W(V,t) \right] = 2\int_{V}^{V_{\max}} \Gamma(V',N(t))\, p(V,V')W(V',t)dV' - \Gamma(V,N(t))W(V,t) \tag{B1}$$

where V and V' are both cell volumes, but the latter referred to cells which undergo division; $V_{\max}$ is the maximum volume that a single cell can attain; N is the cell density; r is the single cell growth rate; Γ is the division rate function; p is the partition probability density function. The PBE is subject to a regularity boundary condition:

$$\int_{0}^{V_{\max}} \frac{\partial}{\partial V}\left[r(V,N(t))W(V,t) \right] dV = 0 \tag{B2}$$

and an appropriate initial distribution. Equations (B1) and (B2) were mathematically derived by Ramkrishna (2000).

B.4.2 Growth

Cell growth rate represents the increase in cell volume with time. The growth rate is defined as the difference between nutrient uptake and product release rates, assuming the first proportional to the cell surface and the latter to the cell volume (Eakman, et al., 1966):

$$r^*(V) = k_1 \cdot V^{2/3} - k_2 \cdot V \,, \tag{B3}$$

where k_1 and k_2 are constants. The maximum volume, $V_{\max}$, that a spherical cell can attain yields a growth rate equal to zero. Thus, once defined the parameter k_1, k_2 is given by:

$$k_2 = k_1 \cdot V_{\max}{}^{-1/3}. \tag{B4}$$

Taking account of the inhibitory process, the growth rate is defined by:

$$r(V,N) = \left(k_1 \cdot V^{2/3} - k_2 \cdot V \right) \cdot G(N)^{n_r}, \quad V \in \left[0, V_{\max}\right], \tag{B5}$$

where $G(N)$ is the inhibition factor described successively in Equation (B10), and n_r a model parameter.

B.4.3 Cell division

We assume that cell division volume is normally distributed around the mean cell division volume, V_c. From this assumption, cell division rate is defined as in Eakman, et al. (1966) and modified to take into account contact inhibition:

$$\Gamma(V,N)=\frac{2\exp\left[-\left(\frac{V-V_c}{\varepsilon}\right)^2\right]\cdot r(V)}{\varepsilon\sqrt{\pi}erfc\left(\frac{V-V_c}{\varepsilon}\right)}\cdot G(N)^{n_\Gamma}, \tag{B6}$$

where $\varepsilon/\sqrt{2}$ is the cell division volume standard deviation and n_Γ is a model parameter.

The division process is further characterized by the partition probability density function $p(V,V')$, which describes the probability that a cell with volume V' will produce upon cell division two cells with volumes V and $V'-V$. As in Hatzis, et al. (1995), it is assumed that the newborn cells probability density function is a symmetric beta distribution:

$$p(V,V')=\frac{1}{\beta(q,q)}\frac{1}{V'}\left(\frac{V}{V'}\right)^{q-1}\left(1-\frac{V}{V'}\right)^{q-1}, \tag{B7}$$

where V' is the mother cell volume and V the daughter one, $\beta(q,q)$ is the beta function and q is a model parameter. We assume that, even though division can be asymmetric, the most probable is a symmetric cell division; the acceptability of this assumption is discussed later in the sensitivity analysis.

B.4.4 Contact inhibition

During the cell culture, frequent medium changes allow bulk properties to be almost constant, thus, we neglect bulk changes in the intercellular microenvironment. However endogenous factors are very diluted regulatory molecules, and even small variations in their concentration have a consistent impact on cell behavior (Lauffenburger and Linderman, 1993). These molecules

are produced by cells themselves and it is reasonable to assume that their influence on cell growth and division parameters is related to cell density. We call “contact inhibition” a complex network of phenomena which increase in importance as cell density on the culture dish increases, and we define an inhibition term G to represent a lumped function where all these phenomena are taken into account. In this way it is possible to develop a basic model that considers only the macroscopic effect of complex molecular signaling, which has not been totally elucidated yet. Inhibition is taken into account by using the radial distribution function (RDF) that gives the probability of cell-cell contact as function of cell packing fraction, i.e. cell density. It is defined by Bravo Yuste and Santos (1993) for hard disks (we refer to a two-dimensional culture system):

$$g(\eta) = \frac{1 - a\eta}{(1-\eta)^2} \in \left[1, g\ \ \eta_{\max}\ \right], \tag{B8}$$

where $a = \frac{2\sqrt{3}}{\pi} - \frac{2}{3}$ and η. is the packing factor, defined as:

$$\eta = N \cdot v \cdot d_{inhib}{}^2 \in [0; \eta_{\max}], \tag{B9}$$

N is the cell density (number of cells per unit surface), $v = \pi/4$ and d_{inhib} represents, in general, the hard disk diameter. η represents the fraction of surface on the Petri dish occupied by the cells. In particular, as cell inhibition is present before contact occurs, d_{inhib} is the cell “diameter” considering also the area around the cell where it has an influence by molecular signals.

The RDF is used to define the inhibition factor, G, which represents the probability of contact between different cell influence areas:

$$G(\eta) = 1 - \frac{g\ \eta\ - 1}{g\ \eta_{\max}\ - 1} \in\ 0,1\ . \tag{B10}$$

B.4.5 Numerical solution

The PBE in (B1) is solved by the method of moments (Ramkrishna, 2000). The initial cell number density, $W_0(V)$, is taken as being lognormal and subsequent time-dependent cell number densities, $W(V,t)$, are assumed to remain lognormal:

$$W(V,t) = \frac{N/\varepsilon}{\sigma\sqrt{2\pi}\cdot(V/\varepsilon)} \exp\left[-\frac{\log(V/\varepsilon) - \mu\ ^2}{2\sigma^2} \right], \tag{B11}$$

where μ, σ and N are the distribution parameters. Although the solution is restricted to a lognormal distribution, the three parameters are allowed to vary with time. The experimental results indicate that the lognormal function is a good fitting for the cell volume distributions.

Taking the zeroth, first and second moments of equation (B1) in dimensionless variables, the following equations system is obtained:

$$\begin{cases} \dfrac{d\tilde{N}}{d\tilde{t}} = \dfrac{t_m k_1}{\varepsilon^{1/3}} \displaystyle\int_0^{\infty} \tilde{\Gamma}\tilde{W} d\tilde{V} \\ \dfrac{d}{d\tilde{t}}\left[\tilde{N} \exp\left(\mu + \dfrac{\sigma^2}{2} \right) \right] = \dfrac{t_m k_1}{\varepsilon^{1/3}} \displaystyle\int_0^{\infty} \tilde{r}\tilde{W} d\tilde{V} \\ \dfrac{d}{d\tilde{t}}\left[\tilde{N} \exp\left[2\ \mu + \sigma^2\ \right] \right] = 2\dfrac{t_m k_1}{\varepsilon^{1/3}} \displaystyle\int_0^{\infty} \tilde{r}\tilde{W}\tilde{V} d\tilde{V} +\ 2\cdot K_2 - 1\ \dfrac{t_m k_1}{\varepsilon^{1/3}} \displaystyle\int_0^{\infty} \tilde{\Gamma}\tilde{W}\tilde{V}^2 d\tilde{V} \end{cases} \tag{B12}$$

where t_m represents the maximum time of experimental observation and $\tilde{N}$, $\tilde{t}$, $\tilde{\Gamma}$, $\tilde{W}$, $\tilde{V}$, $\tilde{r}$ are dimensionless variables. The resulting nonlinear ordinary differential equation system (B12) is integrated by a variable-order solver based on the

numerical differentiation formulas (NDFs), to find the lognormal parameters as functions of time. The initial conditions are derived from the experimental data at $t = 48\,\text{hour}$, end of the lag phase.

B.4.6 Description of generations

The model is extended to track the temporal evolution of cell number densities for each cell generation (Liou, et al., 1997). The proposed model is a system of n_g^f (total number of generations) partial-integro-differential equations similar to (B1) one for each generation, in dimensionless form it is:

$$\begin{cases} \dfrac{\partial \tilde{W}_{n_g}}{\partial \tilde{t}} + \dfrac{t_m k_1}{\varepsilon^{1/3}} \dfrac{\partial}{\partial \tilde{V}} \left[\tilde{r} \cdot \tilde{W}_{n_g} \right] = -\dfrac{t_m k_1}{\varepsilon^{1/3}} \tilde{\Gamma} \cdot \tilde{W}_{n_g} & n_g = 1 \\ \dfrac{\partial \tilde{W}_{n_g}}{\partial \tilde{t}} + \dfrac{t_m k_1}{\varepsilon^{1/3}} \dfrac{\partial}{\partial \tilde{V}} \left[\tilde{r} \cdot \tilde{W}_{n_g} \right] = 2 \dfrac{t_m k_1}{\varepsilon^{1/3}} \int_{\tilde{V}}^{\infty} \tilde{\Gamma} \cdot \tilde{p} \cdot \tilde{W}_{n_g - 1} d\tilde{V}' - \dfrac{t_m k_1}{\varepsilon^{1/3}} \tilde{\Gamma} \cdot \tilde{W}_{n_g} & n_g = 2, 3, \ldots, (n_g^f - 1) \\ \dfrac{\partial \tilde{W}_{n_g}}{\partial \tilde{t}} + \dfrac{t_m k_1}{\varepsilon^{1/3}} \dfrac{\partial}{\partial \tilde{V}} \left[\tilde{r} \cdot \tilde{W}_{n_g} \right] = 2 \dfrac{t_m k_1}{\varepsilon^{1/3}} \int_{\tilde{V}}^{\infty} \tilde{\Gamma} \cdot \tilde{p} \cdot \tilde{W}_{n_g - 1} d\tilde{V}' & n_g = n_g^f \end{cases}$$

. (B13)

Cells are assumed to be all in the first generation at $t = 0$. In the first generation there is no source term, and in the last one there is no exit term. In fact stem cells undergo a finite number of replicative cycles before showing cellular senescence, differentiation and fusion into myotubes. Thus, after $(n_g^f - 1)$ divisions cells stop duplicating.

As experimental data were available only for the overall population, model parameters were not changed from generation to generation, even though it is possible to define differently the growth and cell division rates, and the inhibition influence for each generation.

In the numerical solution we assume that the cell number density functions of each generation, $\tilde{W}_{n_g}$ for $n_g = 1, 2, ..., n_g^f$, can be approximated by lognormal distributions. The equation system (B13) is solved by the method of moments, as reported before. The resulting nonlinear ordinary differential equation model is integrated by a variable-order solver based on the numerical differentiation formulas (NDFs), to find the lognormal parameters as functions of time for each generation.

B.5 Results

B.5.1 Experimental data and model fitting

Figure 1 shows a schematic representation of the phenomena that are described by the population balance equation: cell growth, mitosis and contact inhibition which becomes prevailing at high cell density values ($\eta_{\max}$).

The cell growth is responsible for the cell volume increase, while mitosis is the process occurring when a cell divides and unequally partitions its volume into two daughter cells. Both growth and division are influenced by contact inhibition, a complex network of cell-density-dependent phenomena, related to autocrine and paracrine communication.

In a first set of experiments, we seeded $N_0 = 500\,\text{cell/cm}^2$ on 14 plastic dishes. Every 24 hours, the cells from two different Petri dishes where analyzed by the Coulter Counter®, giving similar results according to the Kolmogorov-Smirnov test. The measurements from a second set of experiments at the same culturing conditions confirmed the results from the first set. Therefore, the experimental

method turns out to be reproducible even for different cell biopsies, which is a fundamental prerequisite for the experimental validation of the model.

The experimental data from the first set of experiments are shown in Figure 2. At each time point, experimental cell number densities from the Coulter Counter® measurements are fitted by lognormal distributions.

Between day 1 and 3 the volume distributions do not change visibly probably because of the lag phase; the model simulation starts from day 2 neglecting this period. In the lower part of the graph in Figure 2a, the contour plot shows lines connecting points of equal number densities as functions of time and cell volume. For comparison, the cell mean volume (--■--) is also reported as a function of time. During the 7-day culture, the cell mean volume remains almost constant between 2000 and $3000 \mu m^3$, whereas the cell volume distribution is wider for the last experimental time points (day 5-7).

Figure 3 shows a comparison between the experimental data and the model calculation for cell density (Fig. 3a) and cell volume (Fig. 3b). The values of the parameters used in the population balance equation are reported in Table I. These values are used for the correlation and the prediction of both set of experiments. The cell density is the zeroth moment of the number density, while the average cell volume is the ratio between the first moment and the zeroth moment. For both cases, the model is able to give a fair description of the experimental data within the experimental uncertainties. In Figure 3a the increase of experimental uncertainty at longer times in culture, represented by larger error bars, is mostly related to the cell differentiation process which ends in myoblast fusion and myofiber formation.

Figure 4 shows a comparison between the time evolution of experimental (Figure 4a) and calculated (Figure 4b) cell volume distribution. The population balance equation reasonably reproduces both the average cell volume (--■--) and the cell volume distribution.

Our results show that the PBE may be successfully used to accurately represent the time evolution of average and segregated properties of the population of satellite cells in a bi-dimensional culture. The volume was chosen as the only independent variable, however the use of other internal properties, such as cell age, protein or gene expression levels could be implemented as internal variables of the model.

B.5.2 Sensitivity analysis

In order to rationally understand the dependence of the model output on each parameter, a local sensitivity analysis (LSA) is performed (Saltelli, et al., 2000) for two model outputs: the cell density, N, and the cell mean volume, $\bar{V}$. An experiment (lag phase excluded) is simulated for 5 days and the sensitivity coefficients, $S_{ij}(t)$, are calculated by the following expression:

$$S_{ij}(t) = \frac{Y_j(t, k_i + \Delta k_i) - Y_j(t, k_i)}{\Delta k_i} \qquad \begin{matrix} i = 1...8 \\ j = 1,2 \end{matrix} \tag{B14}$$

where Y_j is a normalized output variable (N or $\bar{V}$), k_i is a dimensionless parameter value from Table I and $\Delta k_i = 1\% \cdot k_i$.

Figure 5 shows the results of the LSA. Parameters $N_{\max}$, n_r, n_Γ and q are scarcely relevant for both outputs. In particular, the observation that the partitioning function constant (q) is not a significant parameter, justifies our definition of a

symmetric partition probability density function, $p(V,V')$. However, more accurate definition of $p(V,V')$ would be required for better describing the self-renewal and the asymmetric cell division phenomena which can be relevant in satellite cell cultures (Holterman and Rudnicki, 2005).

The parameter related to cell growth, k_1, influences the cell density (N) because cell volume controls cell division. Both N and $\bar{V}$ are very sensitive to V_c and ε variations, which are involved in the model description of cell division.

N_{max} is the parameter that takes into account contact inhibition. It increases in importance in the last phase of the simulation when N is larger. By plotting N vs. t (Figure 3a) we obtain a sigmoid curve which tends to a constant value of N_{max} for large t.

B.5.3 Model prediction

The capability of the model to predict the time-evolution of a cell population properties is of overwhelming importance to optimize cell expansion processes.

A second set of experiments was performed to validate the model. The double repetition of the same experiment as in the first set ($N_0 = 500$ cell/cm^2) gave very similar results, confirming the reliability of the experimental procedure.

Changing the seeding cell density ($N_0 = 100, 1000$ cell/cm^2), we obtained data shown in Figure 6. The experimental data in Figure 6b show that the average cell volume remains quite constant for both $N_0 = 100$ and $N_0 = 1000$ cell/cm^2 and shows values within the range of $2000 - 3000 \mu m^3$ as reported for the experiment at $N_0 = 500$ cell/cm^2. A comparison between experimental data and model

simulations in terms of cell density is shown in Figure 6a for two time points: day 3 and 7. The model reveals a good predictive ability.

Even if our model does not contain variables related to external conditions in culture that can be controlled for optimization purposes, it is a first important step to predict experimental data generated at different cell seeding densities.

B.5.4 Generation model description

In a clinical perspective of using stem cells for tissue engineering, regenerative medicine or cell therapy, it is of paramount importance not only to rapidly and easily expand the stem cells isolated from a biopsy, but also to preserve cell quality in terms of both viability and myogenic differentiative potential. This latter requirement is relevant in order to realize an effective integration of the implanted cells within the damaged or injured tissue (Montarras, 2005).

Because it was recently shown that the myogenic potential is related to the cell generation (Wernig, et al, 2005), it is possible to have a measure of the culture myogenic potential by identifying which generation cells belong to. This is attainable by applying PBEs to each individual generation as reported in (B13).

For instance, Figure 7 shows the simulation results at two time points for the initial condition $N_0 = 500\,\text{cell/cm}^2$ and assuming $n_g^f = 10$. This model can reproduce the number density of each generation as a function of time: as the number densities of the first generations move to the right (larger volumes), cells from new generations appear with smaller cell volumes. To ease the result view, in Figure 8 the evolution of the cell density is presented as in Figure 3a highlighting the contribution of each generation to the total cell density.

Data from Figure 8 are normalized with respect to the total cell density and shown in Figure 9a. This is a useful representation in a clinical perspective, as it is immediately apparent the proliferative senescence degree of the cell population. In Figure 9b, the model results are shown from a simulation where the initial conditions were determined from the model results at day 7 for each generation, but the overall cell density was dropped again to $N_0 = 500\,\text{cell/cm}^2$. In this way, it is simulated the situation that occurs after detaching the cells from the plastic dish and seeding them again at a lower concentration. The time in Figure 9b starts from day 9 because of the lag phase of two days in the second Petri dish. This kind of simulation could result particularly useful to determine the conditions (time for cell passages and seeding concentration) that minimize the proliferative senescence of the cell population.

Further studies will be required to experimentally validate the time evolution of segregated properties described for each generation by the PBE; in particular it would be important to determine the model parameters related to the biological processes from generation to generation. In this simulation the values of the parameters are common to all the generations and are given in Table I.

B.6 Conclusion

In this paper we develop a mathematical model that determines the volume distribution of a satellite cell population as a function of time. The model incorporates growth and cell division processes, both influenced by contact inhibition, a consequence of cell-cell interactions. The model is based on a PBE using cell volume as the internal variable to describe the cell state. An original

approach is adopted to consider the contact inhibition influence, defining an inhibition factor related to the radial distribution function. The model is supported by experimental data to obtain parameters values. A sensitivity analysis on the parameters is performed; in particular, we report the influence of those controlling growth, cell division and inhibition processes. The model is validated by further experimental data at different initial conditions and it results reliable in predicting the temporal evolution of the cell culture. Besides, an enhancement of the model is introduced applying the PBE to each generation in the cell population.

Our model can be used to improve cell expansion efficiency *in vitro*. In fact, as shown in Figure 3a, it is advisable to design cell expansion protocol where the average duplication rate, represented by the curve slope, is kept at the maximum values. This can be achieved by adjusting the initial cell seeding density, the number of cell passages and, in general, avoiding culture conditions where contact inhibition starts preventing cell division.

As future work, it would be opportune to explicitate the contact inhibition term, for instance by including ligand-receptor kinetics, in order to define the cell processes dependence on the micro-environment surrounding the cells.

B.5.4 Nomenclature

a	constant in RDF (dimensionless)
d_{inib}	cell inhibition diameter (cm)
g	radial distribution function (dimensionless)
G	contact inhibition factor function (dimensionless)
k_1	cell growth parameter ($\mu m\ h^{-1}$)

k_2 cell growth parameter (h^{-1})

n_r model parameter for cell growth inhibition (dimensionless)

n_Γ model parameter for cell mitosis inhibition (dimensionless)

N cell density (cm^{-2})

p distribution of cell volumes for the newborn cells (μm^{-3})

q constant in newborn cell volume distribution (dimensionless)

r cell growth rate ($\mu m^3 h^{-1}$)

r^* cell growth rate according to Eakman, et al. (1966) ($\mu m^3 h^{-1}$)

t time (h)

t_m experiment time (h)

v constant for the packing factor calculation (dimensionless)

V cell volume (μm^3)

V_c cell mean division volume (μm^3)

W cell number density ($cm^{-2}\mu m^{-3}$)

Greek Symbols

Γ cell division rate (h^{-1})

ε cell division volume standard deviation times $\sqrt{2}$ (μm^3)

η packing factor (dimensionless)

μ parameter of cell number density (dimensionless)

σ parameter of cell number density (dimensionless)

Subscripts

n_g generation number (dimensionless)

n_g^f first generation without myogenic potential (dimensionless)

max maximum

0 initial condition

tot referred to the whole cell population

Superscripts

' referred to mother cells

~ dimensionless

B.5.5 References

Bravo Yuste S, Santos A. 1993. A heuristic radial distribution function for hard disks. J Chem Phys 99:2020-2024.

Chargé S B P, Rudnicki M A. 2004. Cellular and molecular regulation of muscle regeneration. Physiol Rev 84:209-238.

Davey R E, Zandstra P W. 2004. Signal processing underlying extrinsic control of stem cell fate. Curr Opin Hematol 11:95-101.

Deasy B M, Qu-Peterson Z, Greenberger J S, Huard J. 2002. Mechanisms of muscle stem cell expansion with cytokines. Stem Cells 20:50-60.

Eakman J M, Fredrickson A G, Tsuchiya H M. 1966. Statistics and dynamics of microbial cell populations. Chem Eng Prog Symp Series No 69 62:37-49.

Hatzis C, Srienc F, Fredrickson A G. 1995. Multistaged corpuscular models of microbial growth: Monte Carlo simulations. Biosystems 36:19-35.

Holterman C E, Rudnicki M A. 2005. Molecular regulation of satellite cell function. Semin Cell Dev Biol 16:575-584.

Lauffenburger D A, Linderman J J. 1993. Receptors. Model for binding, trafficking and signaling. New York: Oxford University Press.

Liou J J, Srienc F, Fredrickson A G. 1997. Solutions of population balance models based on a successive generations approach. Chem Eng Sci 52:1529-1540.

Mantzaris N V. 2005. Single-cell gene-switching networks and heterogeneous cell population phenotypes. Comp Chem Eng 29:631-643.

Mauro A. 1961. Satellite cell of skeletal muscle fibers. J Biophys Biochem Cytol 9:493-495.

Montarras D, Morgan J, Collins C, Relaix F, Zaffran S, Cumano A, Partridge T, Buckingham M. 2005. Direct isolation of satellite cells for skeletal muscle regeneration. Science 309(5743):2064-7.

Negroni E, Butler-Browne G S, Mouly V. 2006. Myogenic stem cells: regeneration and cell therapy in human skeletal muscle. Pathol Biol 54:100-108.

Pisu M, Lai N, Cincotti A, Concas A, Cao G. 2004. Modeling of engineered cartilage growth in rotating bioreactors. Chem Eng Sci 59:5035-5040.

Ramkrishna D. 2000. Population balances. Theory and applications to particulate systems in engineering. San Diego: Academic Press.

Rosenblatt J D, Lunt A I, Parry D J, Partridge T A. 1995. Culturing satellite cells from living single muscle fiber explants. In Vitro Cell Dev Biol Anim 31:773-779.

Saltelli A, Chan K, Scott E M. 2000. Sensitivity analysis, probability and statistics series. London: Wiley.

Seale P, Rudnicki M A. 2000. A new look at the origin, function, and "stem-cell" status of muscle satellite cells. Dev Biol 218:115-124.

Sidoli F R, Mantalaris A, Asprey S P. 2004. Modelling of mammalian cells and cell culture processes. Cytotechnology 44:27-46.

Viswanathan S, Zandstra P W. 2003. Towards predictive models of stem cell fate. Cytotechnology 41:75-92.

Viswanathan S, Davey R E, Cheng D, Raghu R C, Lauffenburger D A, Zandstra P W. 2005. Clonal evolution of stem and differentiated cells can be predicted by integrating cell-intrinsic and extrinsic parameters. Biotechnol & Appl Biochem. Published on the web.

Wernig A, Schafer R, Knauf U, Mundegar R R, Zweyer M, Hogemeier O, Martens U M, Zimmermann S. 2005. On the regenerative capacity of human skeletal muscle. Artificial Organs 29:192-198.

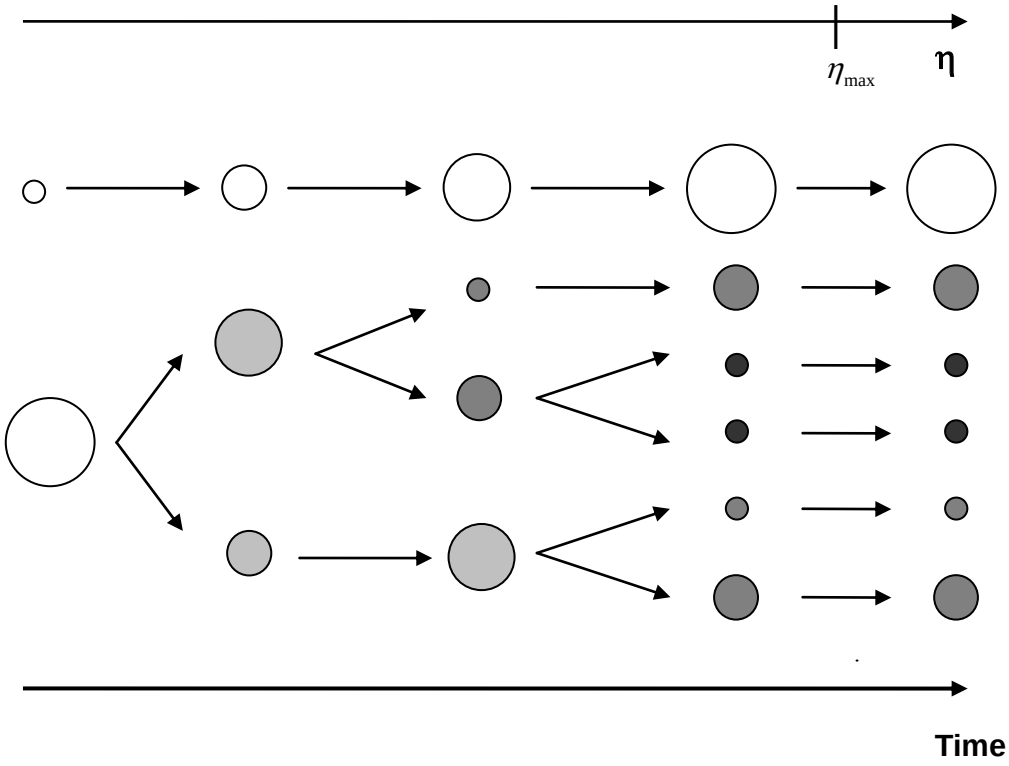

§

Figure 1

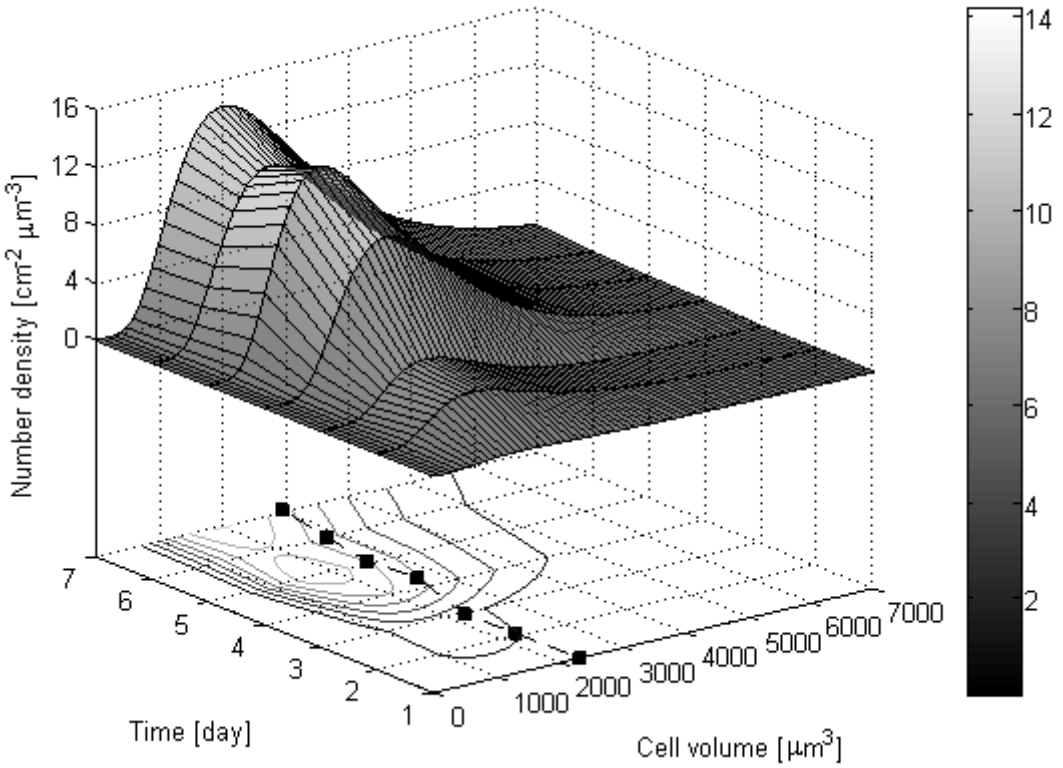
Number density [cm^{-2} μm^{-3}]
16
12
8
4
0
7
6
5
4
3
2
1
0
Time [day]
1000
2000
3000
4000
5000
6000
7000
Cell volume [μm^3]
14
12
10
8
6
4
2

Figure 2

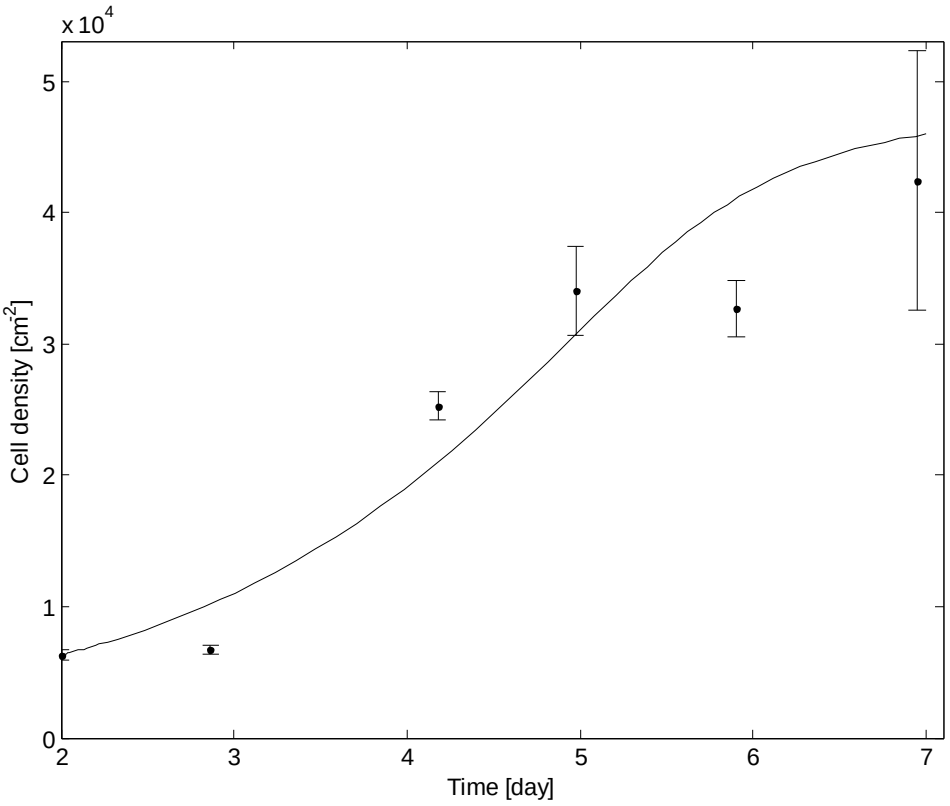

Figure 3a

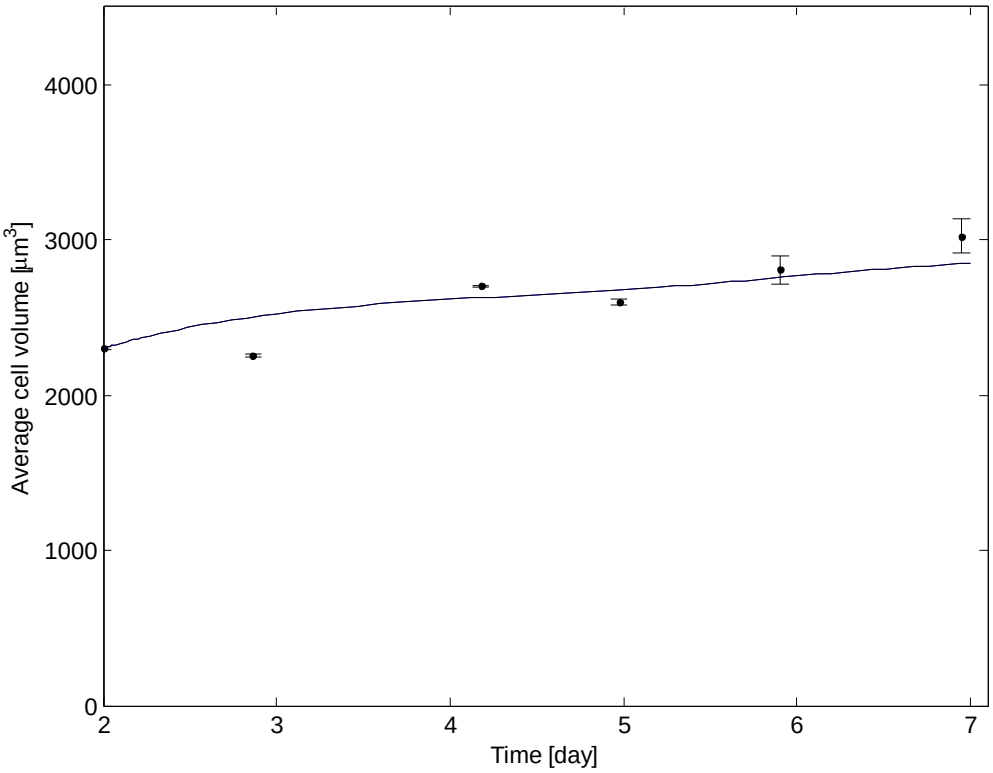

Figure 3b

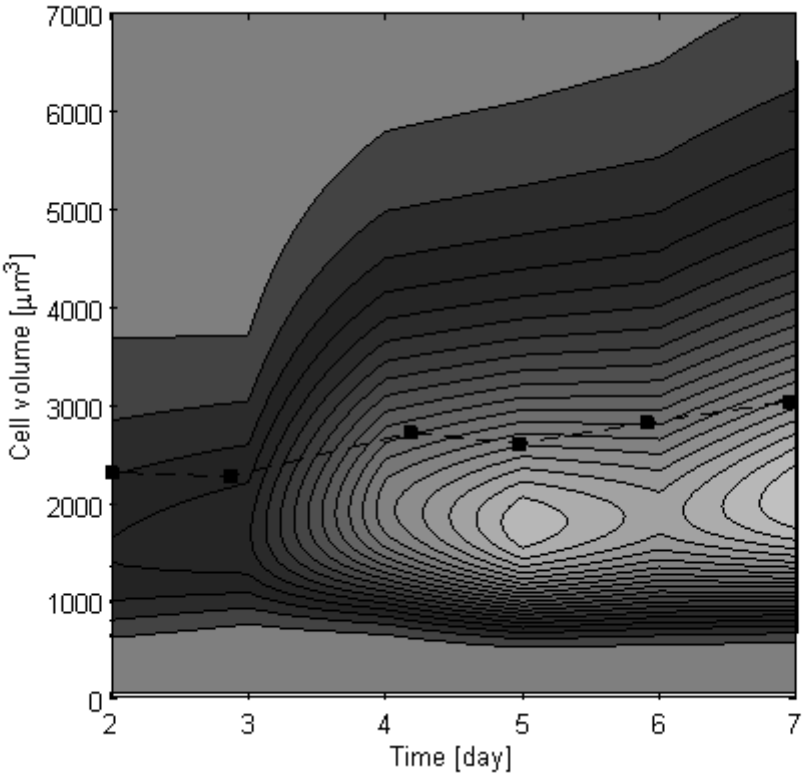

Figure 4a

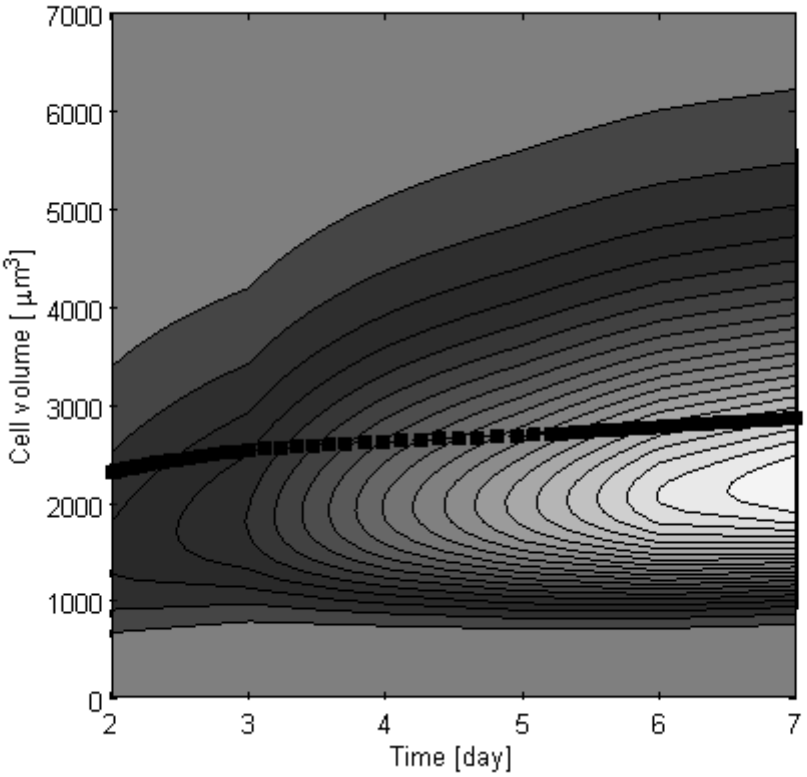

Figure 4b

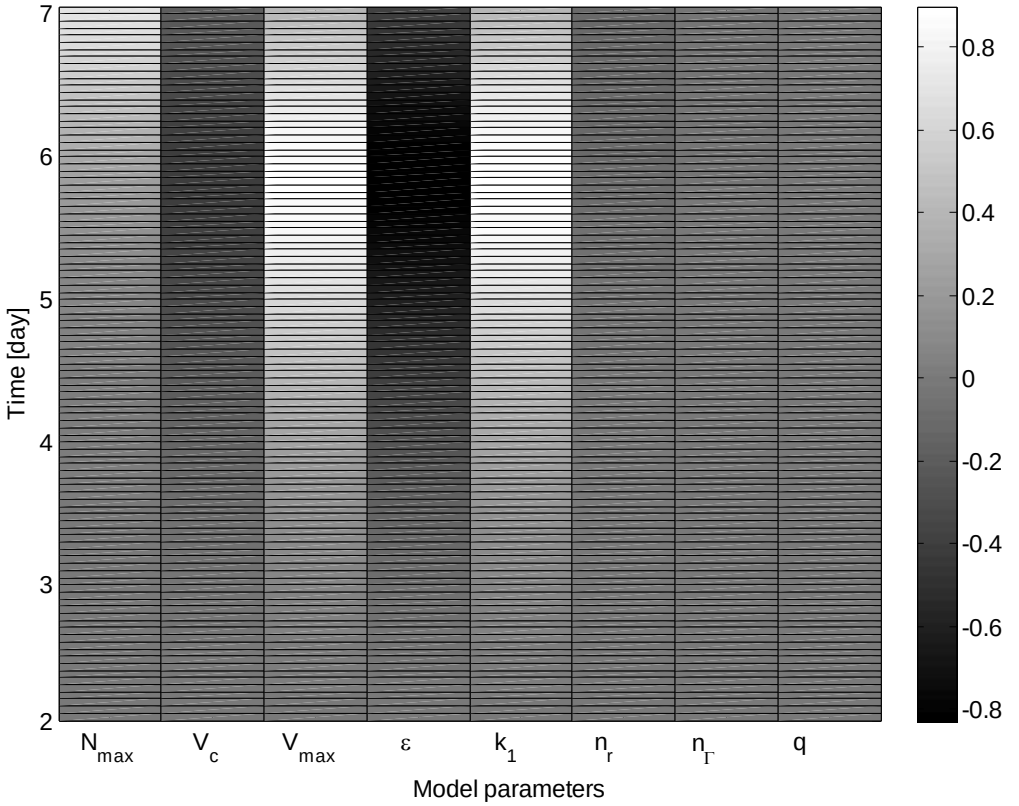

Figure 5a

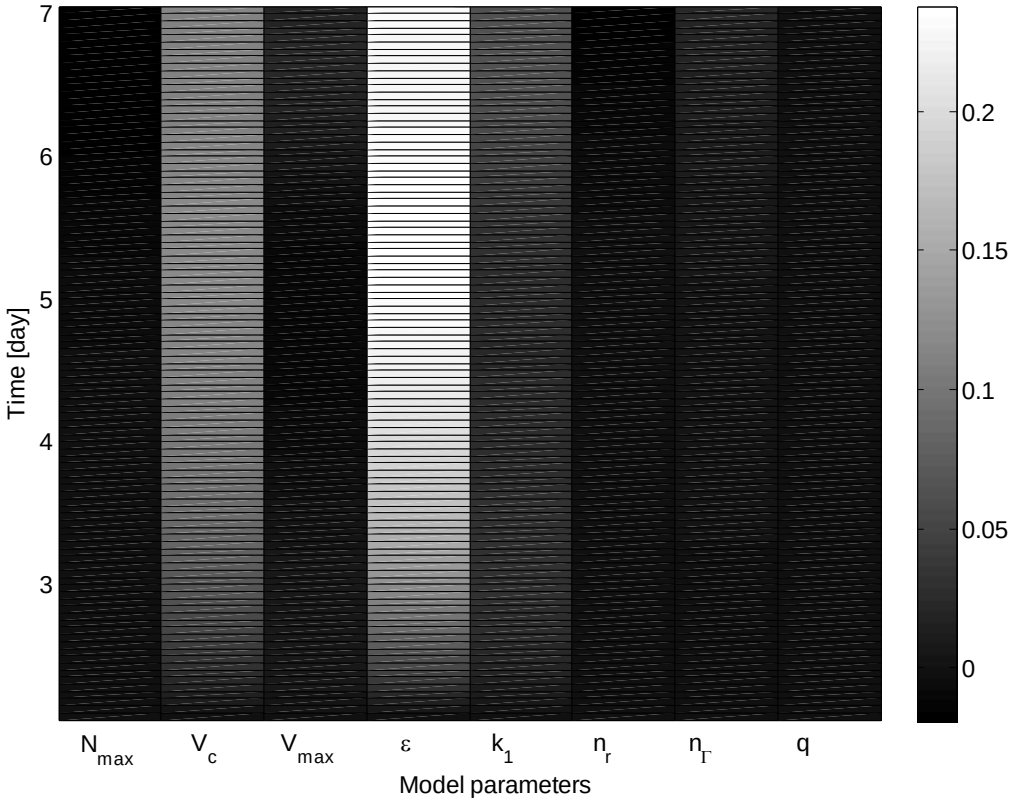

Figure 5b

Figure 6a

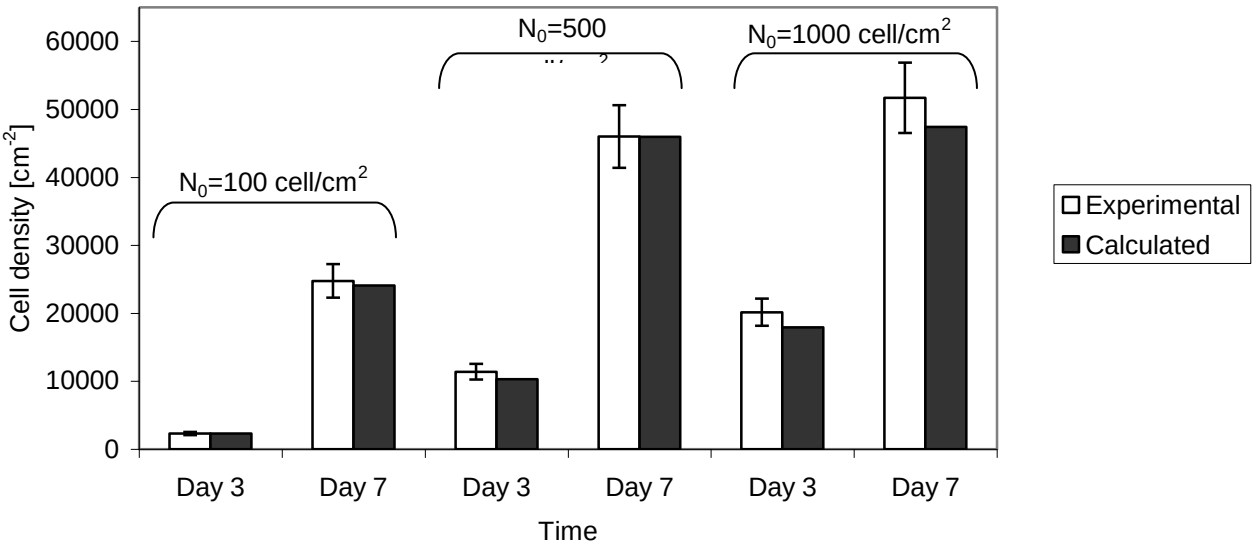

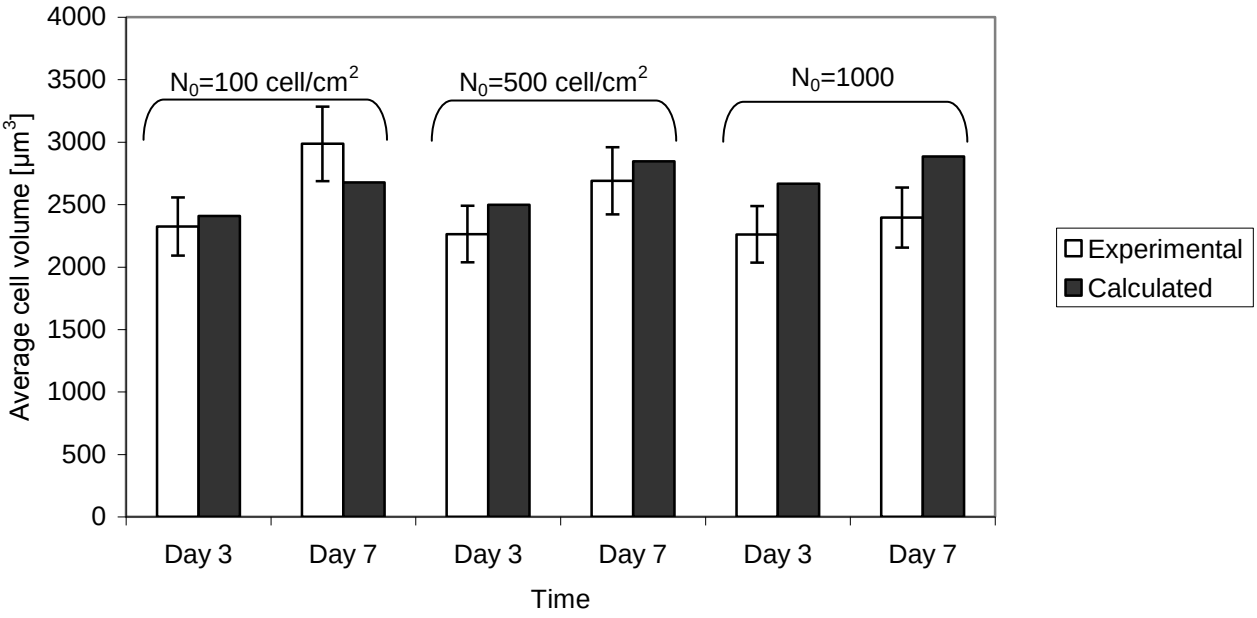

Figure 6b

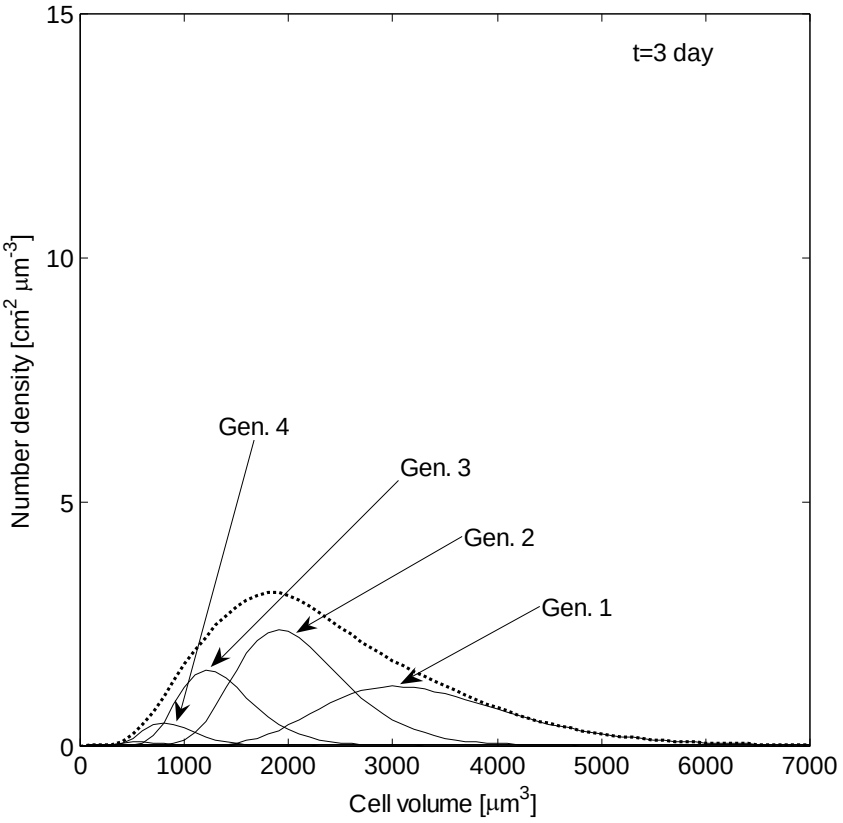

Figure 7a

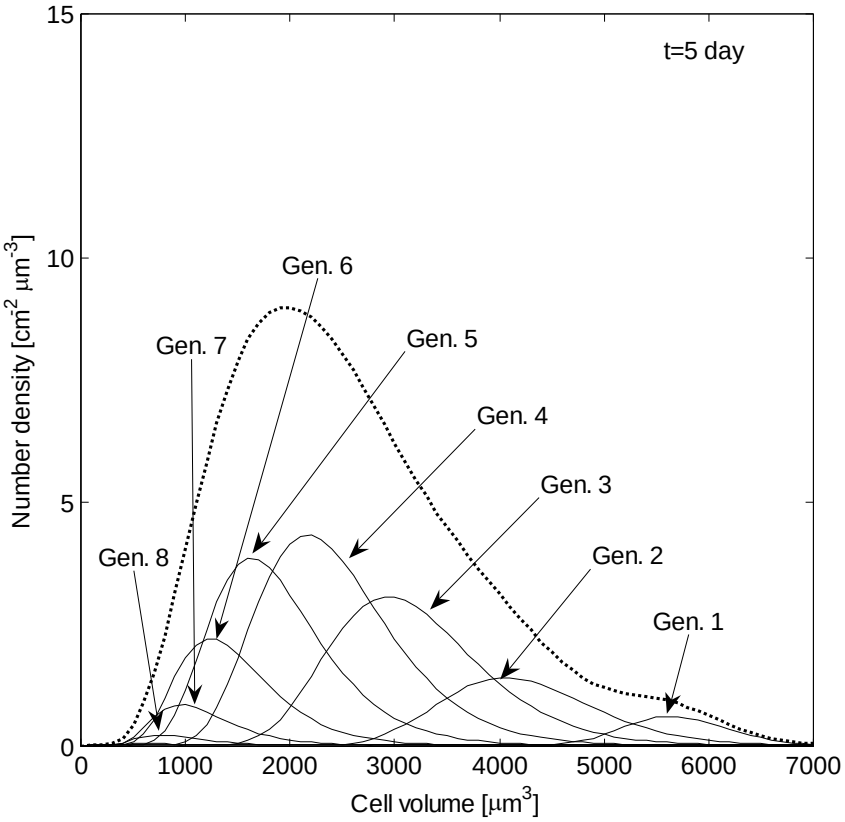

Figure 7b

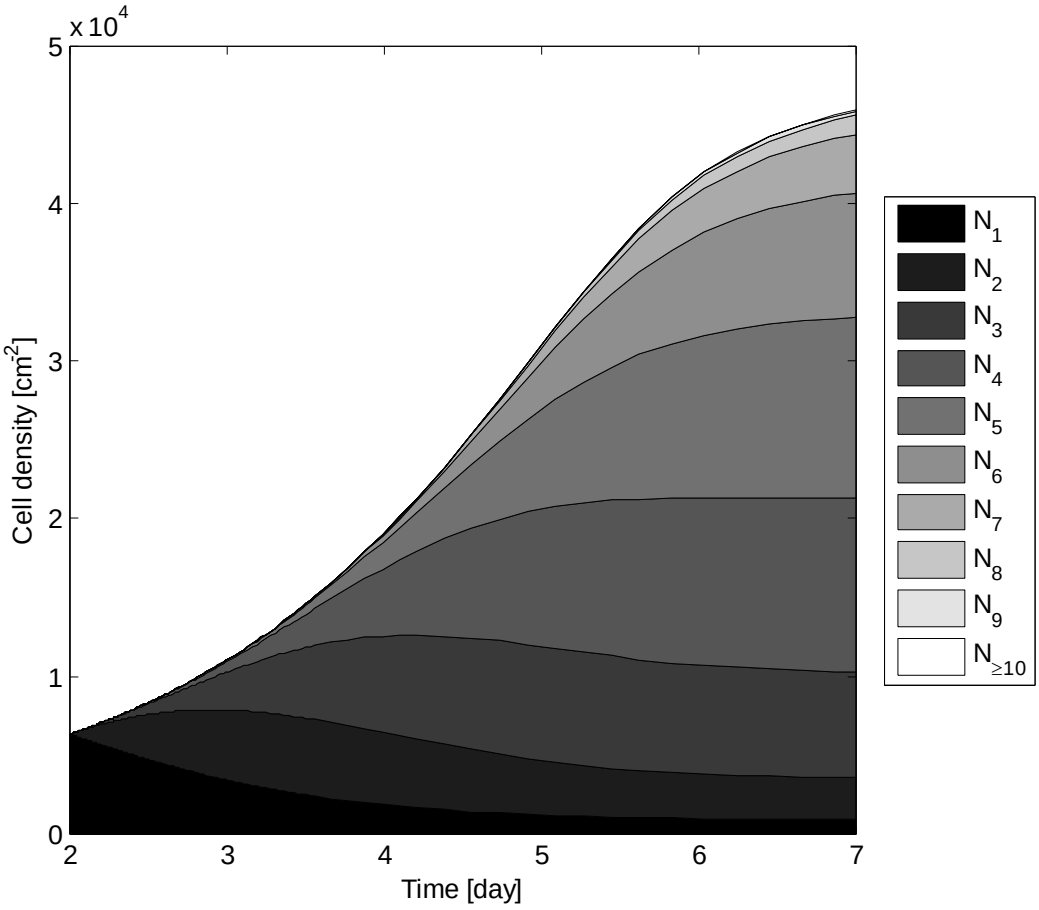
x 10^4
5
4
3
2
1
0
Cell density [cm^-2]
2
3
4
5
6
7
Time [day]
N1
N2
N3
N4
N5
N6
N7
N8
N9
N≥10

Figure 8

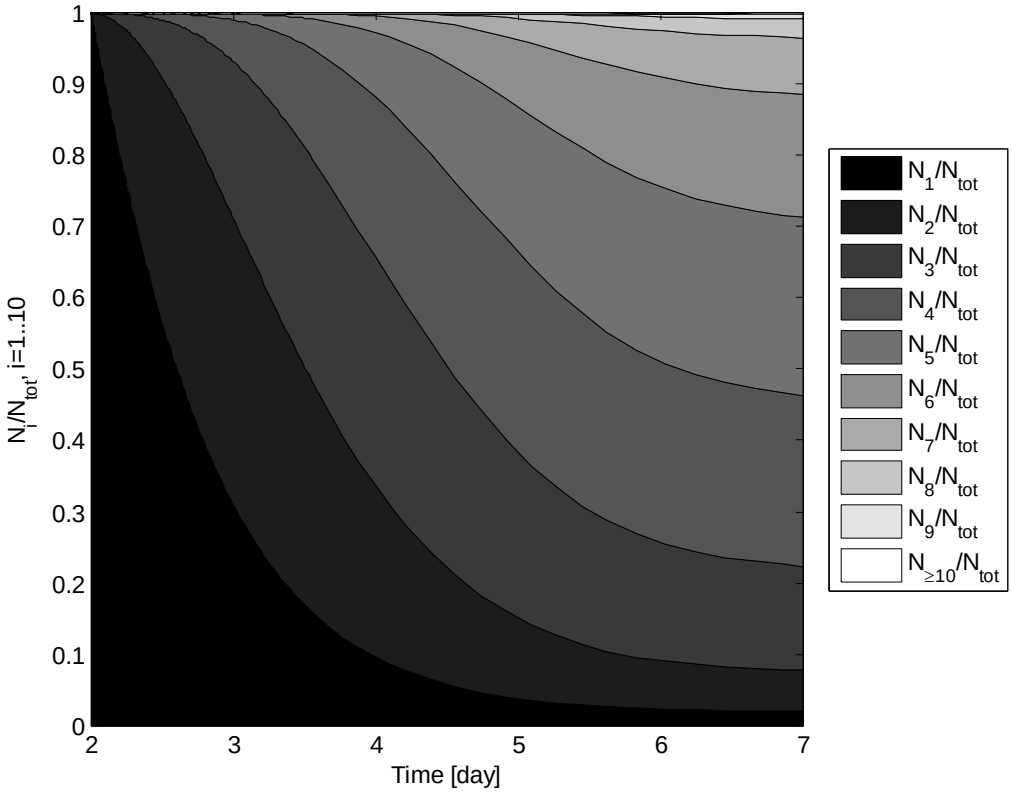

Figure 9a

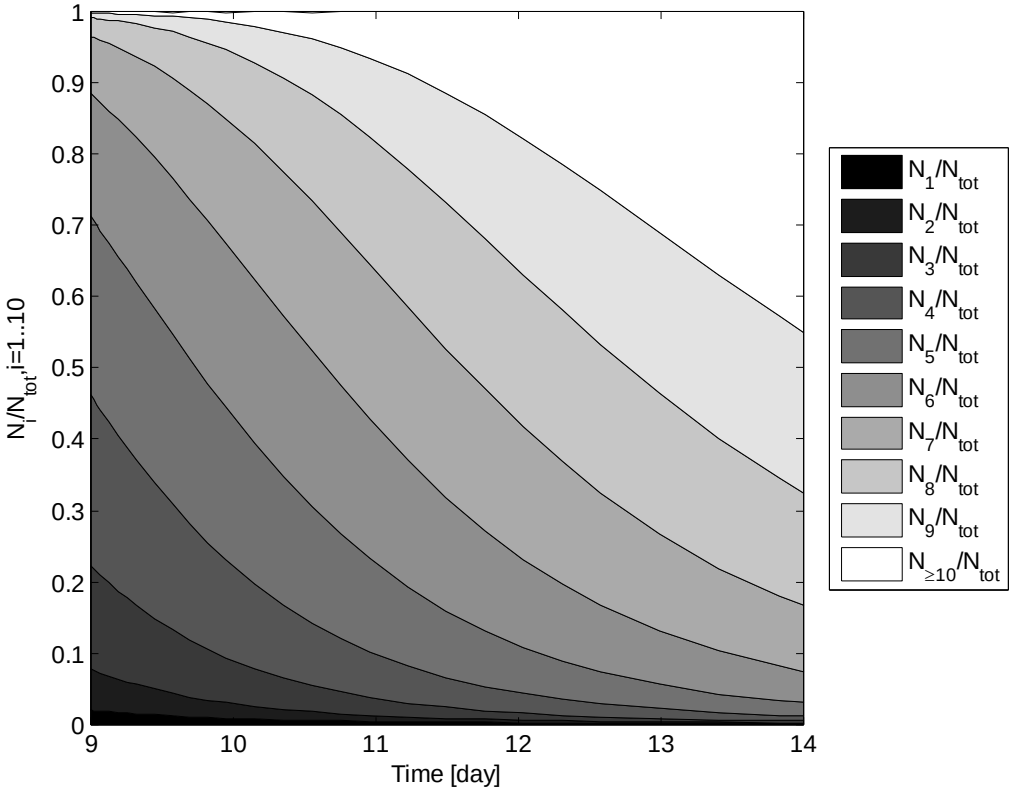

Figure 9b

Appendix C

Dispositivo di miscelazione meccanica per piastre di coltura

In this Appendix the patent application for the device described in Chapter 4 is reported, whose details are:

- Application number: PD2008A000371
- Applicant: Università degli Studi di Padova
- Inventors: Nicola Elvassore, Camilla Luni, Laura Gallimberti
- Class: C12M106
- Camera di Commercio Industria, Artigianato e Agricoltura of Padova
- Date of deposit: 2008/12/17

C.1 Riassunto

Dispositivo per la miscelazione meccanica di colture cellulari in sospensione contenute in una piastra di coltura, comprendente: - un coperchio 10 destinato ad

essere amovibilmente associato ad una piastra di coltura P per schermare il pozzetto o i pozzetti W di quest'ultima limitando l'ingresso di solidi sospesi nell'aria ambiente, e al contempo permettendo l'ingresso di gas e umidità esterni; - almeno una girante di miscelazione 20 per ciascun pozzetto W della piastra di coltura P; - mezzi motori 30 collegabili cinematicamente a ciascuna girante 20.
La girante 20 è rotazionalmente associata al coperchio 10 in corrispondenza della faccia di quest'ultimo destinata ad essere rivolta verso detta piastra di coltura P. Almeno il coperchio 10 e le giranti 20 sono realizzate con materiali che possono essere sottoposti a trattamenti di sterilizzazione e sono in grado di resistere alle condizioni di umidità, temperatura e pH che si creano in un incubatore biologico.
[Fig. 1]

C.2 Descrizione

C.2.1 Campo di applicazione

Forma oggetto della presente invenzione un dispositivo di miscelazione meccanica per piastre di coltura. Vantaggiosamente, il dispositivo secondo l'invenzione può essere utilizzato in tutti i settori che prevedano l'utilizzo di piastre coltura, in particolare per colture cellulari o microbiologiche in sospensione, quali il settore biotecnologico, alimentare, farmaceutico e biomedico.

C.2.2 Stato della tecnica

Come è noto, alcuni tipi di cellule coltivate *in vitro* non aderiscono ad un supporto (es. fondo di una piastra di coltura), ma crescono in sospensione.
Comunemente questi tipi di cellule si coltivano in *medium* liquido non mescolato contenuto in piastre di coltura, come ad esempio piastre Petri a singolo pozzetto o

piastre a pozzetti multipli o multiwell (come illustrato nella Figura A allegata), oppure in fiasche che garantiscono volumi maggiori rispetto alle piastre. In questi sistemi di coltura "statici" le cellule sono portate ad accumularsi sul fondo a causa del proprio peso con distribuzioni non ripetibili da esperimento a esperimento. Nel volume di coltura vengono inoltre a formarsi gradienti di concentrazione di nutrienti, gas e fattori di crescita. Ciò rende sostanzialmente impossibile ottenere condizioni ambientali omogenee in tutto l'ambiente di coltura.

Si stanno quindi sempre più diffondendo sistemi di coltura in sospensione di tipo mescolato, allo scopo di ottenere colture più ripetibili e condizioni ambientali omogenee in termini, ad esempio, di concentrazioni di metaboliti e principi attivi. Sistemi mescolati permettono inoltre di migliorare lo scambio di gas con l'ambiente esterno.

La necessità di colture in condizioni dinamiche ha quindi portato allo sviluppo di diversi sistemi di mescolamento.

In generale i sistemi di mescolamento attualmente utilizzati possono essere ricondotti a tre tipologie principali: agitatori magnetici; agitatori a scuotimento (scuotitori); agitatori meccanici o a giranti.

Per applicazioni specifiche su piastre di coltura, Petri o multipozzetto, si adottano solo agitatori magnetici o a scuotimento. Tipicamente le piastre multipozzetto possono avere 6 pozzetti (come illustrato in Figura A), oppure 12, 24, 48 o 96 pozzetti. Queste piastre sono utilizzate in particolare per colture cellulari molto costose (come possono essere quelle di cellule staminali). I pozzetti hanno volumi da 200 microlitri a 10 millilitri (e comunque mai superiori a 20 ml).

Per applicazioni su piastre di coltura ed in generale su volumi di pochi millilitri non si utilizzano, invece, agitatori meccanici.

Com'è noto, infatti, aspetti critici di un sistema di coltura mescolato sono il controllo contemporaneo di temperatura e pH e il mantenimento di condizioni di sterilità. Per "mantenimento della sterilità" si intende impedire o sostanzialmente schermare l'ingresso di solidi sospesi nell'aria, veicolo di contaminazione biologica.

Sono queste esigenze che hanno reso fino ad oggi praticamente inutilizzabili per volumi di pochi millilitri i miscelatori meccanici a girante, che pur garantirebbero ottime prestazioni di mescolamento. La presenza dell'albero di rotazione della girante e il suo collegamento con i relativi mezzi motori impongono, infatti, tutta una serie di complicazioni costruttive per garantire la sterilità del sistema ed il controllo di temperatura e pH, giustificabili solo per contenitori aventi volumi non inferiori a 100 ml.

Per questi motivi i miscelatori meccanici si adottano principalmente in bioreattori, ossia in sistemi costruttivamente complessi e destinati al trattamento di volumi rilevanti, tali da giustificare anche l'utilizzo di sonde per la misura di temperatura e pH, e il controllo della temperatura in genere tramite camicie d'acqua termostatata.

Gli agitatori magnetici - che operano trascinando in rotazione tramite un campo magnetico un'ancoretta magnetica (opportunamente sagomata) posta sul fondo di ciascun singolo pozzetto – ben si adattano invece a sistemi di coltura semplici e con volumi ridotti. Questo tipo di agitatori permette infatti di ottenere una miscelazione efficace e facilmente regolabile in intensità senza imporre complicazioni costruttive particolari per garantire il controllo di pH e della temperatura ed il mantenimento della sterilità. Il limite principale di questi sistemi è legato al fatto che il trascinamento dell'ancoretta magnetica posta sul fondo del pozzetto produce sforzi di taglio, meccanici e di pressione, che possono danneggiare le colture.

Anche gli agitatori a scuotimento, in quanto sistemi “non invasivi”, ben si adattano all’impiego per volumi di coltura ridotti e quindi in sistemi semplici da un punto di vista costruttivo ed impiantistico. Il limite principale è dato dal fatto che il livello di miscelazione che garantiscono è molto blando e quindi sostanzialmente inefficace per colture cellulari in sospensione soprattutto per volumi ridotti in cui, ad esempio, le forze di superficie sono paragonabili alle forze di inerzia.

C.2.3 Presentazione dell'invenzione

Pertanto, scopo della presente invenzione è quello di eliminare gli inconvenienti della tecnica nota sopra descritta, mettendo a disposizione un dispositivo di miscelazione meccanica per piastre di coltura, che non richieda complicazioni impiantistiche per il controllo della temperatura e pH e per il mantenimento della sterilità.

Un ulteriore scopo della presente invenzione è quello di mettere a disposizione un dispositivo di miscelazione meccanica per piastre di coltura, che sia di semplice ed economica realizzazione.

Un ulteriore scopo della presente invenzione è quello di mettere a disposizione un dispositivo di miscelazione meccanica per piastre di coltura, che sia utilizzabile in modo semplice e pratico.

C.2.4 Breve descrizione dei disegni

Le caratteristiche tecniche dell'invenzione, secondo i suddetti scopi, sono chiaramente riscontrabili dal contenuto delle rivendicazioni sotto riportate ed i vantaggi della stessa risulteranno maggiormente evidenti nella descrizione

dettagliata che segue, fatta con riferimento ai disegni allegati, che ne rappresentano una o più forme di realizzazione puramente esemplificative e non limitative, in cui:

- la Figura 1 mostra un vista prospettica di una prima forma realizzativa del dispositivo di miscelazione secondo l'invenzione associato ad una piastra di coltura;
- la Figura 2 mostra in modo schematico una modalità di utilizzo del dispositivo di miscelazione illustrato nella Figura 1;
- le Figure 3 e 4 mostrano una vista prospettica del dispositivo illustrato nella Figura 1, presa rispettivamente dall'alto e dal basso;
- la Figura 5 mostra una vista prospettica in trasparenza di un dettaglio del dispositivo di miscelazione illustrato nella Figura 1 relativo ad un coperchio;
- la Figura 6 mostra il dispositivo illustrato nella Figura 1 parzialmente sezionato, associato ad una piastra di coltura;
- la Figura 7 mostra una vista in esploso del dispositivo di miscelazione illustrato nella Figura 1;
- la Figura 8 mostra una vista in sezione di un dettaglio del dispositivo di miscelazione secondo l'invenzione relativo a mezzi di miscelazione;
- la Figura 9 mostra una vista prospettica di un dettaglio del dispositivo di miscelazione secondo l'invenzione relativo ad una girante;
- la Figura 10 mostra una vista in esploso del dispositivo di miscelazione realizzato in accordo ad una seconda forma realizzativa dell'invenzione;
- le Figure 11 e 12 mostrano una vista prospettica, presa rispettivamente dall'alto e dal basso, di un dettaglio del dispositivo illustrato nella Figura 10 relativo a mezzi di protezione;

- la Figura 13 mostra una vista laterale dei mezzi di protezione illustrati nelle Figure 11 e 12;
- la Figura 14 mostra una vista prospettica del dispositivo illustrato nella Figura 10, in configurazione assemblata, associato ad una piastra di coltura; e - la Figura 15 mostra uno schema cinematico di un sistema di trasmissione del moto di un dispositivo realizzato in accordo ad una soluzione realizzativa particolare dell'invenzione.

C.2.5 Descrizione dettagliata

Il dispositivo di miscelazione meccanica per piastre di coltura secondo l'invenzione verrà indicato nel suo complesso con 1 nella descrizione e nei disegni allegati.

Vantaggiosamente, il dispositivo secondo l'invenzione può essere utilizzato in tutti i settori che prevedono l'utilizzo di piastre di coltura, in particolare per colture cellulari o microbiologiche in sospensione, quali il settore biotecnologico, alimentare, farmaceutico e biomedico.

Il dispositivo di miscelazione secondo la presente invenzione può essere utilizzato – nelle sue diverse varianti – sia con piastre di coltura Petri a singolo pozzetto, sia con piastre di coltura multipozzetto, simili a quella illustrata nella Figura A allegata (dove i pozzetti sono indicati con W e la piastra multipozzetto nel suo complesso con P).

Come già accennato, i pozzetti di piastre di coltura standard definiscono volumi di coltura che variano da un massimo di 10 ml (nel caso di piastra Petri a singolo pozzetto) ad un minimo di 200 μl (nel caso di piastre con 96 pozzetti).

Il dispositivo secondo l'invenzione consente di operare una miscelazione di tipo meccanico tramite giranti sul contenuto dei pozzetti (ad esempio, colture cellulari in sospensione), permettendo il controllo della temperatura e pH ed il

mantenimento della sterilità senza le complicazioni impiantistiche tipiche dei sistemi di miscelazione meccanica di tipo noto. In tal senso - come sarà ripreso nel seguito - il dispositivo 1 secondo l'invenzione è stato ideato e strutturato per poter essere utilizzato all'interno di incubatori biologici (come illustrato nella Figura 2, dove l'incubatore biologico è schematizzato da un riquadro in linea tratteggiata ed indicato con I).

Secondo l'invenzione, il dispositivo di miscelazione meccanica 1 comprende innanzitutto un coperchio 10 destinato ad essere amovibilmente associato ad una piastra di coltura P per schermarne il pozzetto o i pozzetti W limitando così l'ingresso di solidi sospesi nell'aria ambiente A (veicolo di contaminazione biologica), e al contempo permettendo l'ingresso di gas e umidità esterni.

Più in dettaglio, ai fini del mantenimento della sterilità all'interno dei pozzetti W della piastra di coltura P è sufficiente che il coperchio 10 crei un percorso tortuoso per l'ingresso dell'aria esterna. Tale percorso tortuoso impedisce o quantomeno limita l'ingresso di corpi solidi sospesi nell'aria A.

In tal modo il coperchio 10 e la piastra di coltura P viene quindi a crearsi una camera di coltura mantenuta sterile.

Per ciascun singolo pozzetto W di una piastra di coltura P il dispositivo 1 comprende inoltre almeno una girante di miscelazione 20 rotazionalmente associata al suddetto coperchio 10 in corrispondenza della faccia di quest'ultimo destinata ad essere rivolta verso la piastra di coltura P.

Il numero di giranti 20 varia in funzione del numero di pozzetti W della piastra di coltura P.

Il dispositivo 1 comprende inoltre mezzi motori 30 collegabili cinematicamente a ciascuna girante di miscelazione 20.

Secondo l'invenzione, almeno il coperchio 10 e ciascuna girante 20 sono realizzati con materiali biocompatibili che possono essere sottoposti a trattamenti di sterilizzazione e che sono in grado di resistere alle condizioni di umidità, temperatura e pH che si creano in un incubatore biologico.

Per "biocompatibilità" di un materiale si intende la proprietà di un materiale di non interferire con l'attività di organismi, e quindi in particolare la sua inerzia chimica.

Per "trattamento di sterilizzazione" si intende un trattamento di tipo chimico e/o fisico atto ad eliminare da un substrato eventuali organismi o microrganismi, come ad esempio il trattamento termico in autoclave (con temperature non inferiori a 120°C e tempi di trattamento non inferiori a 30 minuti).

Le condizioni di temperatura, umidità e pH che si creano in un incubatore biologico variano in funzione delle esigenze specifiche della coltura biologica. Mediamente, tuttavia, le temperature sono comprese tra 35°C e 38°C, pH tra 4 e 8 e umidità tra 80% e 100%.

Vantaggiosamente, il dispositivo 1 secondo l'invenzione può comunque essere impiegato in un più ampio spettro di condizioni, con temperature tra 0 e 100°C, pH tra 1 e 13 e umidità tra 0 e 100%.

Preferibilmente, vengono usati materiali come il policarbonato (in particolare per realizzare il coperchio 10) o il teflon (in particolare per realizzare le giranti di miscelazione 20).

Possono tuttavia essere usati in alternativa anche altri materiali, come ad esempio polistirene e altri polimeri plastici, vetro, metalli, ceramiche e siliconi, con proprietà tali da risultare biocompatibili e resistere - senza subire deterioramenti - a trattamenti di sterilizzazione e alle condizioni di pH, temperatura e umidità che si vengono a creare in un incubatore biologico.

Il dispositivo di miscelazione 1 secondo l'invenzione può pertanto essere utilizzato direttamente all'interno di un incubatore biologico. In questo modo, pur operando una miscelazione meccanica mediante giranti, è possibile controllare le condizioni di temperatura, umidità e pH (regolando la concentrazione di CO^2 nell'aria) della coltura biologica presente nella piastra di coltura senza dover prevedere soluzioni impiantistiche ad hoc.

Preferibilmente i mezzi motori 30 sono associati meccanicamente al coperchio 10 e sono quindi destinati ad operare all'interno di un incubatore biologico. Ciò rende più semplice e pratico l'utilizzo del dispositivo 1.

In questo caso, vantaggiosamente, i mezzi motori 30 sono provvisti di mezzi di schermatura 32 atti a proteggere le parti elettriche dei mezzi motori 30 sensibili all'umidità.

In alternativa, è possibile prevedere un dispositivo 1 in cui i mezzi motori non sono meccanicamente associati al coperchio 10 per poter operare dall'esterno di un incubatore biologico. Questa soluzione impone tuttavia complicazioni costruttive ed operative in quanto si deve prevedere un collegamento cinematico tra le giranti disposte all'interno dell'incubatore e i mezzi motori disposti all'esterno dello stesso.

Preferibilmente i mezzi motori 30 comprendono almeno un motore elettrico 31 cinematicamente collegabile a ciascuna girante 20.

Preferibilmente, come previsto nelle soluzioni realizzative illustrate rispettivamente nelle Figure 1 e 14, il motore elettrico 31 è destinato ad essere amovibilmente associato sulla parte sommitale del coperchio 10.

Vantaggiosamente, il motore elettrico 31 è provvisto di un contenitore ermetico 32 atto a proteggerlo dall'umidità in modo da consentirne un uso sicuro all'interno di un incubatore biologico I. Come si può osservare in particolare nelle Figure 1 e 12,

il contenitore ermetico 32 è provvisto di un'apposita apertura attraverso la quale passa l'albero 35 del motore 31.

In accordo ad una soluzione realizzativa preferita, i mezzi motori 30 comprendono almeno un alimentatore elettrico 33 collegabile elettricamente al motore elettrico 31.

Operativamente, il motore elettrico 31 è destinato ad operare - associato al coperchio 10 - all'interno di un incubatore biologico I, mentre l'alimentatore 33 è destinato ad operare all'esterno dell'incubatore I (come illustrato schematicamente nella Figura 2).

Funzionalmente, l'alimentatore 33 e il motore 31 vengono collegati tra loro tramite cavi di connessione elettrica 80 che possono essere fatti passare semplicemente attraverso aperture normalmente previste in tutti gli incubatori biologici.

Preferibilmente, l'alimentatore elettrico 33 è atto a fornire corrente elettrica stabilizzata, dalla cui intensità dipende la velocità di rotazione trasmessa dal motore 31 a ciascuna girante 20.

Vantaggiosamente, l'alimentatore elettrico 33 può essere provvisto di un sistema di regolazione dell'intensità della corrente elettrica stabilizzata in modo che sia possibile adattare l'intensità di miscelazione alle specifiche esigenze della coltura biologica.

In accordo ad una soluzione realizzativa alternativa (non illustrata nelle Figure allegate), il motore elettrico 31 può essere alimentato da batterie elettriche alloggiate internamente al contenitore ermetico. In tal modo il motore elettrico 31 può operare autonomamente, senza che sia necessaria alcuna connessione elettrica esternamente all'incubatore biologico. Il dispositivo 1 risulta essere inoltre complessivamente più compatto.

Come già accennato in precedenza, il dispositivo 1 comprende almeno una girante di miscelazione 20 per ogni pozzetto W di una piastra di coltura P.

Vantaggiosamente, la morfologia delle giranti 20 può essere adattata alle particolari esigenze del ambiente di coltura, in funzione di considerazioni fluidodinamiche.

Ciascuna girante di miscelazione 20 è rotazionalmente collegata al coperchio 10 ed è cinematicamente collegabile ai mezzi motori 30.

Preferibilmente, il collegamento cinematico tra ciascuna girante 20 e i mezzi motori 30 può essere di tipo meccanico.

Più in dettaglio, la girante 20 è rotazionalmente associata al coperchio 10 in modo tale che l'albero della girante sia accessibile dall'esterno del coperchio 10. La girante 20 è collegata al coperchio in modo tale che tra l'albero di rotazione 22 della girante 20 e lo spessore del coperchio 10 sia realizzata un'intercapedine 21 (che mette in comunicazione la camera di coltura sottostante il coperchio e l'ambiente esterno) avente un andamento tortuoso (come illustrato ad esempio nella Figura 8). L'intercapedine permette l'ingresso di aria e gas dall'esterno per diffusione, ma il suo andamento tortuoso impedisce la penetrazione di eventuali corpi solidi sospesi salvaguardando il grado di sterilità interno della piastra di coltura. Tra il coperchio 10 e la piastra di coltura P si riesce quindi a mantenere una camera di coltura sterile.

In accordo ad una soluzione realizzativa preferita dell'invenzione, illustrata in particolare nelle Figure 8 e 9, ciascuna girante 20 è provvista di un mozzo 20' atto ad inserirsi rotazionalmente con una prima estremità in un'apposita apertura di innesto 13 ricavata sul coperchio 10 e di una o più pale 23, associate all'altra estremità del mozzo 20'.

Funzionalmente, il mozzo 20' viene associato tramite un elemento assiale di fissaggio 24 (ad esempio, una vite) ad un ingranaggio 36 (ad esempio,una ruotata

dentata o una puleggia), che viene disposto sulla faccia esterna del coperchio ed è a sua volta cinematicamente collegabile ai mezzi motori 30 per ricevere un moto rotativo. L'elemento di fissaggio 24 funge così da albero di rotazione della girante 20.

Più in dettaglio, sempre in accordo alla suddetta soluzione realizzativa preferita illustrata nella Figura 8, in corrispondenza della faccia esterna del coperchio l'apertura di innesto 13 presenta una sezione allargata definente una sede 14. Tale sede 14 è destinata ad alloggiare una boccola 25, che va ad interporsi assialmente tra il mozzo 20' e l'ingranaggio 36 ricevendo internamente l'elemento assiale di fissaggio 22.

La boccola 25 funge da cuscinetto e da elemento distanziatore tra l'ingranaggio 36 e la superficie del coperchio 10. La boccola è realizzata in teflon, così da facilitare il moto rotativo sfruttando le proprietà autolubrificanti di questo materiale.

Questa soluzione costruttiva rende sostanzialmente superfluo l'inserimento di elementi di tenuta ad O-ring. Infatti, grazie alla variazione di sezione lungo l'apertura 13 e alla presenza della boccola 25 viene a crearsi un percorso tortuoso che impedisce l'ingresso di corpi solidi sospesi nell'aria esterna.

Preferibilmente, come si può osservare nella Figura 8, la porzione 20" con la quale il mozzo 20' si inserisce nell'apertura 13 ha una sezione ridotta. In corrispondenza dello scalino formato dalla porzione 20" viene così a crearsi tra la faccia interna del coperchio 10 ed il mozzo 20' una zona di battuta che aumenta ulteriormente la tortuosità del percorso che l'aria deve percorrere per passare dall'esterno all'interno della camera di coltura.

In alternativa al collegamento di tipo meccanico, il collegamento cinematico tra ciascuna girante 20 e i mezzi motori 30 può essere di tipo a trascinamento magnetico.

Più in dettaglio, la girante 20 è ancora rotazionalmente associata al coperchio 10 (in modo tale che le sollecitazioni meccaniche che si generano durante la rotazione possano scaricarsi principalmente sul coperchio 10), ma è portata in rotazione per trascinamento magnetico dall'esterno del coperchio 10. In tal modo si evita di dover realizzare sul coperchio aperture che (pur schermate e protette) sono comunque zone potenziali di ingresso di elementi di contaminazione.

In accordo ad una soluzione realizzativa alternativa (non illustrata nella Figure allegate) ciascuna girante 20 è provvista di un mozzo atto ad inserirsi rotazionalmente con una prima estremità in un'apposita sede cieca ricavata sulla faccia interna del coperchio e di una o più pale, associate all'altra estremità del mozzo. La girante è provvista di un elemento sensibile al campo magnetico. Sulla faccia esterna del coperchio 10 viene rotazionalmente collegato un ingranaggio (ad esempio,una ruotata dentata o una puleggia) provvisto a sua volta di un elemento magnetico. Grazie a tale elemento magnetico l'ingranaggio riesce a trascinare la girante nel movimento di rotazione che a sua volta riceve dai mezzi motori.

Vantaggiosamente, i mezzi motori 30 comprendono un sistema di trasmissione del moto 36, 37 dall'albero motore 35 del motore elettrico 31 all'albero 22 di ciascuna girante 20 (tramite collegamento meccanico o magnetico).

Come già accennato in precedenza il dispositivo di miscelazione 1 secondo l'invenzione può essere utilizzato con piastre di coltura, del tipo Petri a singolo pozzetto o del tipo multipozzetto. Il numero e la disposizione delle giranti 20 varia dunque in funzione del numero di pozzetti W della piastra di coltura P.

Nel caso di utilizzo con piastre Petri a singolo pozzetto, il dispositivo 1 è provvisto di un'unica girante 20. In questo caso l'ingranaggio 36 cinematicamente collegato al mozzo 20' della girante può essere collegato direttamente all'albero motore 35 del motore 31. Il sistema di trasmissione del moto è quindi molto semplice e può

essere realizzato da due ruote dentate oppure da due pulegge collegate da una cinghia o una catena.

Nel caso di utilizzo con piastre di coltura multipozzetto, come illustrato nelle Figure allegate, il sistema di trasmissione del moto 36, 37 deve essere più articolato dovendo essere asservito ad una pluralità di giranti. In funzione della disposizione e del numero delle giranti il sistema di trasmissione comprende una o più catene cinematiche 36, ciascuna delle quali asservita ad una o più giranti 20.

In accordo ad una soluzione realizzativa preferita illustrata nella Figura 1, le catene cinematiche sono costituite da una pluralità di ingranaggi 36 (ruote dentate).

Nel caso di una piastra di coltura a 6 pozzetti (disposte in due file da tre), una soluzione preferita prevede due cascate di ruote dentate 36 in parallelo, ciascuna delle quali asservita a tre giranti.

Più in dettaglio, lo schema cinematico prevede una ruota dentata motrice 35' (associata all'albero motore 35) e due cascate di ruote dentate ciascuna della quali composta da 3 ruote dentate principali 36 cinematicamente collegate alla rispettiva girante 20 e 2 ruote dentate di collegamento 37. Lo schema cinematico di questa soluzione è illustrato nella Figura 15.

La struttura e la disposizione delle catene cinematiche 36 varia in funzione del numero e della disposizione delle giranti 20 e quindi della struttura della piastra di coltura P.

In accordo a soluzioni realizzative alternative le catene cinematiche possono essere realizzate anche con pluralità di pulegge e cinghie o catene.

Vantaggiosamente, gli ingranaggi vengono realizzati con materiali, aventi proprietà tali da risultare biocompatibili e resistere - senza subire deterioramenti - a trattamenti di sterilizzazione e alle condizioni di pH, temperatura e umidità che si

vengono a creare in un incubatore biologico. In particolare le ruote dentate possono essere realizzate in materiale polimerico.

Riprendendo quanto già accennato in precedenza, il coperchio 10 del dispositivo di miscelazione 1 è destinato ad essere amovibilmente associato ad una piastra di coltura P allo scopo di schermarne i pozzetti W impedendo così l'ingresso di solidi sospesi nell'aria ambiente, e al contempo permettendo l'ingresso di gas e umidità esterni.

Preferibilmente, come si può osservare nelle Figure 4 e 5, il coperchio 10 comprende:

- una porzione principale 11, destinata a sovrapporsi alla piastra di coltura P con funzione di schermo e a supportare le catene cinematiche 36 del sistema di trasmissione del moto; ed
- una porzione secondaria 12, destinata a supportare meccanicamente ed amovibilmente i mezzi motori 30 (nello specifico il motore elettrico 31) in posizione scostata rispetto alla piastra di coltura P; in tal modo si riduce l'interferenza che il motore 31 può eventualmente esercitare sulla coltura, in particolare tramite vibrazioni, campi magnetici/elettrici e/o scambi di calore.

Come si può osservare in particolare nella Figura 5, nella porzione principale 11 del coperchio 10 vengono realizzate sulla superficie sommitale le aperture di innesto 13 o sedi cieche (non illustrate) per le giranti, nonché le sedi di rotazione 18 per le ruote dentate di collegamento 37 (nel caso in cui siano previste catene cinematiche con ruote dentate).

Nella porzione secondaria 12, sempre sulla superficie sommitale del coperchio 10, vengono invece realizzate apposite aperture 19 per il fissaggio di mezzi di supporto 90 del motore 31.

Più in dettaglio, i suddetti mezzi di supporto 90 possono consistere semplicemente in una staffa che con un primo braccio viene collegata amovibilmente al coperchio 10 e con un secondo braccio viene associata stabilmente al motore 31 o eventualmente al contenitore ermetico 32.

Vantaggiosamente, le aperture 19 possono essere realizzate in forma di feritoie o serie di fori allineati così da permettere una regolazione nel posizionamento del motore 31 rispetto alle catene cinematiche 36 e alle giranti 20.

Preferibilmente, il coperchio 10 presenta una struttura scatolare aperta avente base sostanzialmente rettangolare. Il volume interno del coperchio 10 è diviso in due camere 16 e 17 tramite una parete divisoria interna 15, che corrispondono rispettivamente alla porzione principale 11 e alla porzione secondaria 12.

La forma e le dimensioni del coperchio possono tuttavia variare per adattarsi alle piastre di coltura P disponibili in commercio.

Vantaggiosamente, il coperchio 10 può essere sagomato opportunamente per facilitarne la presa e la manipolazione.

In accordo alla soluzione realizzativa illustrata in particolare nelle Figure da 3 a 7, il coperchio 10 è realizzato in modo da racchiudere perimetralmente al suo interno la piastra di coltura P appoggiandosi direttamente sullo stesso piano di appoggio della piastra.

In accordo ad una soluzione realizzativa alternativa, il coperchio 10 può essere realizzato per andare invece in appoggio sul bordo perimetrale della piastra di coltura P, almeno limitatamente alla porzione principale 11. Questa soluzione richiede, però, che il coperchio abbia sostanzialmente le stesse dimensioni della piastra di coltura.

In accordo ad una soluzione realizzativa particolare illustrata nelle Figure da 10 a 14, il dispositivo 1 comprende:

- una base di appoggio 40 atta a supportare la piastra di coltura P e almeno la porzione principale 11 del coperchio 10;
- un corpo di protezione 50 destinato ad essere disposto almeno sopra la porzione principale 11 del coperchio 10. Più in dettaglio vengono inoltre previsti:
- primi mezzi di tenuta 61 (ad esempio in materiale elastomerico) destinati ad essere interposti nella zona di battuta tra la base di appoggio 40 e il coperchio 10;
- secondi mezzi di tenuta 62 destinati ad essere interposti nella zona di battuta tra il corpo di protezione 50 e il coperchio 10;
- terzi mezzi di tenuta 63 destinati ad essere inseriti nella zona di innesto dell'albero 35 del motore 31 nel corpo di protezione 50.

Il dispositivo comprende inoltre mezzi di assiemaggio 70 suscettibili di agire in corrispondenza del coperchio 10, della base di appoggio 40 e/o del corpo di protezione 50 per trattenere insieme la varie parti e comprimere i mezzi di tenuta 61, 62 e 63.

Più in dettaglio, i suddetti mezzi di assiemaggio possono essere realizzati da una pluralità di staffe 90, come illustrato nella Figura 14.

Questa forma realizzativa particolare del dispositivo 1 secondo l'invenzione è destinata ad essere utilizzata nel caso in cui ci sia la necessità di garantire all'interno dell'ambiente di coltura un grado di sterilità superiore rispetto a quello ottenibile con il dispositivo 1 realizzato in accordo alla soluzione realizzativa illustrata nelle figure da 1 a 7.

In questo caso specifico, il dispositivo 1 viene provvisto di mezzi di controllo e regolazione dell'atmosfera gassosa (O_2, umidità, CO_2) interna della camera di coltura. Tali mezzi (non illustrati nelle figure allegate) possono consistere

semplicemente in una serie di condotti di ingresso e uscita comunicanti con la camera di coltura e con apposita strumentazione di controllo. Tali condotti vengono inseriti all'interno della camera di coltura tramite apposite aperture ricavate sul coperchio 10 e sul corpo di protezione 50.

Il dispositivo di miscelazione 1 secondo l'invenzione – nelle sue diverse varianti – offre una serie di vantaggi, in parte già esplicitati nel corso della descrizione.

Un primo importante vantaggio del dispositivo 1 è dato dalla sua praticità d'uso e la sua integrabilità con comuni attrezzature presenti in un laboratorio biologico.

L'impiego del dispositivo 1 non va infatti ad influire in maniera rilevante sulla procedura normalmente seguita per una normale coltura biologica.

Una volta preparata la coltura nella piastra P si procede ad associare alla stessa il coperchio 10: è poi sufficiente disporre con poche e semplici operazioni il motore 31 sul coperchio e impostare l'intensità di miscelazione. L'utilizzo del dispositivo 1 non richiede pertanto particolari abilità o conoscenze tecniche.

Il fatto che il dispositivo 1 possa essere usato direttamente su piastre di coltura, Petri o multiwell, di tipo standard permette all'utilizzatore di seguire senza alcuna modifica i protocolli di coltura biologici specificamente studiati per tali piastre. È noto infatti che molte colture cellulari, ad esempio colture di cellule staminali, sono estremamente sensibili alle condizioni ambientali, potendo essere influenzate, ad esempio, anche da semplici variazioni dei volumi e delle proprietà chimiche e meccaniche delle superfici di coltura.

Un altro importante vantaggio dato dal dispositivo 1 secondo l'invenzione è legato alla possibilità di utilizzo in un normale incubatore biologico. Come già ampiamente descritto in dettaglio, ciò semplifica il controllo della temperatura, pH e della composizione dell'atmosfera gassosa.

Il dispositivo 1 può quindi essere utilizzato senza richiedere servizi esterni (come ad esempio acqua o CO_2) ad esso specificamente dedicati.

Il dispositivo 1 non necessita di nessun accorgimento particolare per il mantenimento della sterilità, essendo strutturato per limitare l'ingresso di corpi solidi sospesi nell'aria esterna.

Il dispositivo è infine di semplice ed economica realizzazione non richiedendo componenti sofisticati o complessi.

L'invenzione così concepita raggiunge pertanto gli scopi prefissi.

Ovviamente, essa potrà assumere, nella sua realizzazione pratica anche forme e configurazioni diverse da quella sopra illustrata, senza che, per questo, si esca dal presente ambito di protezione.

Inoltre tutti i particolari potranno essere sostituiti da elementi tecnicamente equivalenti e le dimensioni, le forme ed i materiali impiegati potranno essere qualsiasi a seconda delle necessità.

C.3 Rivendicazioni

1. Dispositivo di miscelazione meccanica per piastra di coltura, comprendente:
   - un coperchio (10) destinato ad essere amovibilmente associato ad una piastra di coltura (P) per schermare il pozzetto o i pozzetti (W) di quest'ultima limitando l'ingresso di solidi sospesi nell'aria ambiente, e al contempo permettendo l'ingresso di gas e umidità esterni;
   - almeno una girante di miscelazione (20) per ciascun pozzetto (W) di detta piastra di coltura (P), detta girante (20) essendo rotazionalmente associata a detto coperchio (10) in corrispondenza della faccia di quest'ultimo destinata ad essere rivolta verso detta piastra di coltura (P);

- mezzi motori (30) collegabili cinematicamente a detta almeno una girante (20);

detto coperchio (10) e detta almeno una girante (20) essendo realizzati con materiali che possono essere sottoposti a trattamenti di sterilizzazione e sono in grado di resistere alle condizioni di umidità, temperatura e pH che si creano in un incubatore biologico.

2. Dispositivo secondo la rivendicazione 1, in cui il collegamento cinematico tra detta almeno una girante (20) e detti mezzi motori (30) è di tipo meccanico.

3. Dispositivo secondo la rivendicazione 1 o 2, in cui detta girante (20) è rotazionalmente associata a detto coperchio (10) in modo tale che tra l'albero (22) di detta girante (20) e detto coperchio (10) sia realizzata un'intercapedine (21) avente un andamento tortuoso per limitare l'ingresso di corpi solidi sospesi.

4. Dispositivo secondo la rivendicazione 1 o 2, in cui il collegamento cinematico tra detta almeno una girante (20) e detti mezzi motori (30) è di tipo a trascinamento magnetico.

5. Dispositivo secondo una qualsiasi delle rivendicazioni precedenti, in cui detti mezzi motori (30) sono associabili meccanicamente a detto coperchio (10).

6. Dispositivo secondo una qualsiasi delle rivendicazioni precedenti, in cui detti mezzi motori (30) sono provvisti di mezzi di schermatura (32) atti a proteggere le parti di detti mezzi motori (30) sensibili all'umidità.

7. Dispositivo secondo una o più delle rivendicazioni precedenti, in cui detti mezzi motori (30) comprendono almeno un motore elettrico (31) cinematicamente collegabile a detta almeno una girante (20).

8. Dispositivo secondo la rivendicazione 7, in cui detto motore elettrico (31) è atto ad essere amovibilmente associato a detto coperchio (10).

9. Dispositivo secondo la rivendicazione 7 o 8, in cui detto motore elettrico (31) è provvisto di un contenitore ermetico (32) atto a proteggerlo dall'umidità.

10. Dispositivo secondo una o più delle rivendicazioni da 4 a 6, in cui detti mezzi motori (30) comprendono almeno un alimentatore elettrico (33) collegabile elettricamente a detto motore elettrico.

11. Dispositivo secondo la rivendicazione precedente, in cui detto alimentatore elettrico (33) è atto a fornire una corrente elettrica stabilizzata, dalla cui intensità dipende la velocità di rotazione trasmessa da detto motore (31) a detta almeno una girante (20).

12. Dispositivo secondo la rivendicazione precedente, in cui detto alimentatore elettrico (33) è provvisto di un sistema di regolazione dell'intensità della corrente elettrica stabilizzata.

13. Dispositivo secondo una o più delle rivendicazione da 7 a 12, in cui detti mezzi motori (30) comprendono un sistema di trasmissione del moto (36, 37) dall'albero motore (35) di detto motore elettrico (31) all'albero (22) di detta almeno una girante (20).

14. Dispositivo secondo la rivendicazione precedente, in cui detto sistema di trasmissione del moto (36, 37) comprende una o più catene cinematiche (36), ciascuna delle quali asservita ad una o più giranti (20).

15. Dispositivo secondo la rivendicazione 14, in cui dette una o più catene cinematiche comprendono una pluralità di ingranaggi (36).

16. Dispositivo secondo la rivendicazione precedente, in cui detti ingranaggi (36) sono cinematicamente collegati a dette giranti (20).

17. Dispositivo secondo la rivendicazione 14, in cui dette una o più catene cinematiche comprendono una pluralità di pulegge e cinghie o catene.

18. Dispositivo secondo la rivendicazione precedente, in cui dette pulegge sono cinematicamente collegate a dette giranti.

19. Dispositivo secondo una o più delle rivendicazioni da 14 a 18, in cui dette catene cinematiche (36) sono supportate da detto coperchio (10).

20. Dispositivo secondo una o più delle rivendicazioni precedenti, in cui detto coperchio (10) comprende una porzione principale (11), destinata a sovrapporsi a detta piastra di coltura (P) con funzione di schermo, ed una porzione secondaria (12), destinata a supportare meccanicamente ed amovibilmente detti mezzi motori (30) in posizione scostata rispetto a detta piastra di coltura (P).

21. Dispositivo secondo una o più delle rivendicazioni precedenti, in cui detto coperchio (10) è atto a racchiudere perimetralmente al suo interno detta piastra di coltura (P) appoggiandosi direttamente sullo stesso piano di appoggio di detta piastra di coltura (P).

22. Dispositivo secondo una o più delle rivendicazioni da 1 a 20, comprendente una base di appoggio (40) atta a supportare detta piastra di coltura (P) e almeno la porzione principale (11) di detto coperchio (10).

23. Dispositivo secondo una o più delle rivendicazioni precedenti, comprendente un corpo di protezione (50) destinato ad essere disposto sopra detta almeno porzione principale (11) di detto coperchio (10).

24. Dispositivo secondo una o più delle rivendicazioni precedenti, comprendente primi mezzi di tenuta (61) destinati ad essere interposti nella zona di battuta tra detta base di appoggio (40) e detto coperchio (10).

25. Dispositivo secondo una o più delle rivendicazioni precedenti, comprendente secondi mezzi di tenuta (62) destinati ad essere interposti nella zona di battuta tra detto corpo di protezione (50) e detto coperchio (10).

26. Dispositivo secondo una o più delle rivendicazioni precedenti, comprendente terzi mezzi di tenuta (63) destinati ad essere inseriti nella zona di innesto dell’albero motore (35) di detto motore (31) in detto corpo di protezione (50).

27. Dispositivo secondo una o più delle rivendicazioni precedenti, comprendente mezzi di assiemaggio (70) suscettibili di agire su detto coperchio (10) e/o su detta base di appoggio (40) e/o su detto corpo di protezione (50) per comprimere detti mezzi di tenuta (61, 62, 63).

28. Dispositivo secondo una o più delle rivendicazioni da 22 a 27, comprendente mezzi di controllo e regolazione dell’atmosfera gassosa interna alla camera di coltura delimitata da detto coperchio (10), detta base di appoggio (40) e detto corpo di protezione (50).

29. Dispositivo secondo una o più delle rivendicazioni procedenti, in cui detto coperchio (10) è realizzato in policarbonato.

30. Dispositivo secondo una o più delle rivendicazioni precedenti, in cui detta almeno una girante (20) è realizzata in teflon.

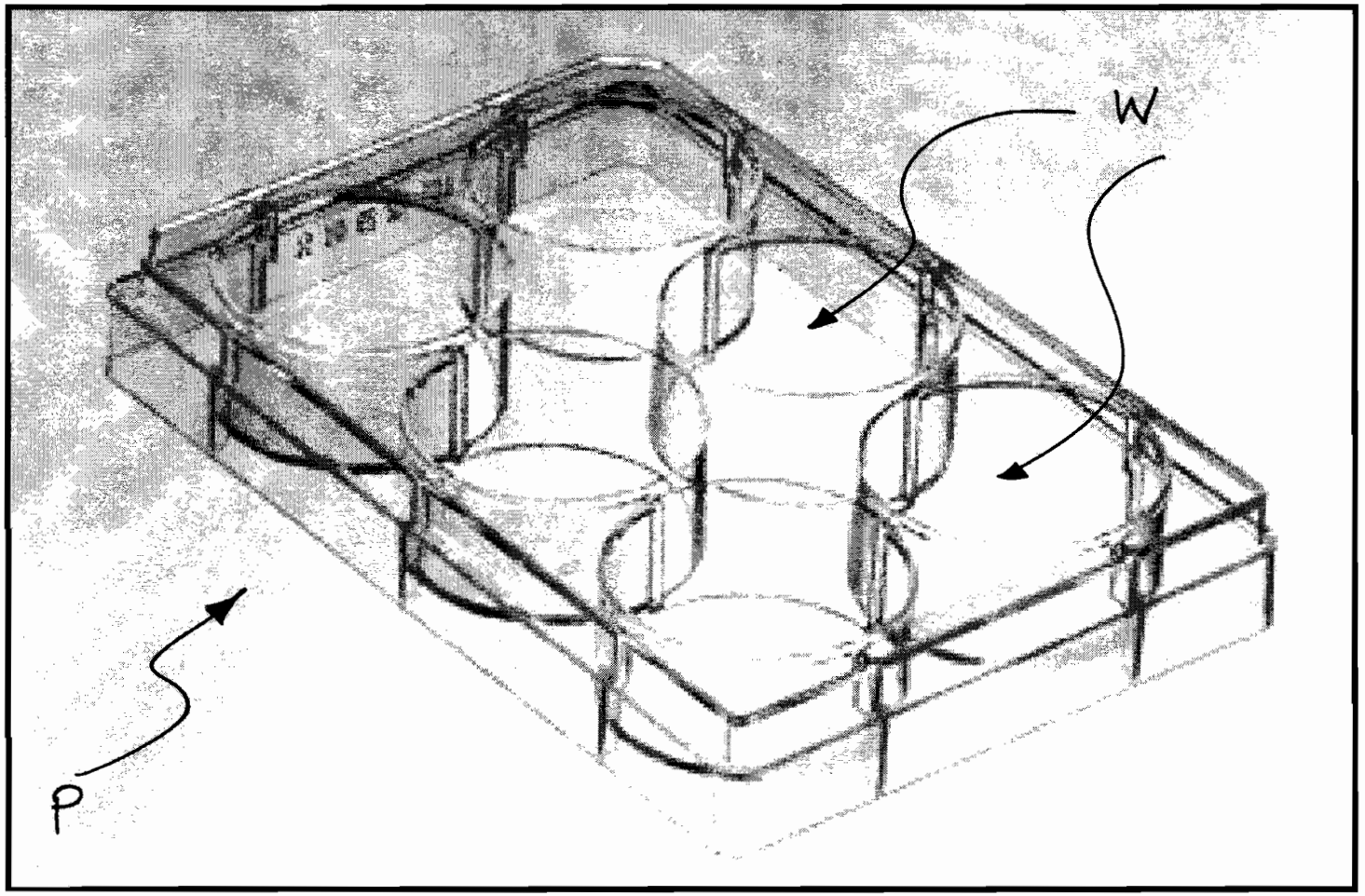

Fig. A

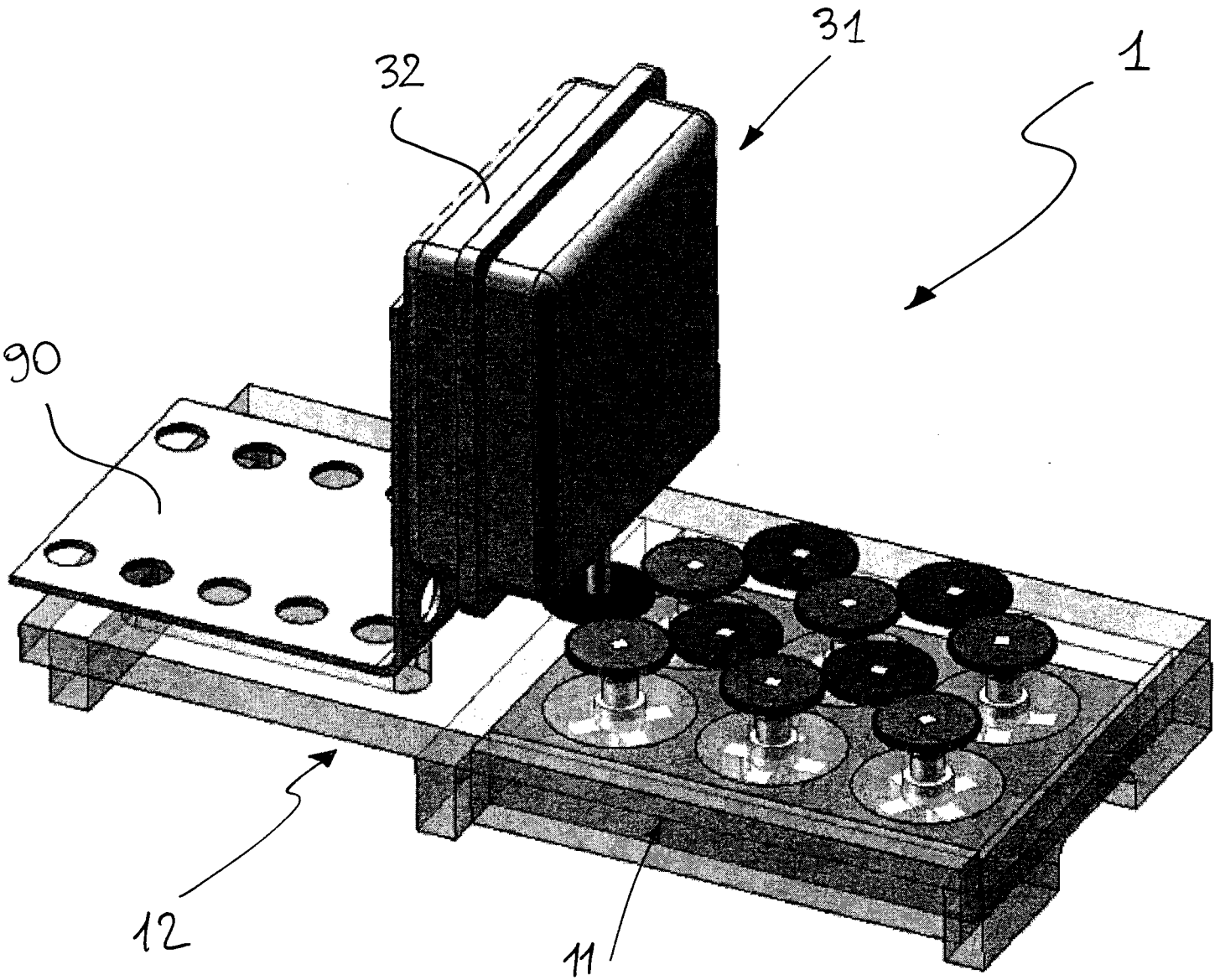

Fig. 1

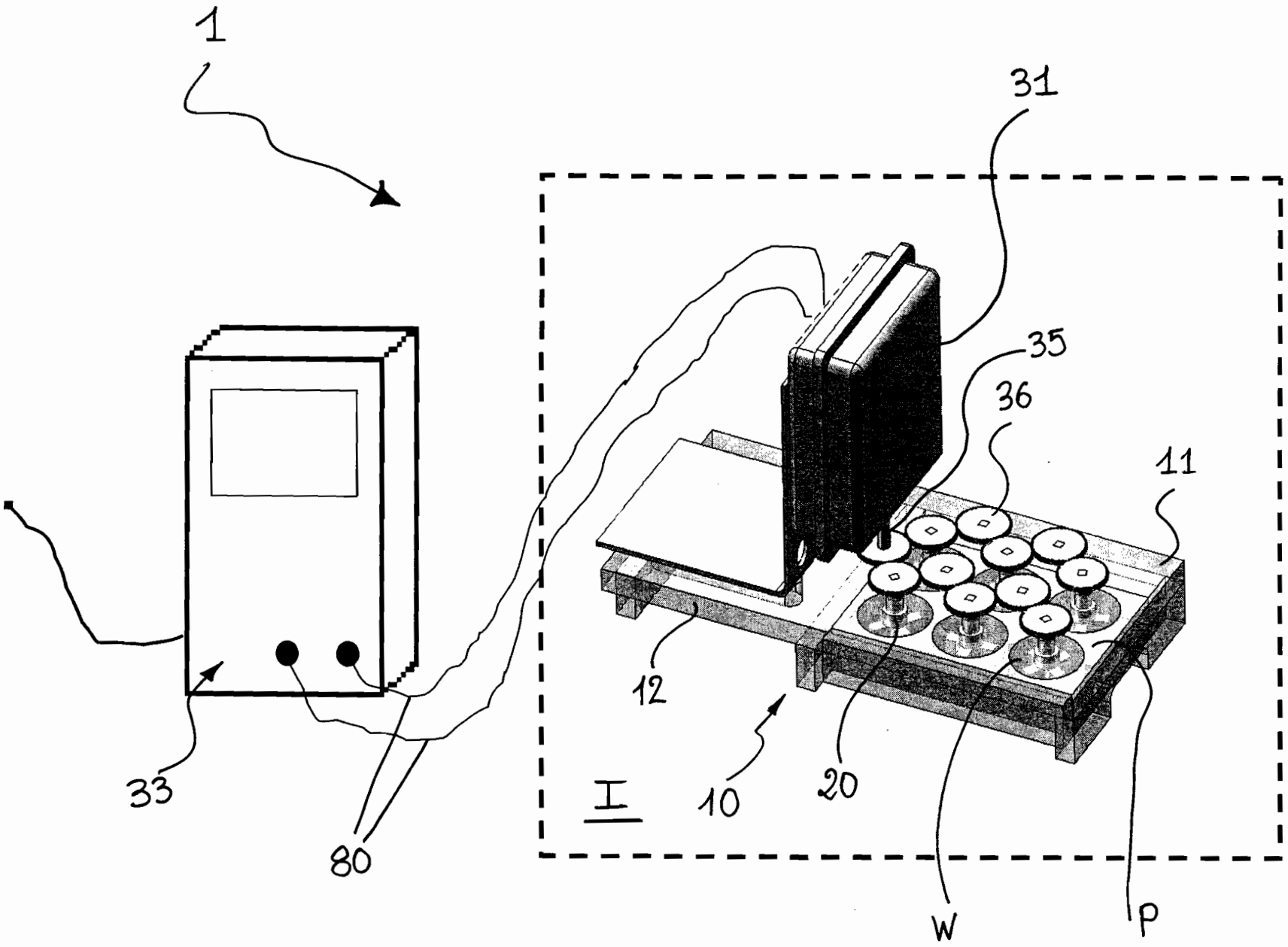

Fig. 2

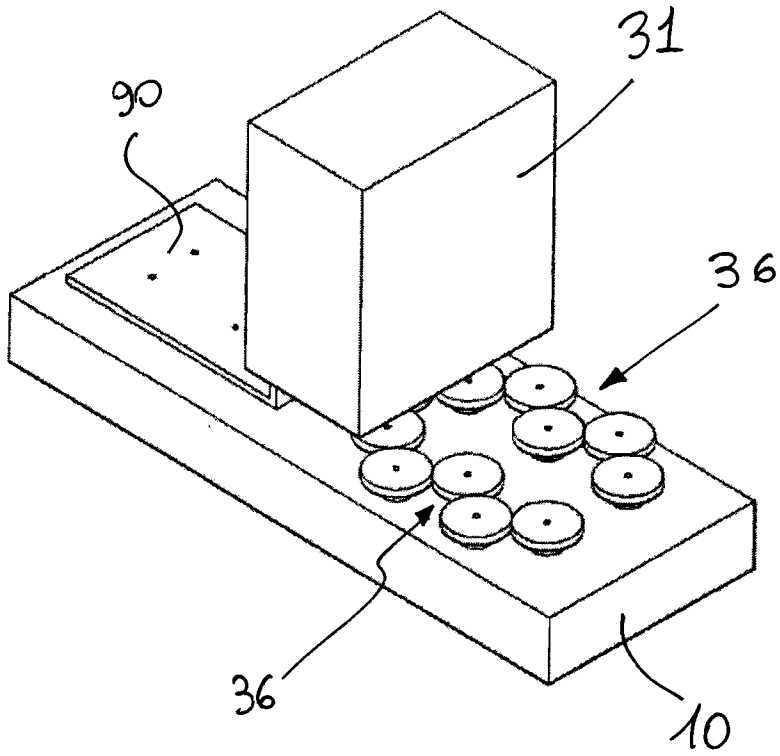

Fig. 3

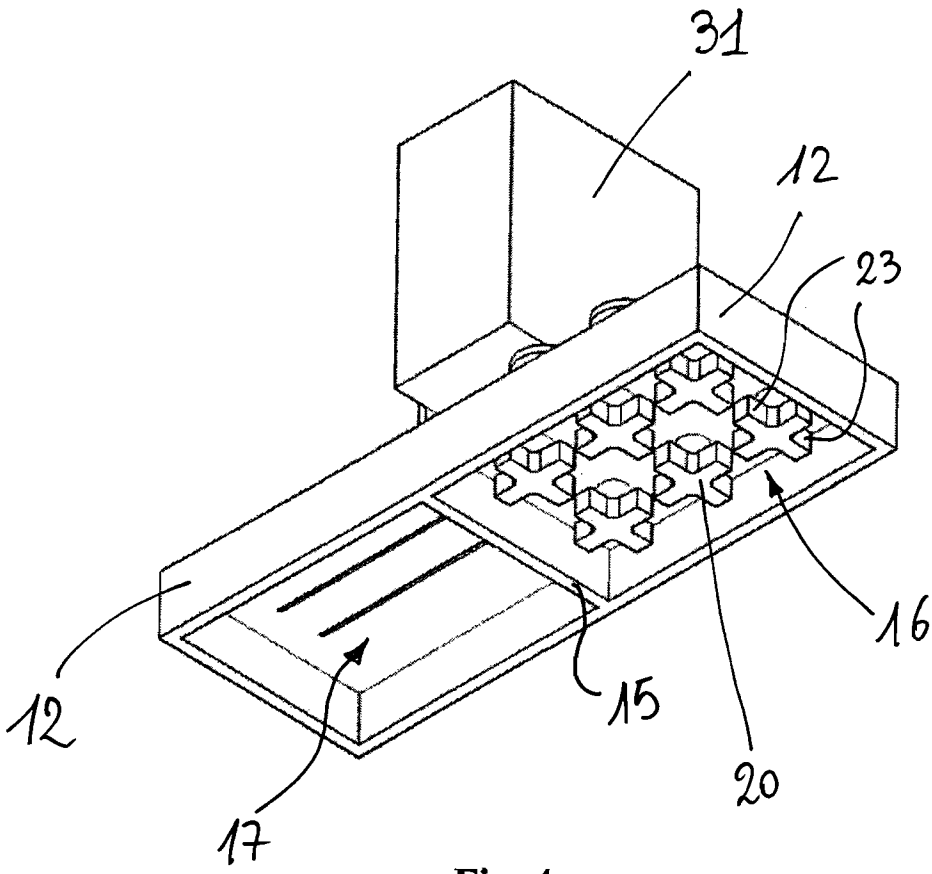

Fig. 4

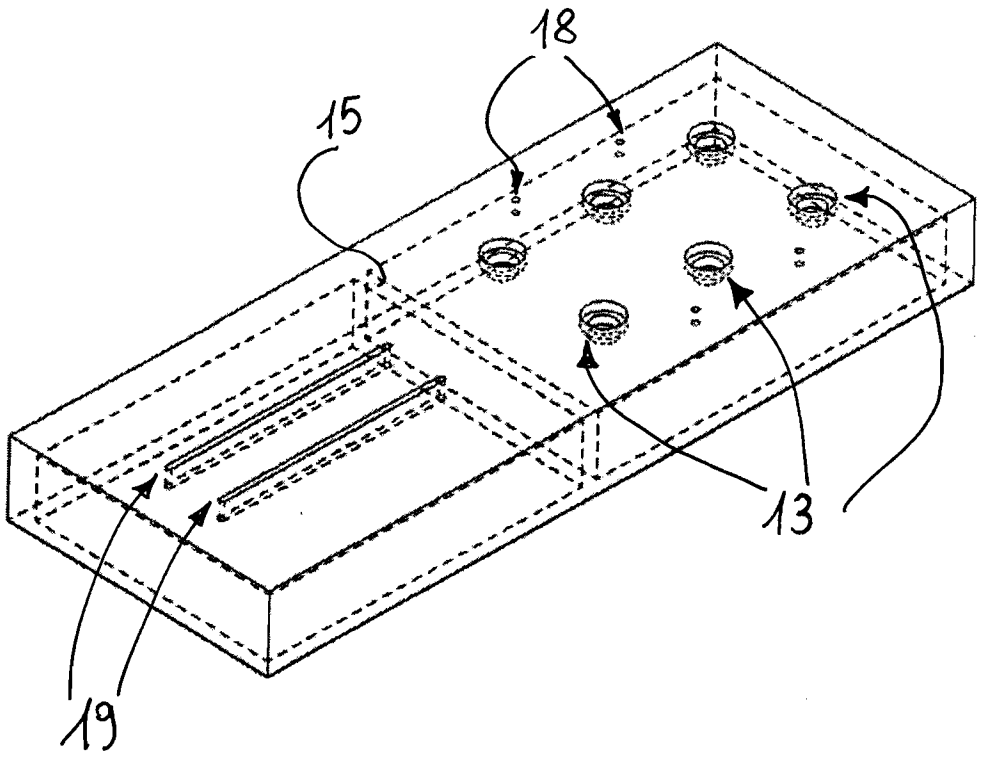

Fig. 5

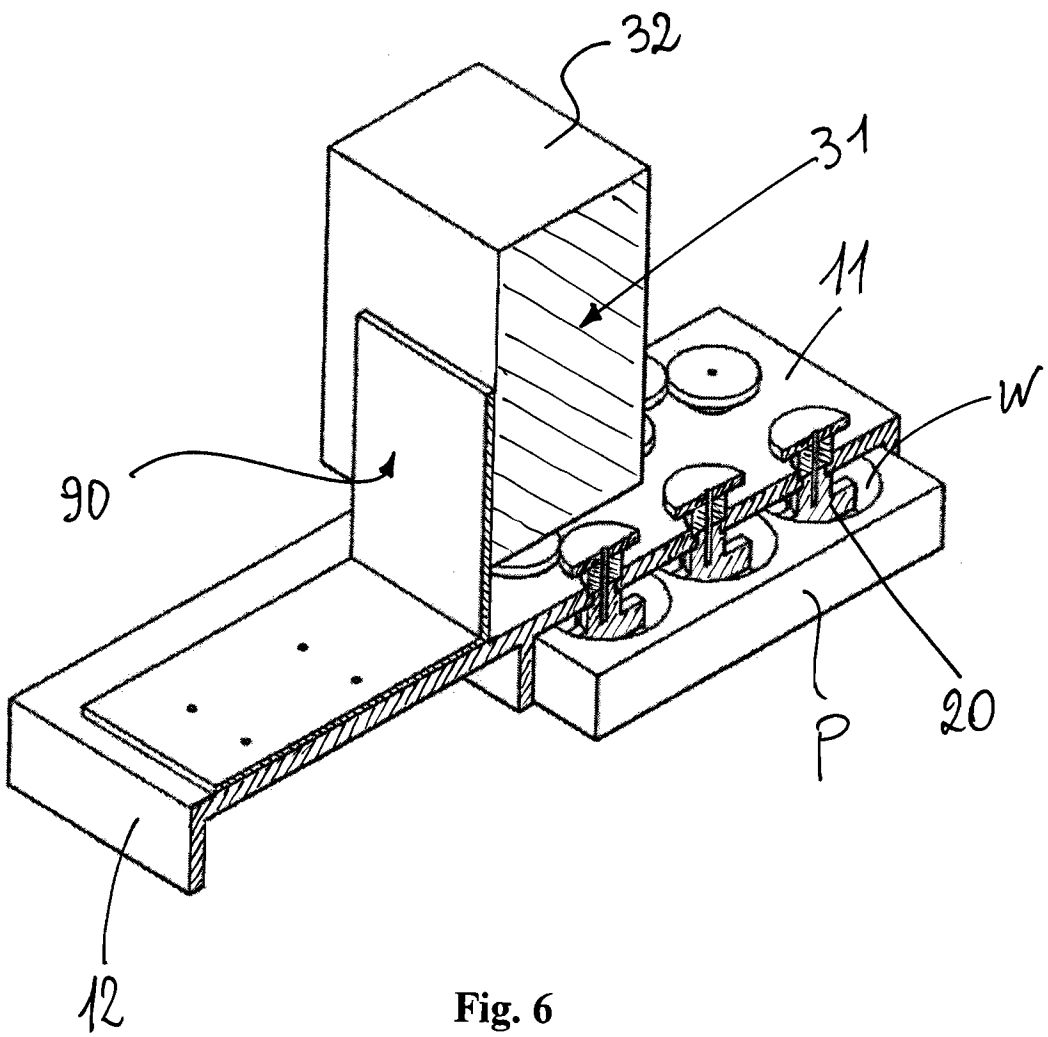

Fig. 6

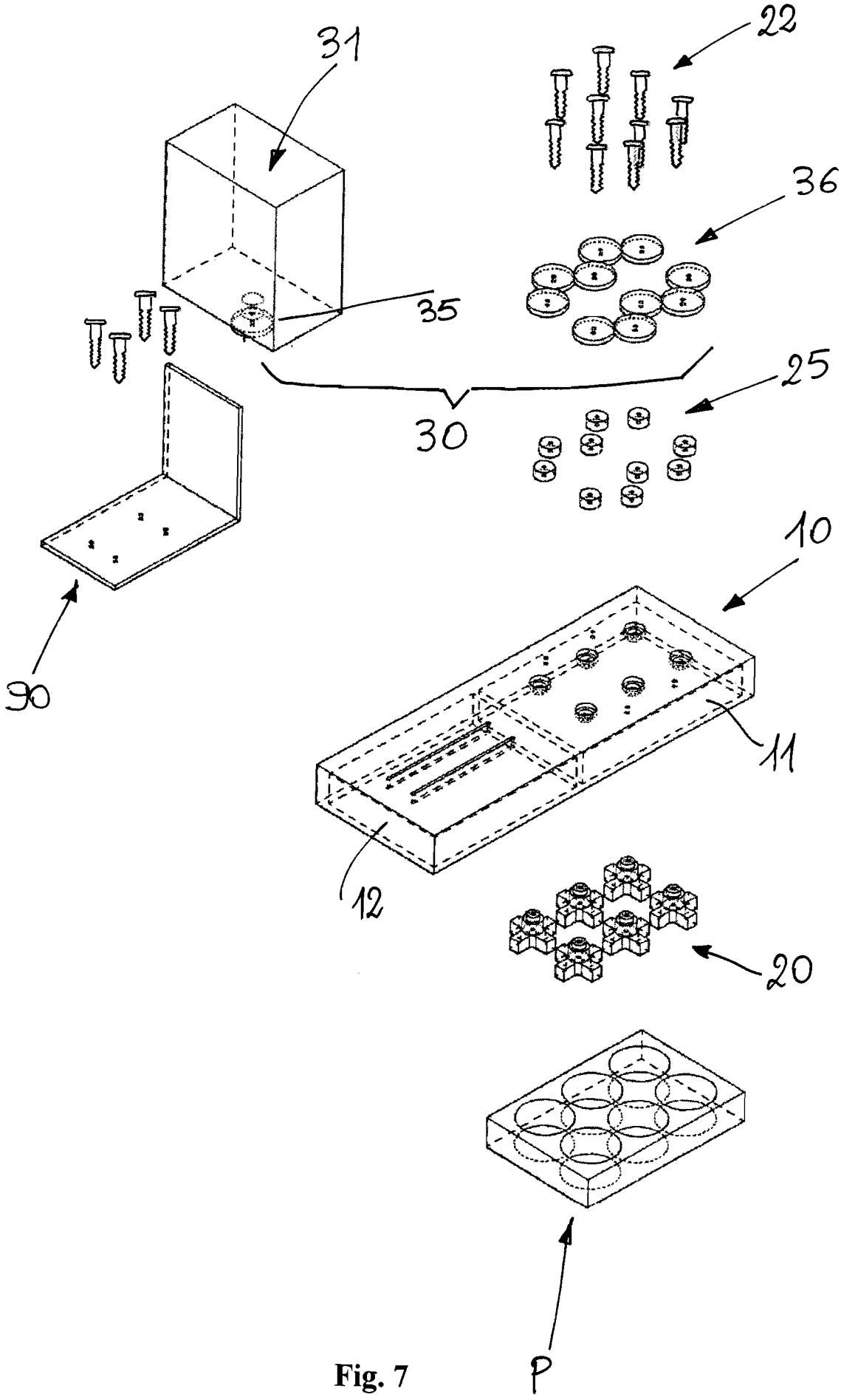

Fig. 7

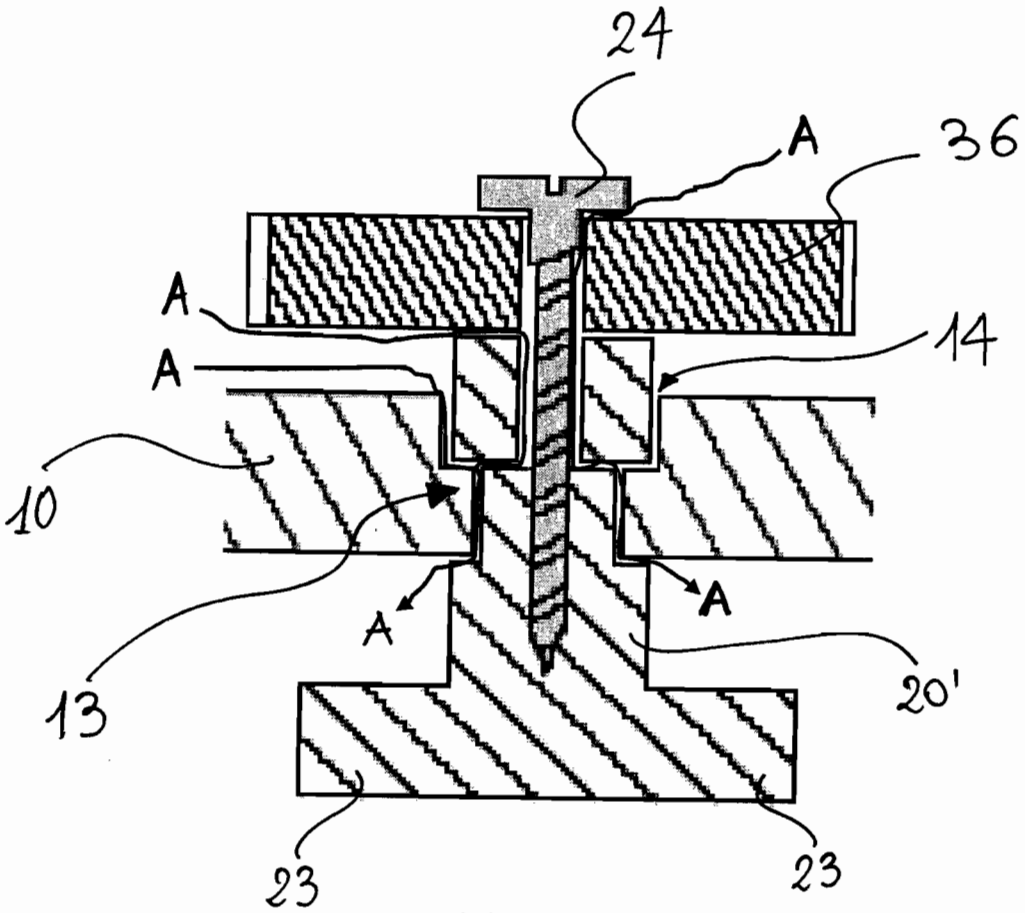

Fig. 8

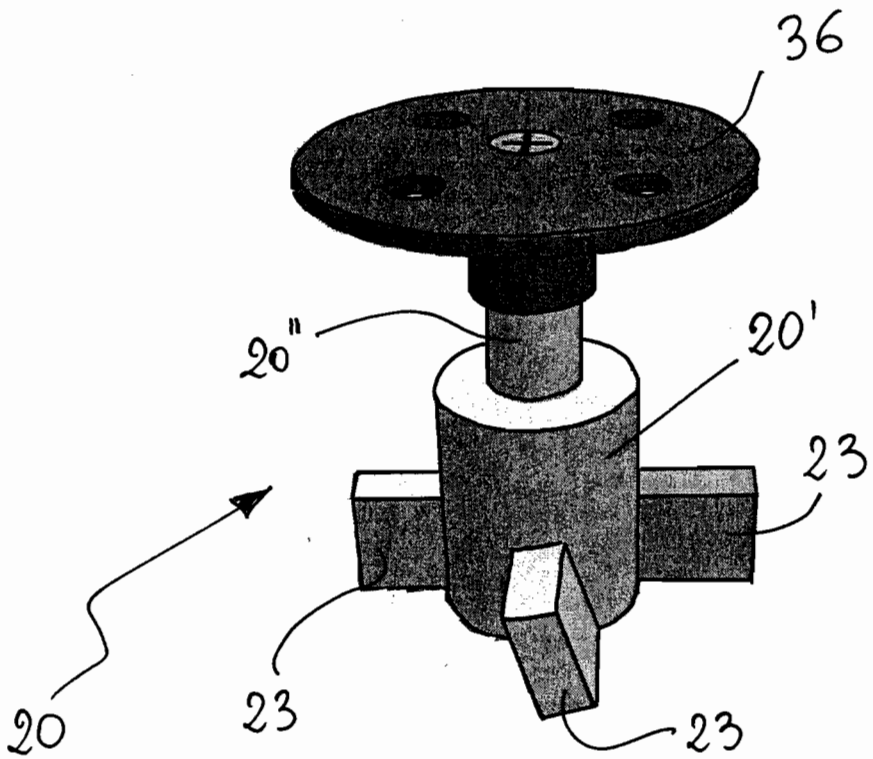

Fig. 9

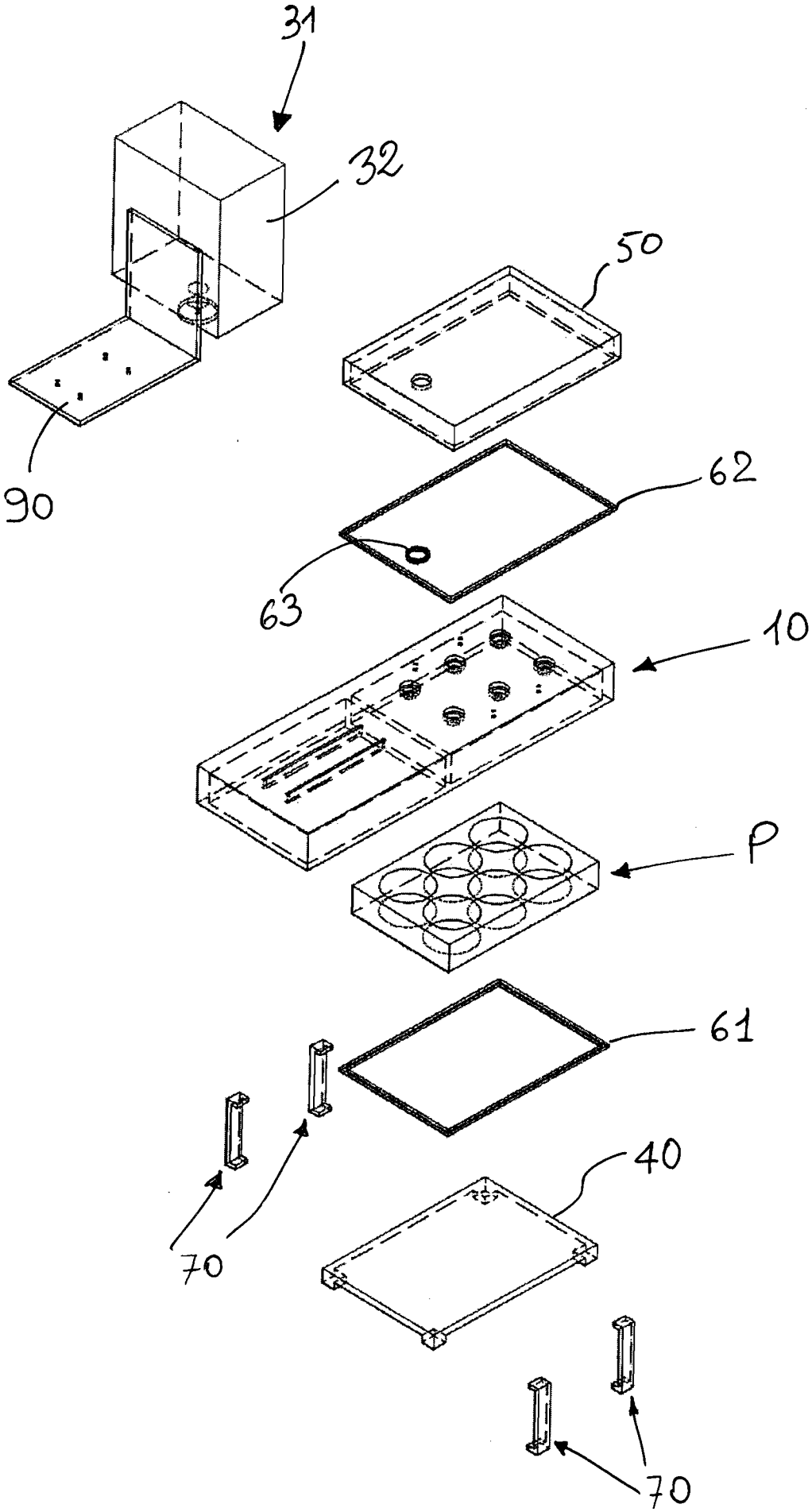

Fig. 10

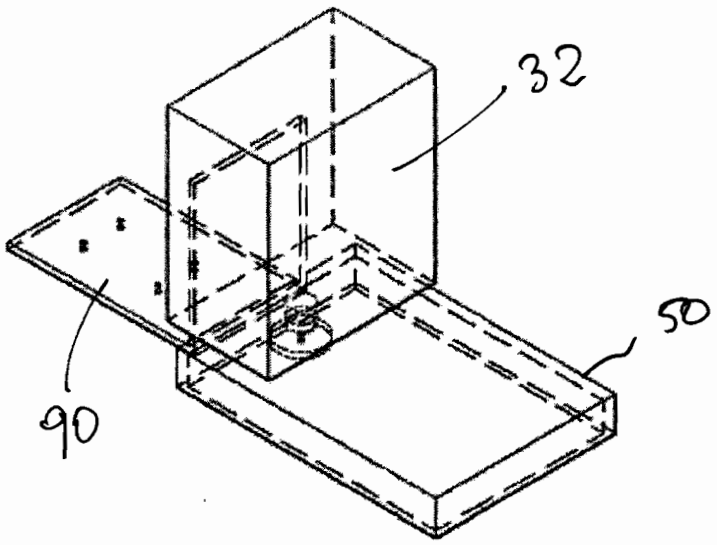

Fig. 11

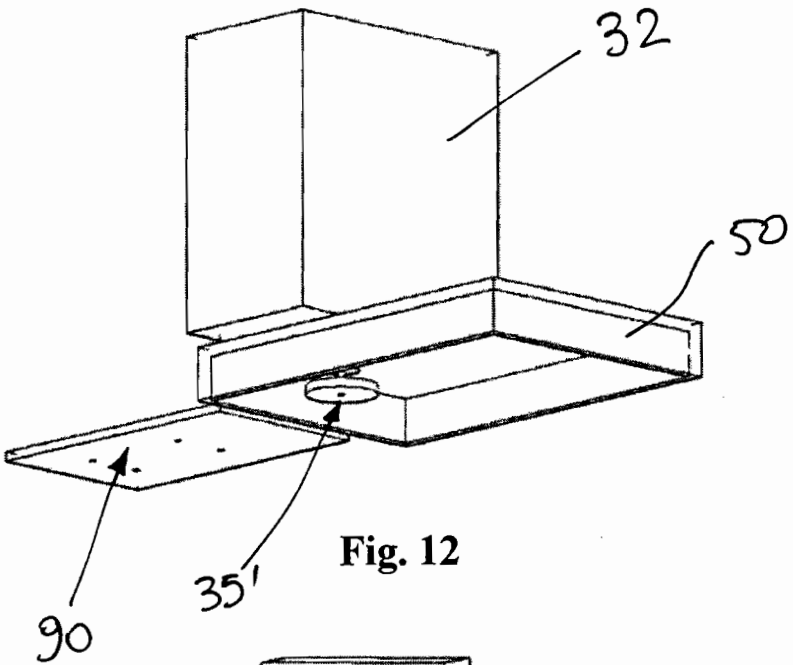

Fig. 12

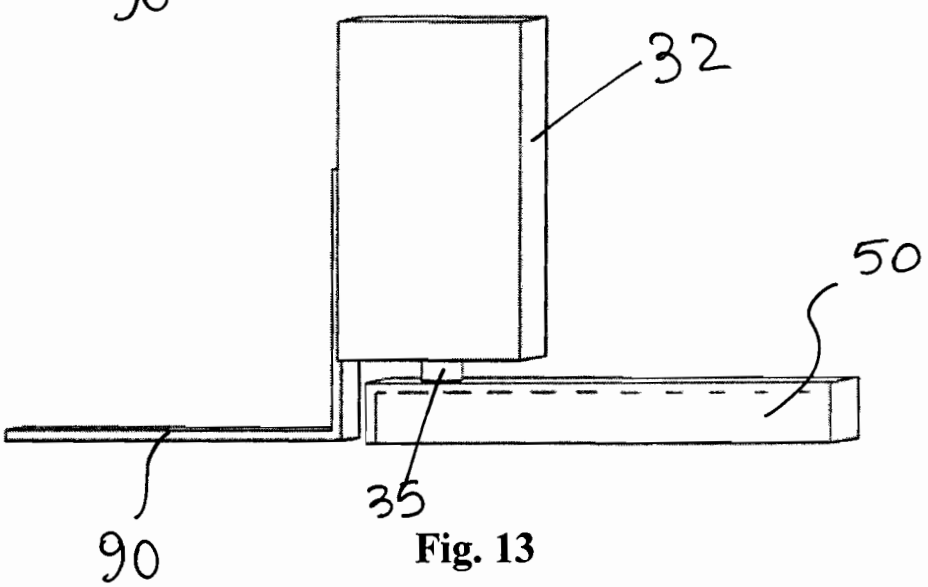

Fig. 13

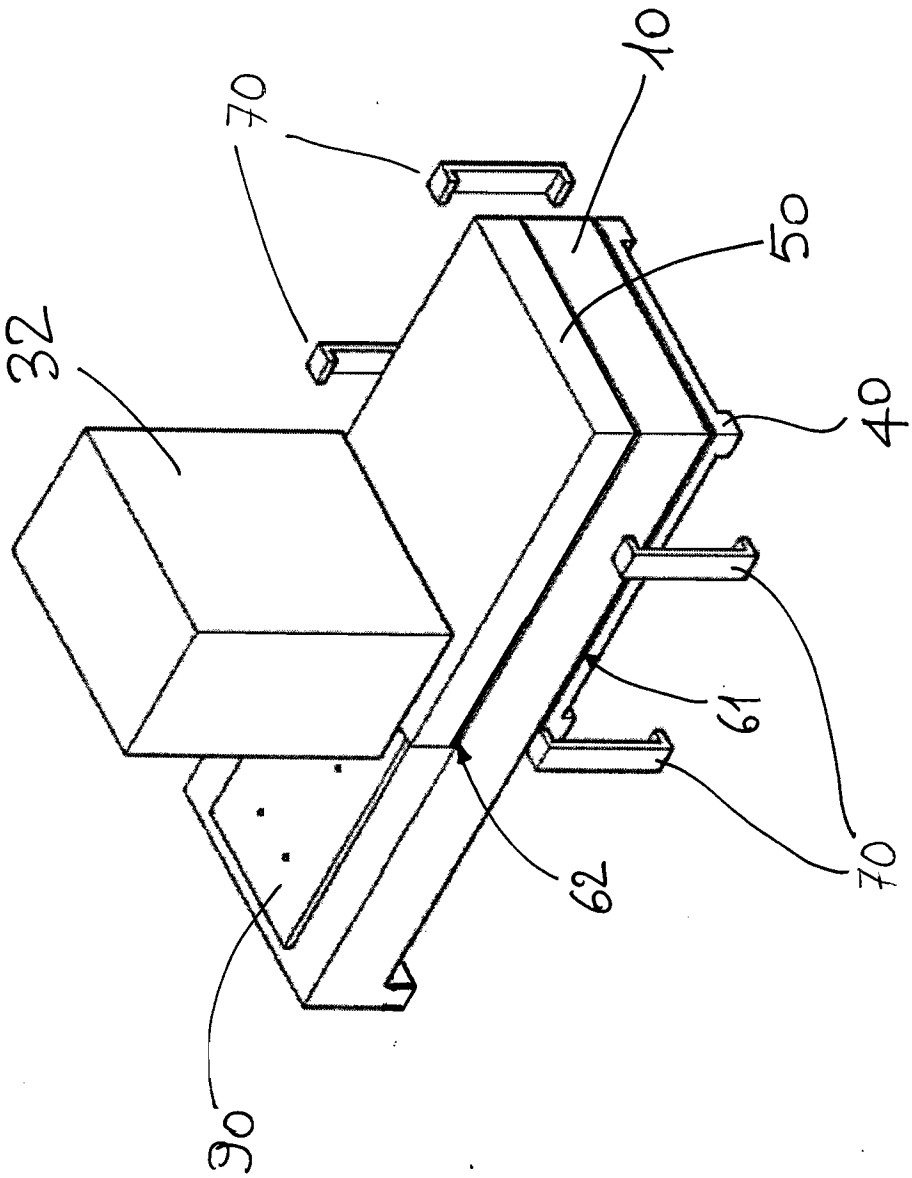

Fig. 14

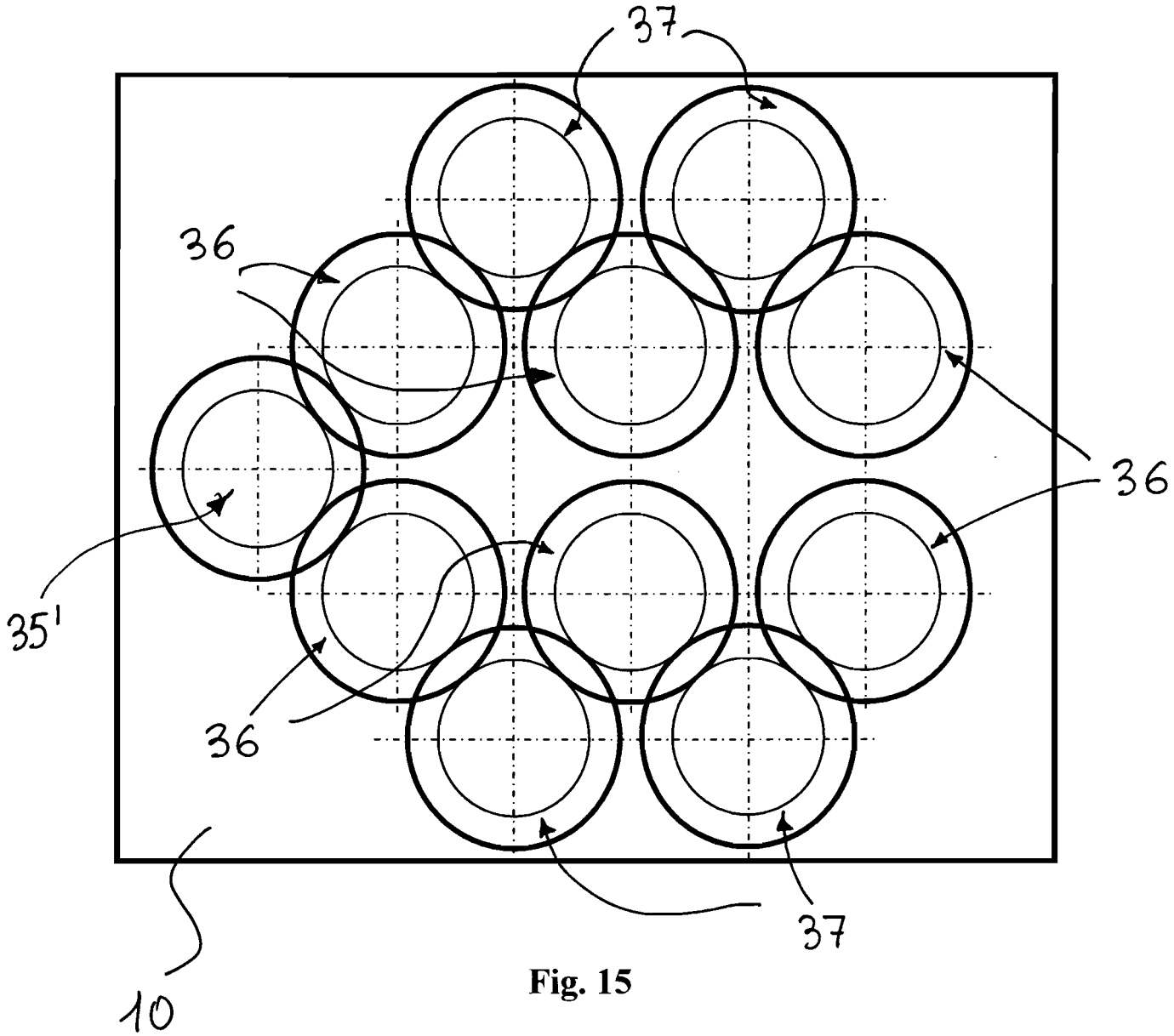

Fig. 15